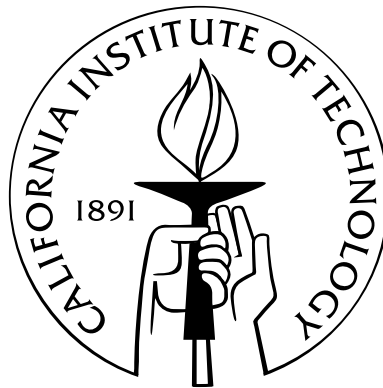# Cavity QED with Multilevel Atoms

Thesis by

Kevin M. Birnbaum

In Partial Fulfillment of the Requirements

for the Degree of

Doctor of Philosophy

California Institute of Technology

Pasadena, California

2005

(Defended May 16, 2005)

Acknowledgements

Thanks Jeff. Thanks Theresa, Tracy, Dominik, Joe, Christina, Andrew. Thanks Andreea, Dave, Russ, Jason. Thanks Scott. Thanks John, Win, James, Dan, Cristoph, Alex, Mike, Ben, Warwick, Liz, Matt, Sergey, Glov. Thanks Mom, Dad, Melissa, Belle, Honey, Gizmo. Thanks everybody I forgot to thank.

Abstract

Cavity QED in the regime of strong coupling is an exciting testbed for quantum information science. Recent progress in cooling and trapping atoms within optical cavities has enabled extensive measurement and manipulation of a cavity coupled to one and the same atom. Future experiments will use new types of optical resonators to greatly increase the rate of atom-cavity interaction, thus improving the fidelity of quantum operations.

In order to accurately calculate the properties of the systems in these current and future experiments, however, we must move beyond the simple model of a two-state atom interacting with a single mode of the electromagnetic field. The models must incorporate the multiple Zeeman and hyperfine states of the atom, as well as all near-detuned modes of the optical resonator. In this thesis, these detailed atom-cavity models are presented, and their properties are explored. We find favorable comparison with recent experimental results and provide predictions for upcoming experiments.

The steady-state transmission spectrum of a cavity with two modes of orthogonal polarization strongly coupled to a single atom with multiple Zeeman states is computed. Effects due to cavity birefringence and atomic ac-Stark shifts are included. The transmission spectrum is compared to experimental results for a single Cesium atom trapped via an intracavity FORT in a Fabry-Perot cavity. The excellent agreement of the theory with the data is used to infer the distribution of the position of the trapped atom.

The intensity correlation function of this system is also calculated, and found to be strongly antibunched and sub-Poissonian. This effect is explained in terms of photon

blockade, based on the structure of the lowest energy eigenvalues. Experimental results confirm the strong nonlinearity at the single-photon level.

We present theoretical predictions of the weak field spectra of microtoroid and photonic bandgap cavities strongly coupled to the D2 transition of single Cesium atoms. These calculations include all hyperfine and Zeeman states of the transition and model the cavity as a single-mode, linearly polarized resonator.

Finally, we outline a technique for using multiple hyperfine and Zeeman levels of a single atom in a strongly coupled atom-cavity system to generate polarized single photons on demand in a well-defined temporal mode via adiabatic passage. The technique is insensitive to cavity birefringence and only weakly sensitive to atomic position. Variations of this technique for generating entanglement of photon polarization and atomic Zeeman state are also discussed.

Contents

Bibliography   **172**

List of Figures

List of Tables

Chapter 1

Introduction

Cavity quantum electrodynamics (QED) provides an exceptional setting in which to study the fundamentals of quantum theory [1]. The model system, a single atom coupled to a mode of the electromagnetic field, has many useful features. It is a quantum system with a small number of degrees of freedom. The coupling to the environment, the continuum of electromagnetic modes, is well understood and can be modeled with high accuracy. In the optical domain, the relevant energy scales are large compared to room temperature. Also, efficient detection of optical photons is readily available. Most importantly, we can achieve strong coupling between the atom and the cavity. Strong coupling means that the coherent, reversible interaction between the two components of the system dominates the dissipative effects of the environment. This allows us to study experimentally many interesting problems in quantum mechanics, such as the dynamics of a measured quantum system and the quantum-classical transition. It also makes cavity QED a great testbed for the emerging ideas of quantum information science.

A single atom coupled to a cavity constitutes one of the most basic systems in optical physics. The usual model of cavity QED is also one of the simplest quantum systems. This model, the Jaynes-Cummings model [2], treats the atom as a two-state system and the cavity as a single harmonic oscillator. While the true system has many more states, in the lab we have restricted the system to a small subspace to match this model. This was accomplished by using optical pumping to reach a cycling transition of the atom; this transition was only coupled to one mode of the cavity [3].

The outstanding experimental problem with cavity QED has been control of the atomic motion. The position of the atom within the cavity determines the coupling strength of the atomic dipole to the cavity field. In order to use the system for quantum information tasks, this coupling strength must be a known constant. Great progress towards the control of atomic motion within a cavity was made with the implementation of a far off-resonant trap (FORT) at the "magic" wavelength which only weakly affects the atomic transition frequency [4]. This has enabled us to move beyond ensemble measurements towards the study of individual quantum systems.

These latest experimental techniques, however, prohibit the use of optical pumping to confine the system to a small subspace. This necessitates developing a more detailed model of the cavity QED system which incorporates multiple atomic states as well as both polarization modes of the Fabry-Perot cavity. Furthermore, future experiments will use microtoroid [5] and photonic bandgap cavities [6], which are expected to couple multiple hyperfine levels of the atom.

This thesis develops and applies these detailed models to current and future experiments with single atoms in the strong coupling regime of cavity QED, and presents an example of how multiple atomic states and polarization modes can be used to perform a quantum information task.

1.1 My History in the Group

I started work in the Quantum Optics Group in the summer of 1999. I began in Lab 1, pestering Christina Hood and Theresa Lynn with questions while they tried to work. They were finishing the rebuild of the cavity QED experiment in that lab and collecting the data on the "atom-cavity microscope" [7, 8]. Eventually I learned how to tweak and became somewhat useful in lab, as Christina graduated and I continued working with Theresa and Joe Buck. We worked on implementing feedback to control the motion of an atom inside the cavity. While this seemed like a straightforward extension of the atom-cavity microscope, it required some major technical improvements in the apparatus, notably a new frequency metrology set-up

to lock the cavity length while modulating the probe light.

While attempting to upgrade the experiment, we were also fighting the pernicious effects of the second law of thermodynamics, which was increasing the entropy and decreasing the usefulness of our apparatus. The worst problems were with the vacuum chamber, which suffered repeated failures. Eventually, after a number of exciting adventures with glove-bags, we found that the cavity transmission had gone to zero.

We decided to rebuild the experiment from the ground up with a new cavity in a new dual-vacuum chamber. Appendix B began as a set of notes about what we learned while designing and building the new chamber. While waiting for vacuum parts to arrive and the chamber to pump down and bake, I worked in Lab 11 with Joe, Jason McKeever, and Alex Kuzmich. There I learned how our group's other cavity QED experiment was designed and was thoroughly intimidated by the complexity of the apparatus.

I returned to Lab 1 to continue the rebuild with Theresa, visiting grad student Dominik Schrader, and new grad student Tracy Northup. As we worked on the experiment, we also did some calculations to find what effect feedback should have on the atomic motion [9, 10]. We found that due to the limited trap lifetime (set by axial motion, which we could not control), feedback would not have time to act on many atoms, and the average effect would be modest. Tracy is currently rebuilding the experiment once again, this time with a longer one-sided cavity, designed to hold atoms in a FORT and entangle them with another atom in the Lab 11 cavity.

While looking at transit data from Lab 1 with its record-holding (until the microtoroid or photonic bandgap experiments come online) single photon Rabi frequency $2g_0/2\pi \simeq 260$ MHz, it occurred to us that this is comparable to the atomic excited-state hyperfine splitting. I started collaborating with Scott Parkins, thinking about the effects this might have on spectral features of the atom-cavity system (see Chapter 6).

While I was calculating the spectra of a multilevel atom coupled to a cavity, the Lab 11 experimentalists (Andreea Boca, Russ Miller, and Dave Boozer) set out to measure that same quantity. Although g_0 was not so large as to couple multiple

hyperfine levels to the cavity, there were multiple Zeeman states of the atom, as well as two cavity modes to consider. We achieved excellent agreement of the theory with the experiment which allowed us to use the spectrum to estimate the temperature of the atom in the trap (see Chapters 2 and 3).

While working on these calculations, I noticed that there was a significant amount of light in the "dark" cavity mode, i.e., the mode which is not driven by the probe laser. After first trying to eliminate this light (thinking it must indicate a mistake in the computer code), I began to investigate its properties. I found that at some detunings, it had extremely sub-Poissonian statistics and asked the experimentalists to measure this to see if it could possibly be true. They found that indeed, there was light in this mode and it was strongly sub-Poissonian, a phenomenon we explain in terms of "photon blockade" in Chapters 4 and 5.

1.2   Overview

In Chapter 2, we describe the measurement of the vacuum-Rabi splitting for one atom trapped in a cavity in the regime of strong coupling. We compare the data to theoretical spectra and infer an approximate temperature for atomic motion.

In Chapter 3, we build up the theory of the vacuum-Rabi splitting, starting with the simplest model and increasing the complexity step by step in order to describe the experiment of Chapter 2. We end with some further extensions to the theory which were not incorporated into the calculations due to limited computer resources.

In Chapter 4, we present the theory and measurement of photon blockade in an atom-cavity system. The photon statistics are also used to infer an approximate temperature, found to be in agreement with the results of Chapter 3.

In Chapter 5, we explore in greater depth the theoretical photon blockade results. We show the relationship of blockade to the eigenvalue structure, compare methods of probing the system, and calculate corrections to the theory.

In Chapter 6, we calculate weak-field spectra for linearly polarized single-mode cavities coupled to multiple hyperfine states. Results should be relevant to planned

experiments with microtoroid and photonic bandgap cavities.

In Chapter 7, we present representative samples of the computer code used to calculate the results of earlier chapters.

In Chapter 8, we describe specific implementations of an improved adiabatic single photon generation protocol, which make use of the two modes of the cavity and the multiple Zeeman and hyperfine states of the atom.

In Appendix A, we present a simple method for determining the length of a Fabry-Perot cavity from measurements of resonant wavelengths and apply it to the Lab 11 cavity.

In Appendix B, we present a user's guide to ultra-high vacuum chambers for atomic physics.

Chapter 2

Observation of the Vacuum-Rabi Spectrum for One Trapped Atom

This chapter is adapted from Ref. [11].

The transmission spectrum for one atom strongly coupled to the field of a high finesse optical resonator is observed to exhibit a clearly resolved vacuum-Rabi splitting characteristic of the normal modes in the eigenvalue spectrum of the atom-cavity system. A new Raman scheme for cooling atomic motion along the cavity axis enables a complete spectrum to be recorded for an individual atom trapped within the cavity mode, in contrast to all previous measurements in cavity QED that have required averaging over $10^3 - 10^5$ atoms.

2.1 Motivation

A cornerstone of optical physics is the interaction of a single atom with the electromagnetic field of a high quality resonator. Of particular importance is the regime of strong coupling, for which the frequency scale g associated with reversible evolution for the atom-cavity system exceeds the rates (γ, κ) for irreversible decay of atom and cavity field, respectively [12]. In the domain of strong coupling, a photon emitted by the atom into the cavity mode is likely to be repeatedly absorbed and re-emitted at the single-quantum Rabi frequency $2g$ before being irreversibly lost into the environment. This oscillatory exchange of excitation between atom and cavity field results from a normal mode splitting in the eigenvalue spectrum of the atom-cavity system

[2, 13, 14], and has been dubbed the 'vacuum-Rabi splitting [13].'

Strong coupling in cavity QED as evidenced by the vacuum-Rabi splitting provides enabling capabilities for quantum information science, including for the implementation of scalable quantum computation [15, 16], for the realization of distributed quantum networks [17, 18], and more generally, for the study of open quantum systems [1]. Against this backdrop, experiments in cavity QED have made great strides over the past two decades to achieve strong coupling [19]. The vacuum-Rabi splitting for single intracavity atoms has been observed with atomic beams in both the optical [20, 21, 22] and microwave regimes [23]. The combination of laser cooled atoms and large coherent coupling has enabled the vacuum-Rabi spectrum to be obtained from transit signals produced by single atoms [3]. A significant advance has been the trapping of individual atoms in a regime of strong coupling [24, 4], with the vacuum-Rabi splitting first evidenced for single trapped atoms in Ref. [24] and the entire transmission spectra recorded in Ref. [25].

Without exception these prior single atom experiments related to the vacuum-Rabi splitting in cavity QED [20, 23, 21, 22, 3, 24, 4, 25] have required averaging over trials with many atoms to obtain quantitative spectral information, even if individual trials involved only single atoms (e.g., 10^5 atoms were required to obtain a spectrum in Ref. [23] and $> 10^3$ atoms were needed in Ref. [25]). By contrast, the implementation of complex algorithms in quantum information science requires the capability for repeated manipulation and measurement of an individual quantum system, as has been spectacularly demonstrated with trapped ions [26, 27] and recently with Cooper pair boxes [28, 29].

2.2   Methodology

With this goal in mind, in this chapter we report measurements of the spectral response of single atoms that are trapped and strongly coupled to the field of a high finesse optical resonator. By alternating intervals of probe measurement and of atomic cooling, we record a complete probe spectrum for one and the same atom. The
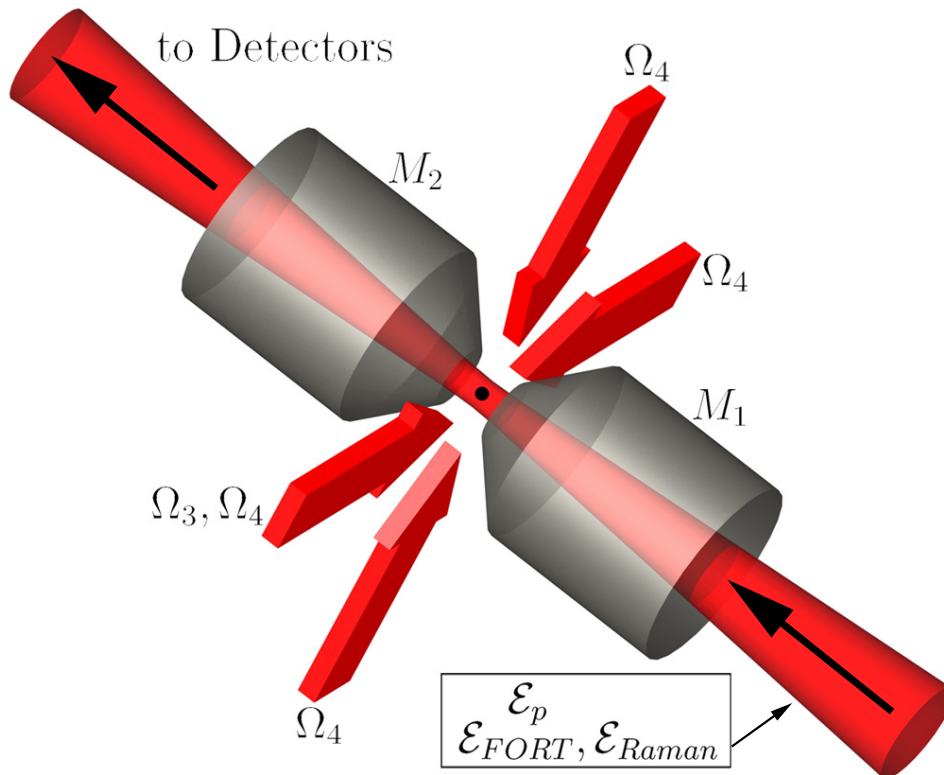
Figure 2.1: A single atom is trapped inside an optical cavity in the regime of strong coupling by way of an intracavity FORT driven by the field $\mathcal{E}_{FORT}$. The transmission spectrum $T_1(\omega_p)$ for the atom-cavity system is obtained by varying the frequency ω_p of the probe beam $\mathcal{E}_p$ and recording the output with single-photon detectors. Cooling of the radial atomic motion is accomplished with the transverse fields Ω_4, while axial cooling results from Raman transitions driven by the fields $\mathcal{E}_{FORT}, \mathcal{E}_{Raman}$. An additional transverse field Ω_3 acts as a repumper during probe intervals.

vacuum-Rabi splitting is thereby measured in a quantitative fashion for each atom by way of a protocol that represents a first step towards more complex tasks in quantum information science. An essential component of our protocol is a new Raman scheme for cooling atomic motion along the cavity axis, that leads to inferred atomic localization $\Delta z_{axial} \simeq 33$ nm, $\Delta \rho_{transverse} \simeq 5.5~\mu$m.

A simple schematic of our experiment is given in Fig. 2.1 [30]. After release from a magneto-optical trap (MOT) located several mm above the Fabry-Perot cavity formed by mirrors (M_1, M_2), single Cesium atoms are cooled and loaded into an intracavity far-off-resonance trap (FORT) and are thereby strongly coupled to a single mode of

the cavity. Our experiment employs the $6S_{1/2}, F = 4 \rightarrow 6P_{3/2}, F' = 5'$ transition of the $D2$ line in Cs at $\lambda_A = 852.4$ nm, for which the maximum single-photon Rabi frequency $2g_0/2\pi = 68$ MHz for $(F = 4, m_F = \pm 4) \rightarrow (F' = 5', m'_F = \pm 5)$. The transverse decay rate for the $6P_{3/2}$ atomic states is $\gamma/2\pi = 2.6$ MHz, while the cavity field decays at rate $\kappa/2\pi = 4.1$ MHz. Our system is in the strong coupling regime of cavity QED $g_0 \gg (\gamma, \kappa)$ [12].

The intracavity FORT is driven by a linearly polarized input field $\mathcal{E}_{FORT}$ at $\lambda_F = 935.6$ nm, resulting in nearly equal AC-Stark shifts for all Zeeman states in the $6S_{1/2}, F = 3, 4$ manifold [31]. Birefringence in the mirrors leads to two nondegenerate cavity modes with orthogonal polarizations $\hat{l}_\pm$ and mode splitting $\Delta\nu_{C_1} = 4.4 \pm 0.2$ MHz. $\mathcal{E}_{FORT}$ ($\mathcal{E}_{Raman}$) is linearly polarized and aligned close to $\hat{l}_+$ ($\hat{l}_-$) for the higher (lower) frequency mode. At an antinode of the field, the peak value of the trapping potential for these states is $U_0/h = -39$ MHz for all our measurements. Zeeman states of the $6P_{3/2}, F' = 5'$ manifold likewise experience a trapping potential, albeit with a weak dependence on m'_F [4]. The cavity length is independently stabilized to length $l_0 = 42.2$ μm such that a TEM_{00} mode at λ_{C_1} is resonant with the free-space atomic transition at λ_A and another TEM_{00} mode at λ_{C_2} is resonant at λ_F. At the cavity center $z = 0$, the mode waists $w_{C_{1,2}} = \{23.4, 24.5\}$ μm at $\lambda_{C_{1,2}} = \{852.4, 935.6\}$ nm.

As illustrated in Fig. 2.1, we record the transmission spectrum $T_1(\omega_p)$ for a weak external probe $\mathcal{E}_p$ of variable frequency ω_p incident upon the cavity containing one strongly coupled atom. $T_1(\omega_p)$ is proportional to the ratio of photon flux transmitted by M_2 to the flux $|\mathcal{E}_p|^2$ incident upon M_1, with normalization $T_0(\omega_p = \omega_{C_1}) \equiv 1$ for the empty cavity. Our protocol consists of an alternating sequence of probe and cooling intervals. The probe beam is linearly polarized and is matched to the TEM_{00} mode around λ_{C_1}. Relative to $\hat{l}_\pm$, the linear polarization vector $\hat{l}_p$ for the probe field $\mathcal{E}_p$ is aligned along a direction $\hat{l}_p = \cos\theta \hat{l}_+ + \sin\theta \hat{l}_-$, where $\theta = 13°$ for Fig. 2.2; however, the theory is relatively insensitive to θ for $\theta \lesssim 15°$. $\mathcal{E}_p$ illuminates the cavity for $\Delta t_{probe} = 100$ μs, and the transmitted light is detected by photon counting. The efficiency for photon escape from the cavity is $\alpha_{e2} = 0.6 \pm 0.1$. The propagation

efficiency from M_2 to detectors (D_1, D_2) is $\alpha_P = 0.41 \pm .03$, with then each detector receiving half of the photons. The avalanche photodiodes (D_1, D_2) have quantum efficiencies $\alpha_P = 0.49 \pm 0.05$. During each probing interval, a repumping beam Ω_3, transverse to the cavity axis and resonant with $6S_{1/2}, F = 3 \rightarrow 6P_{3/2}, F' = 4'$, also illuminates the atom. In successive probe intervals, the frequency ω_p is linearly swept from below to above the common atom-cavity resonance at $\omega_A \simeq \omega_{C_1}$. The frequency sweep for the probe is repeated eight times in $\Delta t_{tot} = 1.2$ s, and then a new loading cycle is initiated.

Following each probe interval, we apply light to cool both the radial and axial motion for $\Delta t_{cool} = 2.9$ ms. Radial cooling is achieved by the Ω_4 beams consisting of pairs of counter-propagating fields in a $\sigma_\pm$ configuration perpendicular to the cavity axis, as shown in Fig. 2.1. The Ω_4 beams are detuned $\Delta_4 \simeq 10$ MHz to the *blue* of the $4 \rightarrow 4'$ transition to provide blue Sisyphus cooling [32] for motion transverse to the cavity axis.

Following each probe interval, we apply light to cool both the radial and axial motion for $\Delta t_{cool} = 2.9$ ms. Radial cooling is achieved by the Ω_4 beams consisting of pairs of counter-propagating fields in a $\sigma_\pm$ configuration perpendicular to the cavity axis, as shown in Fig. 2.1. The Ω_4 beams are detuned $\Delta_4 \simeq 10$ MHz to the *blue* of the $4 \rightarrow 4'$ transition to provide blue Sisyphus cooling [32] for motion transverse to the cavity axis.

To cool the axial motion for single trapped atoms, we have developed a new scheme that employs $\mathcal{E}_{FORT}$ and an auxiliary field $\mathcal{E}_{Raman}$ that is frequency offset by $\Delta_{Raman} = \Delta_{HF} + \delta$ and phase locked to $\mathcal{E}_{FORT}$. Here, $\Delta_{HF} = 9.192632$ GHz is the hyperfine splitting between $6S_{1/2}, F = 3, 4$. $\mathcal{E}_{FORT}$, $\mathcal{E}_{Raman}$ drive Raman transitions between the $F = 3, 4$ levels with effective Rabi frequency $\Omega_E \sim 200$ kHz. By tuning δ near the $\Delta n = -2$ motional sideband (i.e., $-2\nu_0 \sim \delta = -1.0$ MHz, where ν_0 is the axial vibrational frequency at an antinode of the FORT), we implement sideband cooling via the $F = 3 \rightarrow 4$ transition, with repumping provided by the Ω_4 beams. The Raman process also acts as a repumper for population pumped to the $F = 3$ level by the Ω_4 beams. Each cooling interval is initiated by turning on the fields Ω_4, $\mathcal{E}_{Raman}$ during Δt_{cool} and is terminated by gating these fields off before the next probe interval Δt_{probe}.

Figure 2.2: Transmission spectrum $T_1(\omega_p)$ for six randomly drawn atoms. In each case, $T_1(\omega_p)$ is acquired for one-and-the-same atom, with the two peaks of the vacuum-Rabi spectum clearly evident. The error bars reflect the statistical uncertainties in the number of photocounts. The full curve is from the steady-state solution to the master equation.

2.3 Results

Fig. 2.2 displays normalized transmission spectra T_1 and corresponding intracavity photon numbers $\langle n(\omega_p) \rangle$ for individual atoms acquired by alternating probe and cooling intervals. Clearly evident in each trace is a two-peaked structure that represents the vacuum-Rabi splitting observed on an atom-by-atom basis. Also shown is the predicted transmission spectrum obtained from the steady-state solution to the master equation for one atom strongly coupled to the cavity, as discussed below. The quantitative correspondence between theory and experiment is evidently quite reason-

able for each atom. Note that m_F-dependent Stark shifts for $F' = 5'$ in conjunction with optical pumping caused by $\mathcal{E}_p$ lead to the asymmetry of the peaks in Fig. 2.2 via an effective population-dependent shift of the atomic resonance frequency. The AC-Stark shifts of the $(F' = 5', m'_F)$ states are given by $\{m'_F, U_{m'_F}\} = \{\pm 5, 1.18U\}$, $\{\pm 4, 1.06U\}$, $\{\pm 3, 0.97U\}$, $\{\pm 2, 0.90U\}$, $\{\pm 1, 0.86U\}$, $\{0, 0.85U\}$.

To obtain the data in Fig. 2.2, $N_{load} = 61$ atoms were loaded into the FORT in 500 attempts, with the probability that a given successful attempt involved 2 or more atoms estimated to be $P_{load}(N \geq 2) \lesssim 0.06$. Of the N_{load} atoms, $N_{survive} = 28$ atoms remained trapped for the entire duration Δt_{tot}. The six spectra shown in Fig. 2.2 were selected by a random drawing from this set of $N_{survive}$ atoms. Our sole selection criterion for presence of an atom makes no consideration of the spectral structure of $T_1(\omega_p)$ except that there should be large absorption on line center, $T_1(\omega_p = \omega_{C_1}) \leq T_{thresh} \approx 0.2$. Transmission spectra $T_1(\omega_p), \bar{T}_1(\omega_p)$ are insensitive over a range of selection criteria $0.02 \leq T_{thresh} \leq 0.73$. Note that an atom trapped in the FORT in the absence of the cooling and probing light has lifetime $\tau_0 \simeq 3$ s, which leads to a survival probability $p(\Delta t_{tot}) \simeq 0.7$.

In Fig. 2.3 we collect the results for $T_1(\omega_p)$ for all $N_{survive} = 28$ atoms, and display the average transmission spectrum $\bar{T}_1(\omega_p)$, as well as a scatter plot from the individual spectra. This comparison demonstrates that the vacuum-Rabi spectrum observed for any particular atom represents with reasonable fidelity the spectrum that would be obtained from averaging over many atoms, albeit with fluctuations due to Poisson counting and optical pumping effects over the finite duration of the probe. The total acquisition time associated with the probe beam for the spectrum of any one atom is only 40 ms.

2.4 Comparison to Theory

The full curves in Figs. 2.2 and 2.3 are obtained from the steady state solution of the master equation including all transitions $(F = 4, m_F) \leftrightarrow (F' = 5', m'_F)$ with their respective coupling coefficients $g_0^{(m_F, m'_F)}$, as well as the two nearly degenerate
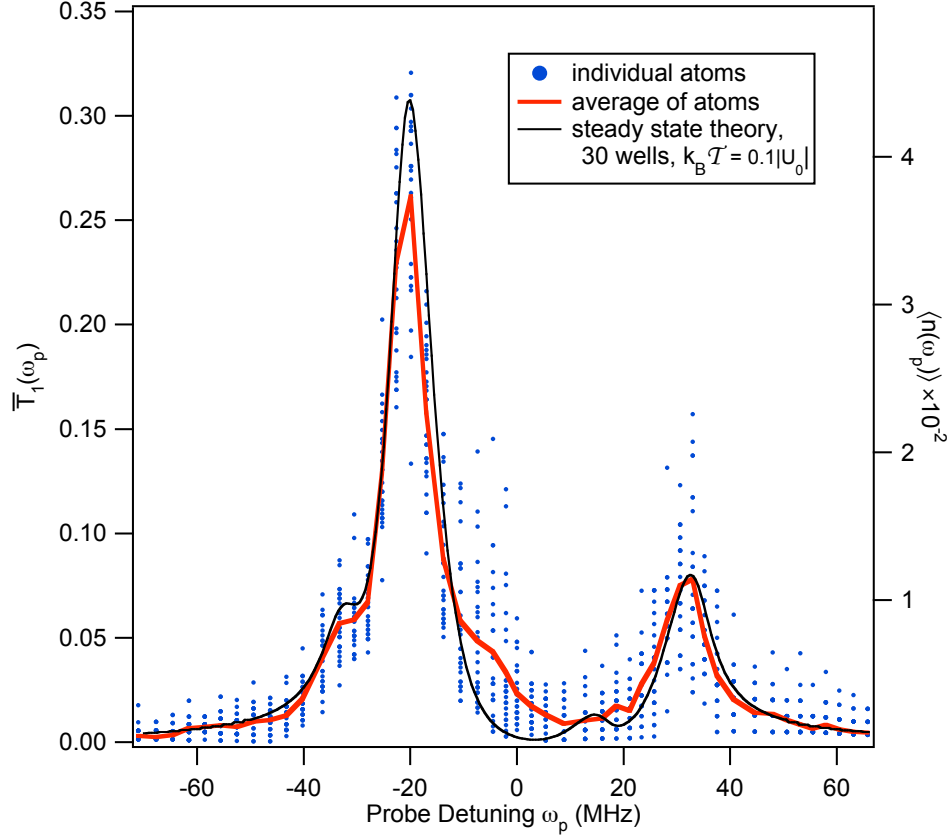
Figure 2.3: Transmission spectrum $\bar{T}_1(\omega_p)$ (thick trace) resulting from averaging all 28 individual spectra $T_1(\omega_p)$ (dots). The thin trace is from the steady-state solution to the master equation, and is identical to that in Fig. 2.2. The only free parameters in the theory are the temperature and the range of FORT antinodes; the vertical scale is absolute.

modes of our cavity. For the comparison of theory and experiment, the parameters $(g_0^{(m_F, m_F')}, \gamma, \kappa, \omega_{C_1} - \omega_A, \omega_p - \omega_A, |\mathcal{E}_p|^2, U_0)$ are known in absolute terms without adjustment. However, we have no *a priori* knowledge of the particular FORT well into which the atom is loaded along the cavity standing wave, nor of the energy of the atom. The FORT shift and coherent coupling rate are both functions of atomic position $\mathbf{r}$, with $U(\mathbf{r}) = U_0 \sin^2(k_{C_2} z) \exp(-2\rho^2/w_{C_2}^2)$ and $g^{(m_F, m_F')}(\mathbf{r}) = g_0^{(m_F, m_F')} \psi(\mathbf{r})$, where $g_0^{(m_F, m_F')} = g_0 G_{m_F, m_F'}$ with $G_{i,f}$ related to the Clebsch-Gordan coefficient for the particular $m_F \leftrightarrow m_F'$ transition. $\psi(\mathbf{r}) = \cos(k_{C_1} z) \exp(-\rho^2/w_{C_1}^2)$, where ρ is the transverse distance from the cavity axis z, and $k_{C_{1,2}} = 2\pi/\lambda_{C_{1,2}}$.

As discussed in connection with Fig. 2.4 below, for the theoretical curves shown
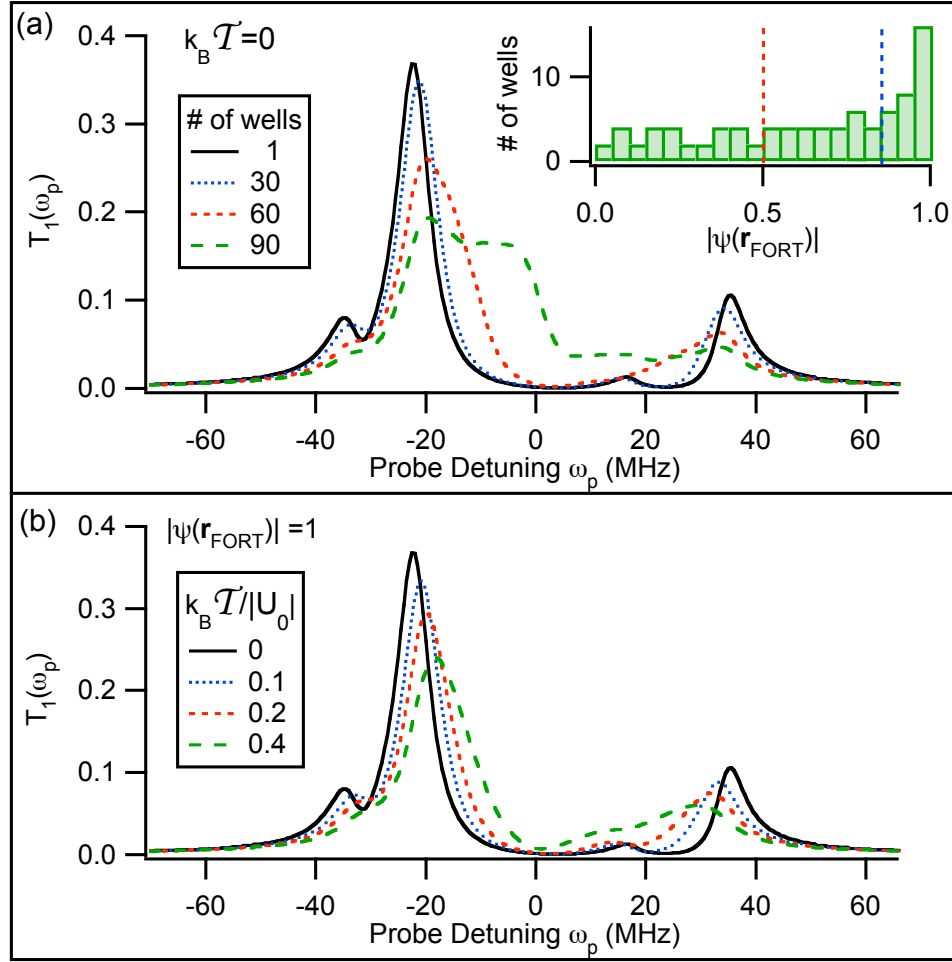
Figure 2.4: Theoretical plots for $T_1(\omega_p)$ from the steady-state solution of the master equation. (a) For zero temperature, $T_1(\omega_p)$ is calculated from an average over various FORT antinodes along the cavity axis, with the inset showing the associated distribution of values for $|\psi(\mathbf{r}_{FORT})|$. (b) For an optimum FORT well (i.e., $|\psi(\mathbf{r}_{FORT})| = 1$), $T_1(\omega_p)$ is computed for various temperatures from an average over atomic positions within the well.

in Figs. 2.2 and 2.3, we have chosen only the 30 out of 90 total FORT wells for which $|\psi(\mathbf{r}_{FORT})| \geq 0.87$, where $\mathbf{r}_{FORT}$ is such that $U(\mathbf{r}_{FORT}) = U_0$. Furthermore, for these wells we have averaged $T_1(\omega_p)$ over a Gaussian distribution in position $\mathbf{r}$ consistent with a temperature $k_B\mathcal{T} = 0.1U_0$ ($\sim 200 \, \mu$K). Since all parameters are known except for those that characterize atomic motion, the good agreement between theory and experiment allows us to infer that our cooling protocol together with the selection criterion $T_{thresh} = 0.2$ results in individual atoms that are strongly coupled in one of

the "best" FORT wells (i.e., $|\psi(\mathbf{r}_{FORT})| \gtrsim 0.87$) with "temperature" $\sim 200\ \mu$K . In Figs. 2.2 and 2.3, the discrepancy between experiment and the *steady-state* theory for $\bar{T}_1(\omega_p)$ around $\omega_p \sim 0$ can be accounted for by a *transient* solution to the master equation which includes optical pumping effects over the probe interval Δt_{probe}. Also, although the spectra are consistent with a thermal distribution, we do not exclude a more complex model involving probe-dependent heating and cooling effects.

In support of these assertions, Fig. 2.4(a) explores the theoretical dependence of $T_1(\omega_p)$ on the set of FORT wells selected, and hence on the distribution of values for $|\psi(\mathbf{r}_{FORT})|$ in the ideal case $\mathcal{T} = 0$. Extending the average beyond the 30 "best" FORT wells leads to spectra that are inconsistent with our observations in Figs. 2.2 and 2.3. Fig. 2.4(b) likewise investigates the theoretical dependence of $T_1(\omega_p)$ on the temperature $\mathcal{T}$ for an atom at an antinode of the FORT with optimal coupling (i.e., $|\psi(\mathbf{r}_{FORT})| = 1$). For temperatures $\mathcal{T} \gtrsim 200\ \mu$K, the calculated spectra are at variance with the data in Figs. 2.2 and 2.3, from which we infer atomic localization $\Delta z \simeq 33$ nm in the axial direction and $\Delta x = \Delta y \simeq 3.9\ \mu$m in the plane transverse to the cavity axis. Beyond these conclusions, a consistent feature of our measurements is that reasonable correspondence between theory and experiment is only obtained by restricting $|\psi(\mathbf{r})| \gtrsim 0.8$.

Our experiment represents an important advance in the quest to obtain single atoms trapped with optimal strong coupling to a single mode of the electromagnetic field. The vacuum-Rabi splitting is the hallmark of strong coupling for single atoms and photons, and all measurements until now have required averaging over many atoms for its observation. By contrast, we are able to observe spectra $T_1(\omega_p)$ on an atom-by-atom basis with clearly resolved normal-mode splittings. These spectra contain detailed quantitative information about the coherent coupling $g(\mathbf{r})$ and FORT shifts for each atom. This information indicates that the coupling g is in a narrow range of near-maximal values. Our observations are made possible by the implementation of a new scheme to cool both the radial and axial atomic motion. The capabilities demonstrated in this chapter should provide the tools necessary to implement diverse protocols in quantum information science [15, 16, 17, 18, 1].

Chapter 3

Calculation of the Vacuum-Rabi Spectrum

As described in Chapter 2, the transmission spectrum of an optical cavity coupled to a single atom was measured. The vacuum-Rabi splitting, the hallmark of strong coupling, was clearly and repeatably observed for each atom loaded and trapped inside the cavity mode. The excellent agreement of the data with theoretical models was used to infer the distribution of atomic position based on the transmission measurement alone. The details of the theoretical models used to draw this inference are presented here.

3.1   The Jaynes-Cummings Model

We begin with the simplest model which exhibits the vacuum Rabi splitting, the Jaynes-Cummings model [2]. In the Jaynes-Cummings model, the atom has one ground state, denoted $|g\rangle$, and one excited state, $|e\rangle$, with a transition frequency ω_a. It is coupled to a single mode resonator (annihilation operator a) with resonant frequency ω_c, which is driven by an external classical field at frequency ω_p. The Hamiltonian describing this system is

$$H_{JC} = \Delta_a |e\rangle\langle e| + \Delta_c a^\dagger a + g(a^\dagger d + d^\dagger a) + \varepsilon a + \varepsilon^* a^\dagger \qquad (3.1)$$

where $d \equiv |g\rangle\langle e|$ is the atomic lowering operator, $\Delta_a \equiv \omega_a - \omega_p$, and $\Delta_c \equiv \omega_c - \omega_p$. The classical driving field, assumed to be a coherent state, is represented by ε and g is half of the single-photon Rabi frequency. We have used the rotating wave approximation, and the Hamiltonian is described in the frame which is rotating with the probe. In this chapter, we use units where $\hbar = 1$ so that energy has the same dimension as frequency.

In order to calculate the transmission of the cavity, we will find the steady state of the system. The time evolution (including decays) of ρ, the density matrix of the atom-cavity system, is determined by the master equation $\dot{\rho} = \mathcal{L}\rho$. In using the master equation, we make a number of assumptions, notably that the environment is Markovian, i.e., it has no memory [33]. This means that the reservoir must have a very large number of degrees of freedom, so that when energy or information from our system of interest enters the reservoir, it takes a very long time (much longer than any time-scale of interest) for unitary evolution of the reservoir to bring that information back into contact with the system. Our environmental reservoirs are the continuum of electromagnetic modes which interact with the atom and with the cavity, for which the Markov approximation is quite excellent for any reasonable time-scale.

The heart of the master equation is $\mathcal{L}$, the Liouvillian superoperator, which for the Jaynes-Cummings system is

$$\mathcal{L}_{JC}\rho = -i[H_{JC}, \rho] + \kappa\mathcal{D}[a]\rho + \gamma\mathcal{D}[d]\rho \qquad (3.2)$$

where $\mathcal{D}$ is the decay superoperator, which for an environment at zero temperature is defined by $\mathcal{D}[c]\rho = 2c\rho c^\dagger - c^\dagger c\rho - \rho c^\dagger c$ for any operator c. We may approximate the environment as being at zero temperature because the relevant energy scales are ω_a for the atom and ω_c for the cavity. Both are around 352 THz (wavelength of 852 nm), which is far above room temperature, 6.25 THz (this is why at room temperature everything does not glow with black-body radiation at our wavelength). The rate of decay of field from the cavity is κ, and the rate of decay of amplitude in the excited state of the atom is γ.

From the Liouvillian, we can find the steady state density matrix, ρ_{ss}, such that $\mathcal{L}\rho_{ss} = 0$. We define the steady state transmission to be $T = \text{Tr}(\rho_{ss}a^\dagger a)(\kappa/|\varepsilon|)^2$. For a cavity with no atom ($g = 0$), the transmission as a function of probe detuning would be $T = \kappa^2/(\kappa^2 + \Delta_c^2)$.

We will restrict our study of atom-cavity systems to the weak driving limit. In this limit, we assume that the driving of the system is sufficiently weak that the system will not have more than one excitation at a time, i.e., the system is constrained to be in the ground state or one of the lowest lying excited states. Operationally, this means that the state space of the cavity can be restricted to $\{0,1\}$ photons. In the weak driving limit, populations in the excited states are linear in driving intensity and T is independent of ε.

The steady state of the Jaynes-Cummings system can be found analytically in the weak driving limit [20], and the transmission is given by

$$T_{JC} = \left| \frac{\kappa(\gamma + i\Delta_a)}{(\kappa + i\Delta_c)(\gamma + i\Delta_a) + g^2} \right|^2, \tag{3.3}$$

which we plot as a function of probe detuning for various atom-cavity detunings in Fig. 3.1. Notice that each spectrum has two peaks separated in frequency by approximately $2\sqrt{g^2 + (\frac{\omega_a - \omega_c}{2})^2}$. This two-peaked structure is called the vacuum-Rabi splitting [13] because it persists for arbitrarily weak drive strength. The vacuum-Rabi splitting arises from the atom-field interaction term in Eq. (3.1), which determines the eigenvalues of the normal modes corresponding to the lowest lying excitations of the system.

3.2 Multiple Zeeman States

We will now consider a more detailed model of the atom in order to more accurately describe the experiment of Chapter 2. Since the atom used in that experiment was ^{133}Cs, and the cavity and probe were tuned near the $F = 4 \rightarrow F' = 5'$ transition, we will now take the atom to have nine possible ground states $\{|F = 4, m_F =$
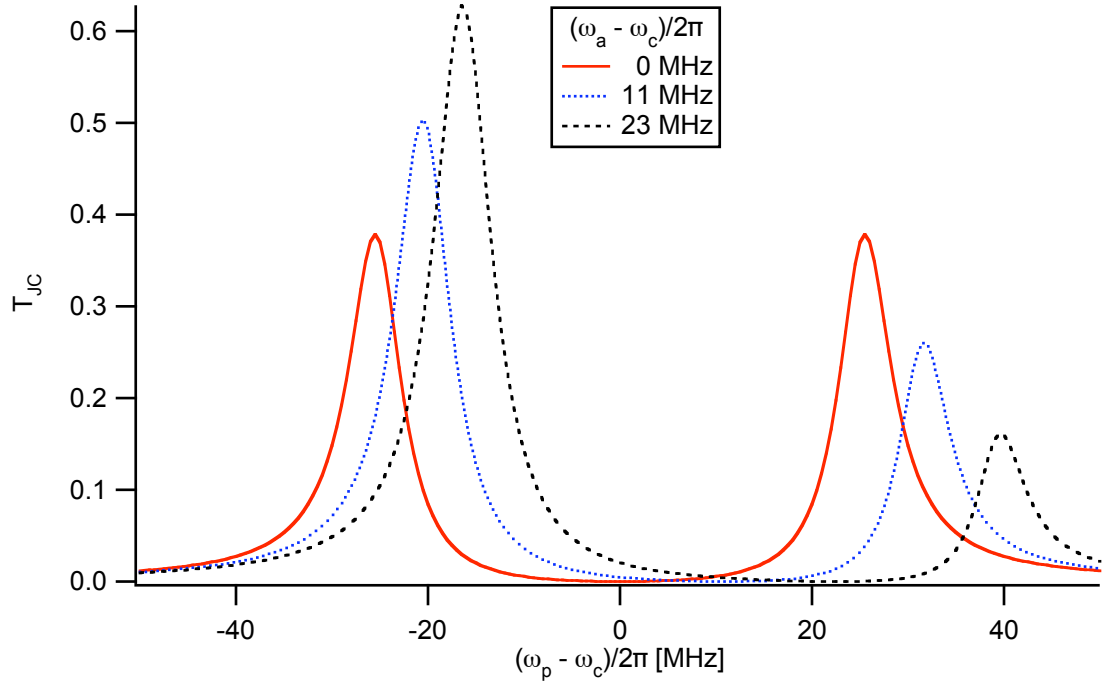
Figure 3.1: The weak field transmission of the Jaynes-Cummings system versus probe detuning. Parameters are $(g, \kappa, \gamma)/2\pi = (25.3, 4.1, 2.6)$ MHz. The atom is detuned from the cavity by 0 MHz (solid red curve), 11 MHz (blue dotted curve), and 23 MHz (black dashed curve).

$-4\rangle \ldots |F = 4, m_F = +4\rangle\}$ and eleven excited states $\{|F' = 5', m_F = -5\rangle \ldots |F' = 5', m_F = +5\rangle\}$. In restricting the space of the atom to these 20 states, we ignore off-resonant excitation to $F' = 4'$ or decay to $F = 3$. In the experiment, a repumping beam tuned to $F = 3 \rightarrow F' = 4'$ was used to prevent accumulation of population in $F = 3$.

We will use the dipole approximation for all atom-field interactions. We define the atomic dipole transition operators for the $F = 4 \rightarrow F' = 5'$ transition as

$$D_q = \sum_{m_F=-4}^{4} |F = 4, m_F\rangle\langle F = 4, m_F|\mu_q|F' = 5', m_F + q\rangle\langle F' = 5', m_F + q| \quad (3.4)$$

where $q = \{-1, 0, 1\}$ and μ_q is the dipole operator for $\{\sigma_-, \pi, \sigma_+\}$-polarization respectively, normalized such that for the cycling transition $\langle F = 4, m_F = 4|\mu_1|F' =$

$5', m_F = 5\rangle = 1.$

In the experiment, the cavity was driven with linearly polarized light. One might model the cavity as a single-mode, linearly polarized resonator which is driven by an external field. The Hamiltonian for this model of the cavity coupled to the $F = 4 \rightarrow F' = 5'$ transition of one atom is

$$H_1 = \Delta_{5'} \sum_{m_F=-5}^{5} |F' = 5', m_F\rangle\langle F' = 5', m_F| + \Delta_c a^\dagger a + g(a^\dagger D_0 + D_0^\dagger a) + \varepsilon a + \varepsilon^* a^\dagger \quad (3.5)$$

where $\Delta_{5'} = \omega_{4\rightarrow 5'} - \omega_p$. Here we have chosen coordinates such that the polarization of the cavity mode is π. The Liouvillian for this system is

$$\mathcal{L}_1 \rho = -i[H_1, \rho] + \kappa \mathcal{D}[a]\rho + \gamma \sum_{q=-1}^{1} \mathcal{D}[D_q]\rho \quad (3.6)$$

The steady state transmission of this system T_1 is plotted in Fig. 3.2.

3.3 Two-Mode Cavity

Modeling the cavity as a single-mode resonator, however, is quite inaccurate. In fact, Fabry-Perot cavities, such as that used in the experiment, support two modes with orthogonal polarizations [34]. The Hamiltonian of a single atom coupled to a cavity with two degenerate orthogonal linear modes is

$$\begin{aligned} H_2 &= \Delta_{5'} \sum_{m_F=-5}^{5} |F' = 5', m_F\rangle\langle F' = 5', m_F| + \Delta_c(a^\dagger a + b^\dagger b) \\ &\quad + g(a^\dagger D_0 + D_0^\dagger a) + g(b^\dagger D_y + D_y^\dagger b) + \varepsilon a + \varepsilon^* a^\dagger \end{aligned} \quad (3.7)$$

where $D_y = \frac{i}{\sqrt{2}}(D_{-1} + D_{+1})$ is the dipole operator for linear polarization along the $\hat{y}$-axis. We are using coordinates where the cavity supports $\hat{y}$ and $\hat{z}$ polarizations and $\hat{x}$ is along the cavity axis, and the linearly polarized cavity driving field is along $\hat{z}$. The annihilation operator for the $\hat{z}$ ($\hat{y}$) polarized cavity mode is a (b). The Liouvillian
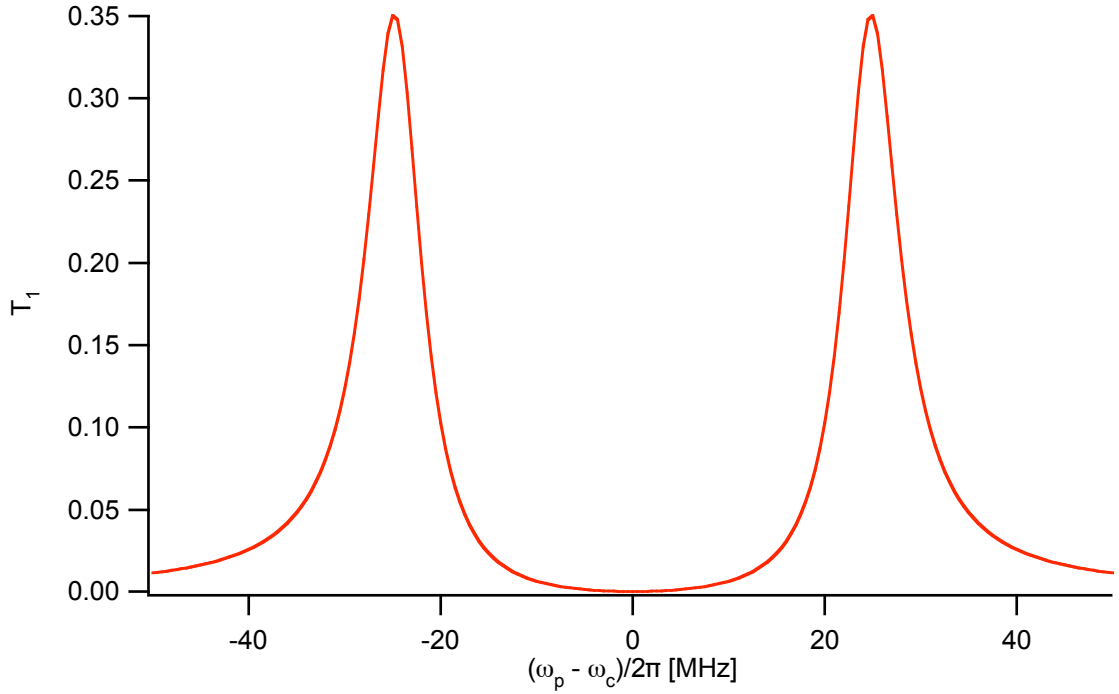
Figure 3.2: The weak field transmission of a single-mode, linearly polarized cavity coupled to a $F = 4 \to F' = 5'$ transition of one atom versus probe detuning. Parameters are $(g, \kappa, \gamma)/2\pi = (33.9, 4.1, 2.6)$ MHz and $\omega_{4\to5'} = \omega_c$. Note that the largest dipole matrix element coupling the atom to the cavity is $\langle F = 4, m_F = 0|\mu_0|F' = 5', m'_F = 0\rangle \approx 0.75$ giving a maximum effective coupling of ≈ 25.3 MHz.

for this system is

$$\mathcal{L}_2\rho = -i[H_2, \rho] + \kappa\mathcal{D}[a]\rho + \kappa\mathcal{D}[b]\rho + \gamma \sum_{q=-1}^{1} \mathcal{D}[D_q]\rho \qquad (3.8)$$

The steady state transmission of a strongly coupled two-mode cavity T_2 is plotted in Fig. 3.3.

The Stark shifts of the atom [4] and the birefringence of the cavity [10] modify the Hamiltonian as follows:

$$
\begin{aligned}
H_{full} &= \sum_{m'_F=-5}^{5} \Delta_{m'_F}|F' = 5', m'_F\rangle\langle F' = 5', m'_F| + \Delta_{c_z} a^\dagger a + \Delta_{c_y} b^\dagger b \\
&\quad + g(a^\dagger D_0 + D_0^\dagger a) + g(b^\dagger D_y + D_y^\dagger b) + \varepsilon a + \varepsilon^* a^\dagger
\end{aligned}
\qquad (3.9)
$$
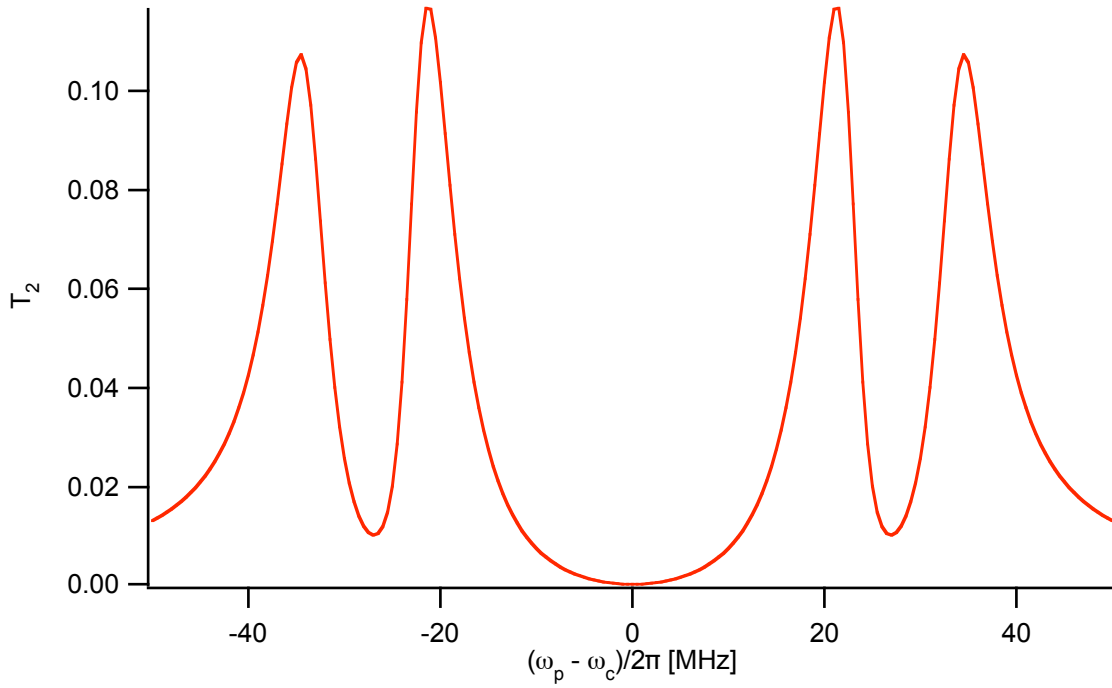
Figure 3.3: The weak field transmission of a two-mode cavity driven by linearly polarized light and coupled to a $F = 4 \rightarrow F' = 5'$ transition of one atom versus probe detuning. Parameters are $(g, \kappa, \gamma)/2\pi = (33.9, 4.1, 2.6)$ MHz and $\omega_{4 \rightarrow 5'} = \omega_c$.

where the birefringent splitting is $\Delta_B = \Delta_{c_z} - \Delta_{c_y}$. The detuning of the $\hat{z}$ ($\hat{y}$) polarized mode from the probe is Δ_{c_z} (Δ_{c_y}). The atomic excited state detunings are given by $\Delta_{m'_F} = \Delta_a + U\beta_{m'_F}$, where Δ_a is the atom-probe detuning of the $F = 4 \rightarrow F' = 5'$ transition in free space, U is the FORT potential, and $\beta_{m'_F}$ for the FORT wavelength of the experiment is given by $\{m'_F, \beta_{m'_F}\} = \{\pm5, 0.18\}, \{\pm4, 0.06\}, \{\pm3, -0.03\}, \{\pm2, -0.10\}, \{\pm1, -0.14\}, \{0, -0.15\}$ [4]. The resulting steady state transmission T_{full} is displayed in Fig. 3.4.
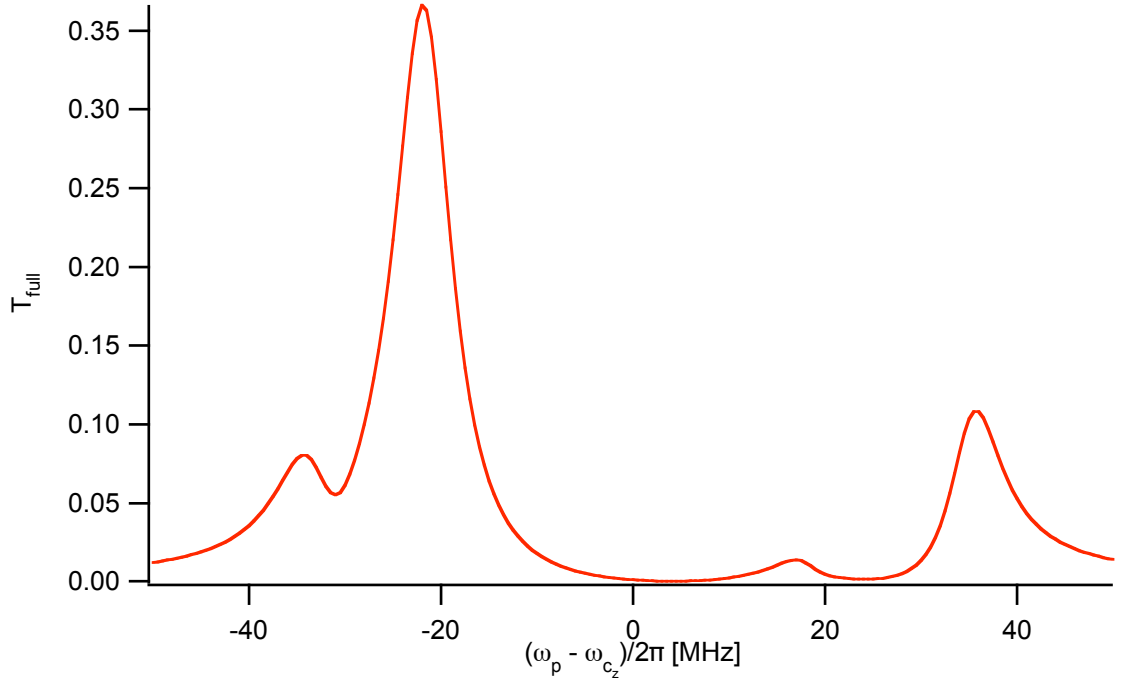
Figure 3.4: The weak field transmission of a birefringent two-mode cavity driven by linearly polarized light and coupled to a $F = 4 \rightarrow F' = 5'$ transition of one atom with Stark shifts versus probe detuning. Parameters are $(g, \kappa, \gamma, \Delta_B, U)/2\pi = (33.9, 4.1, 2.6, 4.4, 38.5)$ MHz and $\omega_{4\rightarrow5'} = \omega_{c_z}$.

3.4 Atomic Position

The parameters g and U depend on the position of the atom within the spatial modes of the cavity. The dependence on the atomic position $\vec{r}$ is

$$U(\vec{r}) = U_0 \sin^2(2\pi x/\lambda_{FORT}) \exp(-2\xi^2/w_{FORT}^2) \tag{3.10}$$

$$g(\vec{r}) = g_0 \cos(2\pi x/\lambda_c) \exp(-\xi^2/w_c^2) \tag{3.11}$$

where $\xi = \sqrt{y^2 + z^2}$ is the radial coordinate, λ_{FORT} (λ_c) is the wavelength of the TEM$_{00}$ mode for the FORT (CQED), and w_{FORT} (w_c) is the beam waist of the mode for the FORT (CQED). We neglect the dependence of w_{FORT} and w_c on x because the cavity is very close to planar, and hence the variation in the waist from the center of the mode to the mirror face is small. The origin of the coordinate system is at
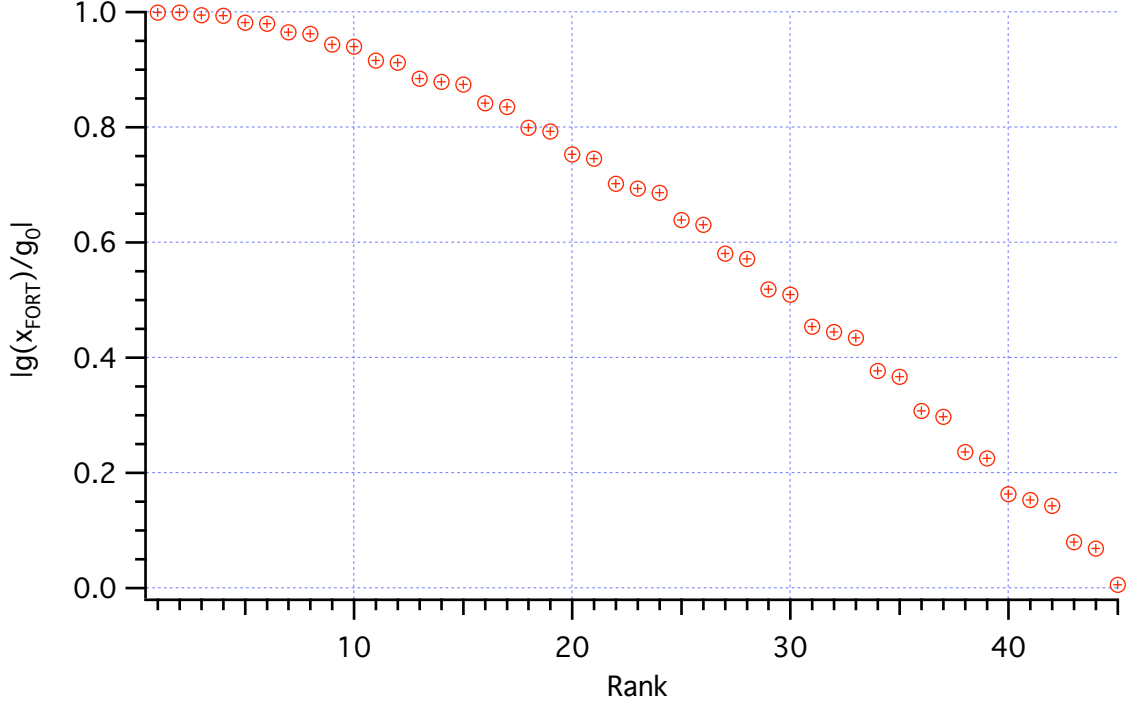
Figure 3.5: The relative strength of the CQED coupling at the different FORT maxima $|g(\vec{r}_{FORT})/g_0|$ are plotted. The values have been rank ordered so that larger strengths are to the left in the plot. Since the cavity is symmetric, only those maxima with $x > 0$ ($n \in \{0, \ldots 44\}$) are considered. Wavelengths are $\lambda_c = 852.358, \lambda_{FORT} = 935.586$.

the center of the cavity, so the mirror faces are at $x = L/2$ and $x = -L/2$, where L is the length of the cavity. Note that $U(\vec{r})$ is proportional to the FORT intensity, whereas $g(\vec{r})$ is proportional the cavity field. $U(x)$ ($g(x)$) varies as sin (cos) because the FORT (CQED) mode supports an even (odd) number of half-wavelengths in the cavity (see Appendix A).

The atoms are trapped near the regions of maximum FORT intensity, namely the points $\vec{r}_{FORT}$ where $U(\vec{r}_{FORT}) = U_0$. These points have $\xi_{FORT} = 0$ and $x_{FORT} = (n + 1/2)\lambda_{FORT}/2$. Since the FORT mode has 90 antinodes within the cavity, $n \in \{-45, \ldots 44\}$. At each of these FORT maxima we can find $g(\vec{r}_{FORT}) = g_0 \cos(\pi(n + 1/2)\lambda_{FORT}/\lambda_c)$. Because of the symmetry of the cavity structure about the center, the well (n) is the same as the well ($-n - 1$). The relative strength of coupling at these FORT maxima are displayed in Fig. 3.5.

In our model, the probability distribution of atomic position for an atom trapped in a particular FORT well is a Gaussian centered at $\vec{r}_{FORT}$. This corresponds to a thermal distribution in a harmonic potential. Note that the experimental system is far more complicated: the potential is not harmonic, we expect heating and cooling rates that are strongly dependent on position in the CQED and FORT modes (and probe detuning), and our system is likely far from thermal equilibrium. Still, given the success of the model, it is instructive to find the correspondence between Gaussian width and "temperature."

For the thermal distribution of a one-dimensional harmonic oscillator with spring constant k_s, the equipartition theorem says $\frac{1}{2}k_s\bar{s^2} = \frac{1}{2}k_B\mathfrak{T}$, where $\bar{s^2}$ is the expectation over the ensemble of the square of the distance from the potential minimum, k_B is Boltzmann's constant, and $\mathfrak{T}$ is the temperature. Hence, the standard deviation σ of the Gaussian distribution ($\sigma = \sqrt{\bar{s^2}}$) is found to be $\sigma = \sqrt{k_B\mathfrak{T}/k_s}$.

Near $\vec{r}_{FORT}$, we can Taylor expand Eq. 3.10 to find the effective spring constant for small oscillations in each dimension. We find $k_x = \frac{d^2U}{dx^2} = -8\pi^2\frac{U_0}{\lambda_{FORT}^2}$, $k_y = k_z = -4\frac{U_0}{w_{FORT}^2}$. This gives a probability distribution function for one well,

$$P(x,\xi) = \frac{\exp\left(\frac{-(x-x_{FORT})^2}{2\sigma_x^2}\right)}{\sqrt{2\pi}\sigma_x}\frac{\exp\left(\frac{-\xi^2}{2\sigma_\xi^2}\right)}{2\pi\sigma_\xi^2} \tag{3.12}$$

where $\sigma_x = \sqrt{k_B\mathfrak{T}/k_x}$ and $\sigma_\xi = \sqrt{k_B\mathfrak{T}/k_y}$. Here we are assuming the same "temperature" for the axial and radial dimension. In general they could be quite different because the system is not in equilibrium and there is a large separation of time scales for motion in each dimension.

We can compute the ensemble average of transmission for an atom trapped in one well,

$$\bar{T} = \int_{x=x_{FORT}-\lambda_{FORT}/4}^{x=x_{FORT}+\lambda_{FORT}/4} \int_{\xi=0}^{\xi=\infty} T(g(\vec{r}), U(\vec{r}))P(x,\xi)2\pi\xi d\xi dx. \tag{3.13}$$

To account for multiple wells, we can perform averages of these $\bar{T}$ for different wells. Note that $T(g) = T(-g)$, so that it is only the magnitude of g which matters. In our model, we average over a varying number of wells, starting with the highest value of

$|g(\vec{r}_{FORT})|$ and proceeding down to some cutoff value. This average implies that the atom is never in the poorly coupled wells, and it has equal probability to be in any of the allowed wells. One could construct a more sophisticated model which would assign probabilities to each well, resulting in a weighted average. However, since we do not quantitatively understand the dynamics that lead to well-selectivity, we chose to use the simplest model which gives reasonable agreement with the experimental data.

3.5 Applicability of Weak Driving and Steady-State Approximations

In the previous sections of this chapter, we have calculated transmission spectra of atom-cavity systems making two major assumptions: that the probe is sufficiently weak such that the transmitted intensity is proportional to the driving intensity; and that the system has reached a steady state consistent with the probe field, including all optical pumping effects. In this section, we will examine the relevance of these assumptions in describing the experiment of Chapter 2.

In the experiment, the drive strength was such that in the absence of an atom, the intracavity photon number was $N_{no\ atom} = (|\varepsilon|/\kappa)^2 = 0.141$. As discussed further in Chapters 4 and 5, the strong coupling condition $g > (\kappa, \gamma)$ makes the system highly non-linear at the level of one photon. How significant, then, are deviations in the transmission spectrum from the weak field limit at this drive strength?

Consider Fig. 3.6 which contrasts the weak field with a calculation for $N_{no\ atom} = 0.141$. It should be noted that due to limited computational power, these calculations were performed with a basis of $\{0, 1\}$ photons in each cavity mode. Corrections due to higher photon numbers may be significant. However, as described in Chapters 4 and 5, we expect that higher photon numbers at the transmission peaks will be suppressed, so that the most notable qualitative effect of finite drive strength – a reduction in the height of the tallest peak – should persist. This effect may account
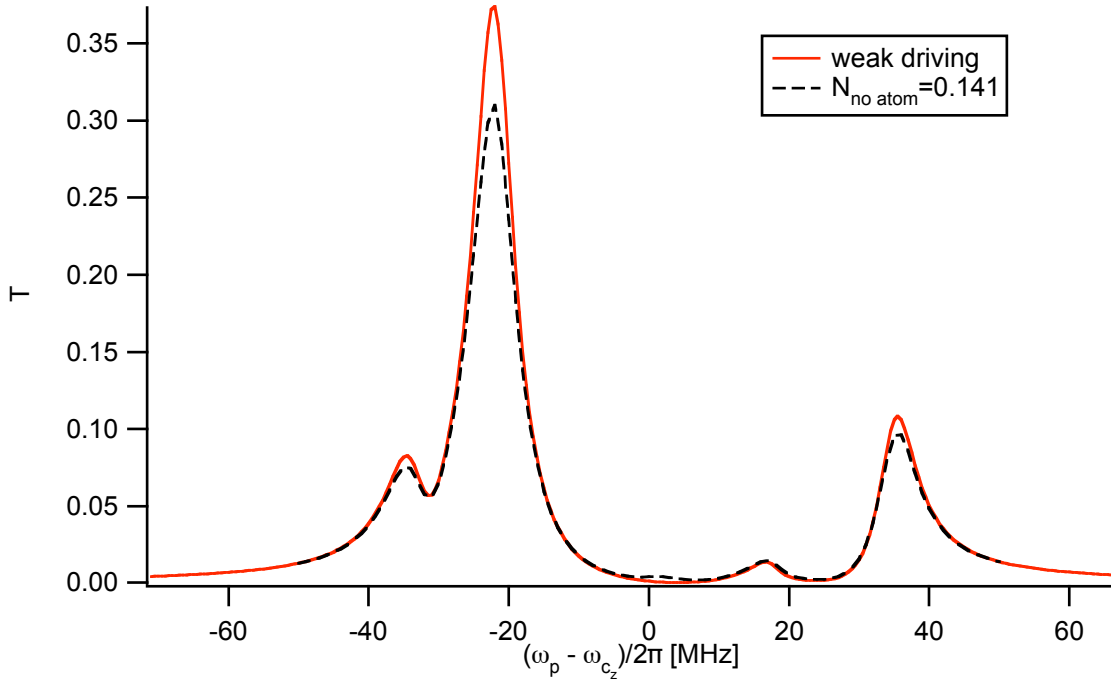
Figure 3.6: The transmission spectrum of Fig. 3.4 (red) and the calculated spectrum with drive strength to match the experimental condition, $N_{no\ atom} = 0.141$ (black, dashed). Both calculations were performed on a basis of $\{0, 1\}$ photons in each cavity mode.

for the discrepancy between theory and experiment in the size of the large peak as shown in Fig. 2.3.

In Fig. 3.7, we explore the effect of finite probe duration. We display the instantaneous transmission (ratio of transmitted to incident photon flux, normalized to an empty cavity) after various probe durations. The system is assumed to start with the atom in an equal mixture of all ground states and the cavity field in the vacuum state. At each detuning, we evolve this density matrix under the Liouvillian for a time t and calculate $T = \mathrm{Tr}(\rho(t)a^\dagger a)(\kappa/|\varepsilon|)^2$. The optical pumping rates are dependent on the probe detuning, but are generally short compared to the experimental probe duration of 100μs. We expect, therefore, that corrections due to the finite probe duration are modest. They could, however, explain in part the discrepancy of theory and experiment around $\omega_p \simeq 0$ in Fig. 2.3.
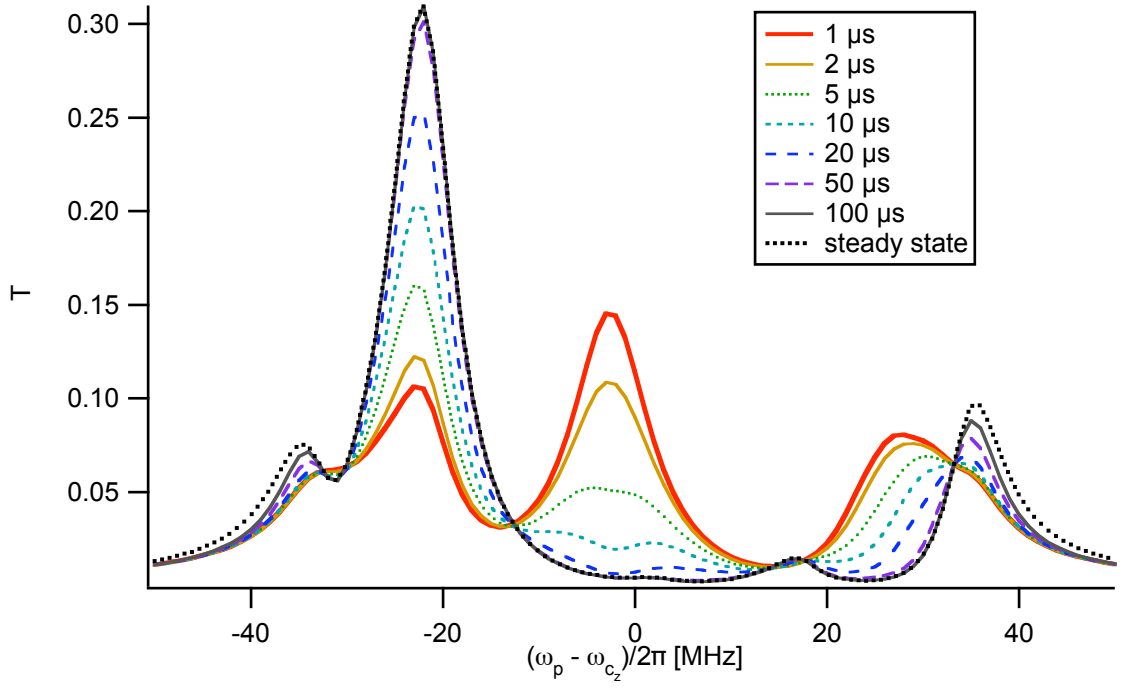
Figure 3.7: The transmission spectrum at various times. Parameters are the same as in Figs. 3.4 and 3.6, with $N_{no\ atom} = 0.141$. All traces were computed with a basis of $\{0, 1\}$ photons in each cavity mode.

Chapter 4

Photon Blockade in an Optical Cavity with One Trapped Atom

This chapter is adapted from Ref. [35].

Observations of photon blockade are reported for the light transmitted by an optical cavity containing one trapped atom. Excitation of the atom-cavity system by a first photon "blocks" the transmission of a second photon, thereby converting an incident Poissonian stream of photons into a sub-Poissonian, antibunched stream, as confirmed by measurements of the photon statistics of the transmitted field. The intensity correlations of the cavity transmission also reveal the energy distribution for oscillatory motion of the trapped atom via the anharmonic trapping potential.

4.1 Background

Sufficiently small metallic [36] and semiconductor [37] devices at low temperatures exhibit "Coulomb blockade," whereby charge transport through the device occurs on an electron-by-electron basis. For example, a single electron on a metallic island of capacitance C can block the flow of another electron if the charging energy $e^2/2C \gg k_B T$ and the tunneling resistance $R \gg h/4e^2$. In 1997, Imamoḡlu *et al.* proposed that an analogous effect might be possible for photon transport through an optical system by employing photon-photon interactions in a nonlinear optical cavity [38]. In this scheme, strong dispersive interactions enabled by electromagnetically induced transparency (EIT) cause the presence of a "first" photon within the cavity to block

the transmission of a "second" photon, leading to an ordered flow of photons in the transmitted field.

After resolution of an initial difficulty [39], subsequent work has confirmed that such photon blockade is indeed feasible for a single intracavity atom by way of a multi-state EIT scheme [40, 41, 42]. Photon blockade is possible in other settings, including in concert with Coulomb blockade [43] and via tunneling with localized surface plasmons [44]. Photon blockade has also been predicted for a two-state atom coupled to a cavity mode [45, 46, 8]. As illustrated in Fig. 4.1(a), the underlying mechanism is the anharmonicity of the Jaynes-Cummings ladder of eigenstates [2, 47]. Resonant absorption of a photon of frequency ω_- to reach the state $|1, -\rangle$ (where $|n, +(-)\rangle$ denotes the higher (lower) energy eigenstate with n excitations) "blocks" the absorption of a second photon at ω_- because transitions to $|2, \pm\rangle$ are detuned from resonance.

Scattering from a single atom in free space also provides a fundamental example of photon blockade [48], albeit with the fluorescent field distributed over 4π and the flux limited by the rate of spontaneous decay γ. By contrast, cavity-based schemes offer the possibility for photon emission into a collimated spatial mode with high efficiency and at a rate set by the cavity decay rate κ, which can be much larger than γ. Achieving photon blockade for a single atom in a cavity requires operating in the regime of strong coupling, for which the frequency scale g_0 associated with reversible evolution of the atom-cavity system exceeds the dissipative rates (γ, κ) [12].

4.2   Overview

In this chapter, we report observations of photon blockade in the light transmitted by an optical cavity containing one atom strongly coupled to the cavity field. For coherent excitation at the cavity input, the photon statistics for the cavity output are investigated by measurement of the intensity correlation function $g^{(2)}(\tau)$, which demonstrates the manifestly nonclassical character of the transmitted field. Explicitly, we find $g^{(2)}(0) = (0.13 \pm 0.11) < 1$ with $g^{(2)}(0) < g^{(2)}(\tau)$, so that the output light
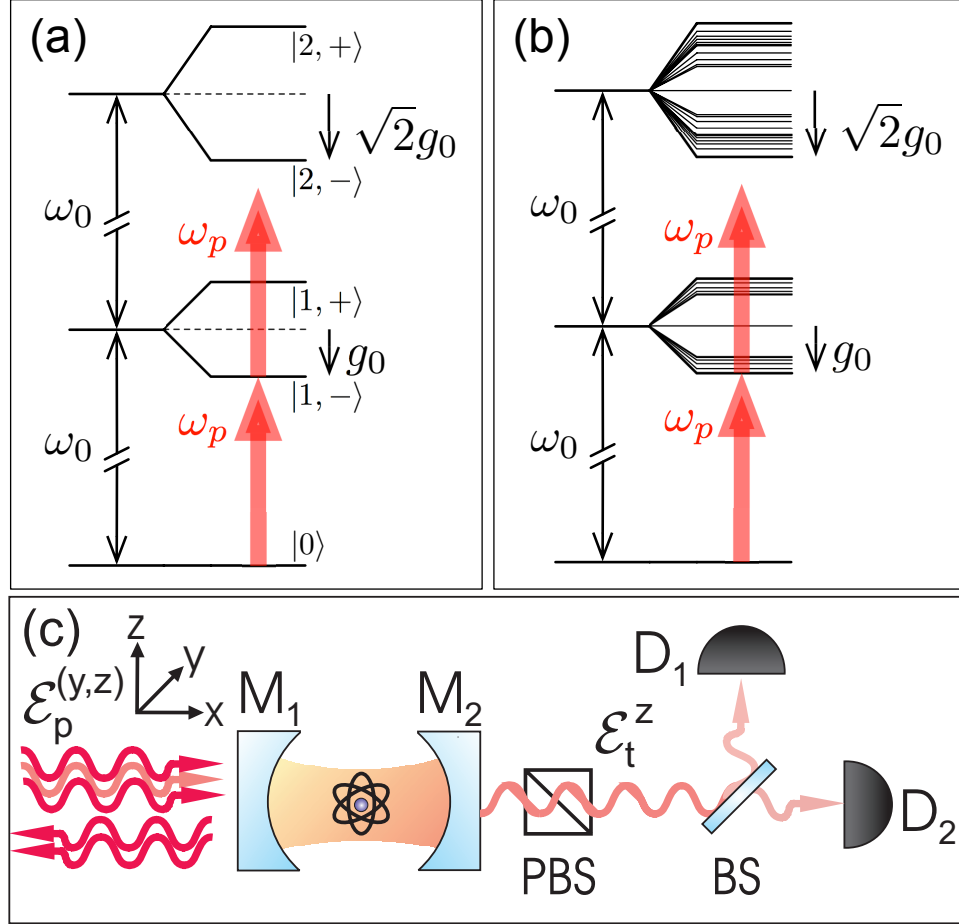
Figure 4.1: (a) Level diagram showing the lowest energy states for a two-state atom of transition frequency ω_A coupled (with single-photon Rabi frequency g_0) to a mode of the electromagnetic field of frequency ω_C, with $\omega_A = \omega_C \equiv \omega_0$ [2]. Two-photon absorption is suppressed for a probe field ω_p (arrows) tuned to excite the transition $|0\rangle \rightarrow |1, -\rangle$, $\omega_p = \omega_0 - g_0$, leading to $g^{(2)}(0) < 1$ [8]. (b) Eigenvalue structure for the $(F = 4, m_F) \leftrightarrow (F' = 5', m'_F)$ transition coupled to two degenerate cavity modes $l_{y,z}$. Two-photon absorption is likewise blocked for excitation tuned to the lowest eigenstate (arrows). (c) Simple schematic of the experiment.

is both sub-Poissonian and antibunched [49]. We find that $g^{(2)}(\tau)$ rises to unity at a time $\tau = \tau_B \simeq 45$ns, which is consistent with the lifetime $\tau_- = 2/(\gamma + \kappa) = 48$ ns for the state $|1, -\rangle$ associated with the blockade. Over longer time scales, cavity transmission exhibits modulation arising from the oscillatory motion of the atom trapped within the cavity mode. We utilize this modulation to make an estimate of the energy distribution for the atomic center-of-mass motion and infer a maximum

energy $E/k_B \sim 250$ μK.

The schematic of our experiment in Fig. 4.1(c) illustrates the Fabry-Perot cavity formed by mirrors (M_1, M_2) into which single optically cooled Cesium atoms are loaded. The physical length of the cavity is 42.2 μm and the finesse is 4.3×10^5. The cavity length is independently stabilized such that a TEM_{00} longitudinal mode at λ_{C_1} is resonant with the free-space atomic transition at λ_A and another TEM_{00} mode at λ_{C_2} is resonant at λ_F. At the cavity center $x = 0$, the mode waists $w_{C_{1,2}} = \{23.4, 24.5\}$ μm at $\lambda_{C_{1,2}} = \{852.4, 935.6\}$ nm. Atoms are trapped within the cavity by a far-off-resonance trap (FORT) which is created by exciting a TEM_{00} cavity mode at $\lambda_F = 935.6$ nm [4]. To achieve strong coupling, we utilize the $6S_{1/2}, F = 4 \rightarrow 6P_{3/2}, F' = 5'$ transition of the $D2$ line in Cs at $\lambda_A = 852.4$ nm, for which the maximum rate of coherent coupling is $g_0/2\pi = 34$ MHz for $(F = 4, m_F = \pm 4) \rightarrow (F' = 5', m'_F = \pm 5)$. The transverse decay rate for the $6P_{3/2}$ atomic states is $\gamma/2\pi = 2.6$ MHz while the cavity field decays at rate $\kappa/2\pi = 4.1$ MHz.

A variety of factors make our atom-cavity system more complex than the simple situation described by the Jaynes-Cummings eigenstates, including most significantly that (1) the cavity supports two modes $l_{y,z}$ with orthogonal linear polarizations $(\hat{y}, \hat{z})$ near $\lambda_A = 852.4$ nm and (2) a multiplicity of Zeeman states are individually coupled to these modes for transitions between the manifolds $(F = 4, m_F) \leftrightarrow (F' = 5', m'_F)$. An indication of the potential for this system to achieve photon blockade is provided in Fig. 4.1(b), which displays the actual eigenvalue structure for the first two excited manifolds obtained by direct diagonalization of the interaction Hamiltonian. As for the basic two-state system, excitation to the lowest energy state in the one-excitation manifold "blocks" subsequent excitation because the transitions to the two-excitation manifold are out of resonance.

4.3 Theoretical Prediction

To substantiate this picture quantitatively, we present in Fig. 4.2 theoretical results from the steady-state solution to the master equation in various situations, all for

the case of coincident atomic and cavity resonances $\omega_A = \omega_{C_1} \equiv \omega_0$. Beginning with the ideal setting of a two-state atom coupled to a single cavity mode, we display in Fig. 4.2(a) results for the probe transmission spectrum $T(\omega_p)$ and the intensity correlation function $g^{(2)}(0)$ of the field $\mathcal{E}_t$ transmitted by mirror M_2 for excitation by a coherent-state probe $\mathcal{E}_p$ of variable frequency ω_p incident upon the cavity mirror M_1. $T(\omega_p)$ is proportional to the ratio of photon flux $\langle \mathcal{E}_t^\dagger \mathcal{E}_t \rangle$ transmitted by M_2 to the flux $|\mathcal{E}_p|^2$ incident upon M_1, and normalized such that a cavity without an atom has a resonant transmission of unity, i.e., $T(\omega_p = \omega_{C_1}) = 1$. For a field with intensity operator $\hat{I}(t)$, $g^{(2)}(\tau) \equiv \langle : \hat{I}(t)\hat{I}(t + \tau) : \rangle / \langle : \hat{I}(t) : \rangle \langle : \hat{I}(t + \tau) : \rangle$, where the colons denote time and normal ordering [49].

Clearly evident in $T(\omega_p)$ are two peaks at $\omega_p = \omega_\pm \equiv \omega_0 \pm g_0$ associated with the vacuum-Rabi splitting for the states $|1, \pm\rangle$. At these peaks, $\mathcal{E}_p$ is detuned for excitation $|1, \pm\rangle \to |2, \pm\rangle$, resulting in $g^{(2)}(0) < 1$ for $\mathcal{E}_t$. The Poissonian photon statistics of the incident probe are thereby converted to sub-Poissonian statistics for the transmitted field by way of the photon blockade effect illustrated in Fig. 4.1(a). For strong coupling in the weak-field limit, $g^{(2)}(0) \propto (\kappa + \gamma)^2 / g_0^2$ for $\omega_p = \omega_\pm$ [46], hence the premium on achieving $g_0 \gg (\kappa, \gamma)$. By contrast, for $\omega_p = \omega_0 \pm g_0/\sqrt{2}$, $\mathcal{E}_p$ is resonant with the two-photon transition $|0\rangle \to |2, \pm\rangle$, resulting in super-Poissonian statistics with $g^{(2)}(0) \gg 1$. For $\omega_p = \omega_0$, there is extremely large bunching due to quantum interference between $\mathcal{E}_p$ and the atomic polarization [46, 50].

In Fig. 4.2(b), we examine the more complex situation relevant to our actual experiment, namely a multi-state atom coupled to two cavity modes with orthogonal polarizations $\hat{y}, \hat{z}$. Most directly related to the simple case of Fig. 4.2(a) is to excite one polarization eigenmode with the incident probe, taken here to be $\mathcal{E}_p^z$, and to detect the transmitted field $\mathcal{E}_t^z$ for this same polarization, with the transmission spectrum and intensity correlation function denoted by $T_{zz}(\omega_p)$, $g_{zz}^{(2)}(0)$, respectively. Even for the full multiplicity of states for the $F = 4 \to F' = 5'$ transition coupled to the two cavity modes $l_{y,z}$, $T_{zz}(\omega_p)$ displays a rather simple structure, now with a multiplet structure in place of the single vacuum-Rabi peak around $\omega_p \simeq \omega_0 \pm g_0$. For a probe frequency tuned to the eigenvalues $\omega_p = \omega_0 \pm g_0$, $g_{zz}^{(2)}(0) \simeq 0.7$, once again dropping
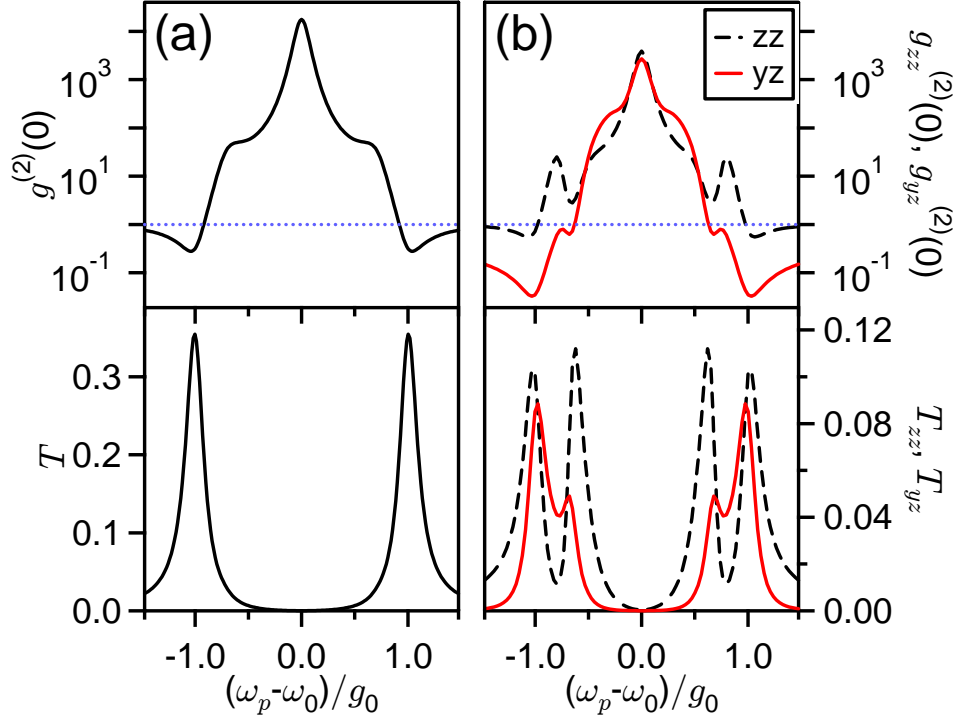
Figure 4.2: Theoretical results for the transmission spectrum and intensity correlation functions: (a) $T(\omega_p)$, $g^{(2)}(0)$; (b) $T_{zz}(\omega_p)$, $g_{zz}^{(2)}(0)$ (dashed) and $T_{yz}(\omega_p)$, $g_{yz}^{(2)}(0)$ (red) from the steady-state solution to the master equation. Included are all transitions $(F = 4, m_F) \leftrightarrow (F' = 5', m_F')$ with their respective coupling coefficients $g_0^{(m_F, m_F')}$, as well as the two cavity modes $l_{y,z}$ here assumed to be degenerate in frequency. The blue dotted lines indicate Poissonian statistics. Parameters are $(g_0, \kappa, \gamma)/2\pi = (33.9, 4.1, 2.6)$ MHz, and the probe strength is such that the intracavity photon number on resonance without an atom is 0.05.

below unity as in Fig. 4.2(a).

An alternate scheme is to detect along $\hat{z}$, but excite along orthogonal polarization $\hat{y}$, with the respective transmission and correlation functions $T_{yz}(\omega_p)$, $g_{yz}^{(2)}(0)$ also shown in Fig. 4.2(b). Similar to $T_{zz}(\omega_p)$, $T_{yz}(\omega_p)$ exhibits a multiplet structure in the vicinity of $\omega_p \simeq \omega_0 \pm g_0$ due to the nature of the first excited states of the atom-cavity system. At the extremal $\omega_p = \omega_0 \pm g_0$, $g_{yz}^{(2)}(0)$ reaches a value $g_{yz}^{(2)}(0) \simeq 0.03$ much smaller than for either $g^{(2)}(0)$ in (a) or $g_{zz}^{(2)}(0)$ in (b) for the same values of (g_0, κ, γ). Our preliminary hypothesis is that this reduction relates to the absence of the superposed driving field $\mathcal{E}_p^y$ for the transmitted field $\mathcal{E}_t^z$ with orthogonal polarization $\hat{z}$

[51]; photons in the mode l_z derive only from emissions associated with the atomic components of atom-field eigenstates.

Tuning the probe to $\omega_p = \omega_0 \pm g_0$ has the additional benefit of reducing sensitivity to atomic position, which varies experimentally due to atomic motion and the multiplicity of trapping sites within the cavity [11]. The atomic position affects the transmission via the position dependence of the coupling $g = g_0 \psi(\vec{r})$, where ψ is the TEM_{00} spatial mode at λ_{C_1} with maximum $|\psi| = 1$ and $\vec{r}$ is the position of the atom. Since $T_{yz}(\omega_p)$ is small when $|\omega_p - \omega_0| \gtrsim g$, atoms which have a lower than expected value of g will have a reduced contribution to the photon statistics.

An important step in the implementation of this strategy is our recent measurement of the vacuum-Rabi spectrum $T_{zz}(\omega_p)$ for one trapped atom (see Chapter 2). In that work, we obtained quantitative agreement on an atom-by-atom basis between our observations and an extension of the theoretical model employed to generate the various plots in Fig. 4.2(b). The extended model incorporates ac-Stark shifts from the FORT as well as cavity birefringence.

The TEM_{00} longitudinal mode for the FORT is driven by a linearly polarized input field $\mathcal{E}_{FORT}$, resulting in nearly equal ac-Stark shifts for Zeeman states in the $6S_{1/2}, F = 3, 4$ manifold. At an antinode of the field, the peak value of the trapping potential for these states is $U_0/h = -43$ MHz for all our measurements. Zeeman states of the $6P_{3/2}, F' = 5'$ manifold experience a similar trapping potential, but with a weak dependence on m'_F [4]. Stress-induced birefringence in the cavity mirrors leads to a mode splitting $\Delta\omega_{C_1}/2\pi = 4.4 \pm 0.2$ MHz of the two cavity modes $l_{y,z}$ with orthogonal linear polarizations $(\hat{y},\hat{z})$. $\mathcal{E}_{FORT}$ is linearly polarized and aligned along $\hat{z}$, the higher frequency mode.

The extended model predicts that corrections to $g_{yz}^{(2)}(0)$ due to these effects are small for our parameters (see Section 5.3).

4.4 Experimental Results

With these capabilities in hand, we now report measurements of $g_{yz}^{(2)}(\tau)$ for the light transmitted by a cavity containing a single trapped atom. We tune the probe $\mathcal{E}_p^y$ to $(\omega_p - \omega_0)/2\pi = -34$ MHz, near $-g_0$, and acquire photoelectric counting statistics of the field $\mathcal{E}_t^z$ by way of two avalanche photodiodes (D_1, D_2), as illustrated in Fig. 4.1(c). From the record of these counts, we are able to determine $g_{yz}^{(2)}(\tau)$ by way of the procedures discussed in Ref. [52]. The efficiency for photon escape from the cavity is $\alpha_{e2} = 0.6 \pm 0.1$. The propagation efficiency from M_2 to detectors (D_1, D_2) is $\alpha_P = 0.41 \pm .03$, with then each detector receiving half of the photons. The avalanche photodiodes (D_1, D_2) have quantum efficiencies $\alpha_P = 0.49 \pm 0.05$.

Data are acquired for each trapped atom by cycling through probing, testing, and cooling intervals (of durations $\Delta t_{probe} = 500$ μs, $\Delta t_{test} = 100$ μs and $\Delta t_{cool} = 1.4$ ms, respectively) using a procedure similar to that of Ref. [11]. All probing/cooling cycles end after an interval $\Delta t_{tot} = 0.3$ s, at which point a new loading cycle is initiated. The test beam is polarized along $\hat{z}$ and resonant with the cavity. We select for the presence of an atom by requiring that $T_{zz}(\omega_p \simeq \omega_{C_1}) \lesssim 0.35$ for the test beam. We employ only those data records associated with probing intervals after which the presence of an atom was detected. The intracavity photon number in mode l_y due to the probe field $\mathcal{E}_p^y$ on resonance, in the absence of an atom, is 0.21, and the polarizing beam splitter at the output of the cavity (PBS in Fig. 4.1(c)) suppresses detection of this resonant light by a factor of ~ 94. A repumping beam transverse to the cavity axis and resonant with $6S_{1/2}, F = 3 \rightarrow 6P_{3/2}, F' = 4'$ also illuminates the atom during the probe and test intervals. This beam prevents accumulation of population in the $F = 3$ ground state caused by the probe off-resonantly exciting the $F = 4 \rightarrow F' = 4'$ transition.

Fig. 4.3 presents an example of $g_{yz}^{(2)}(\tau)$ determined from the recorded time-resolved coincidences at (D_1, D_2). In Fig. 4.3(a), the manifestly nonclassical character of the transmitted field is clearly observed with a large reduction in $g_{yz}^{(2)}(0)$ below unity, $g_{yz}^{(2)}(0) = (0.13 \pm 0.11) < 1$, corresponding to the sub-Poissonian character of the
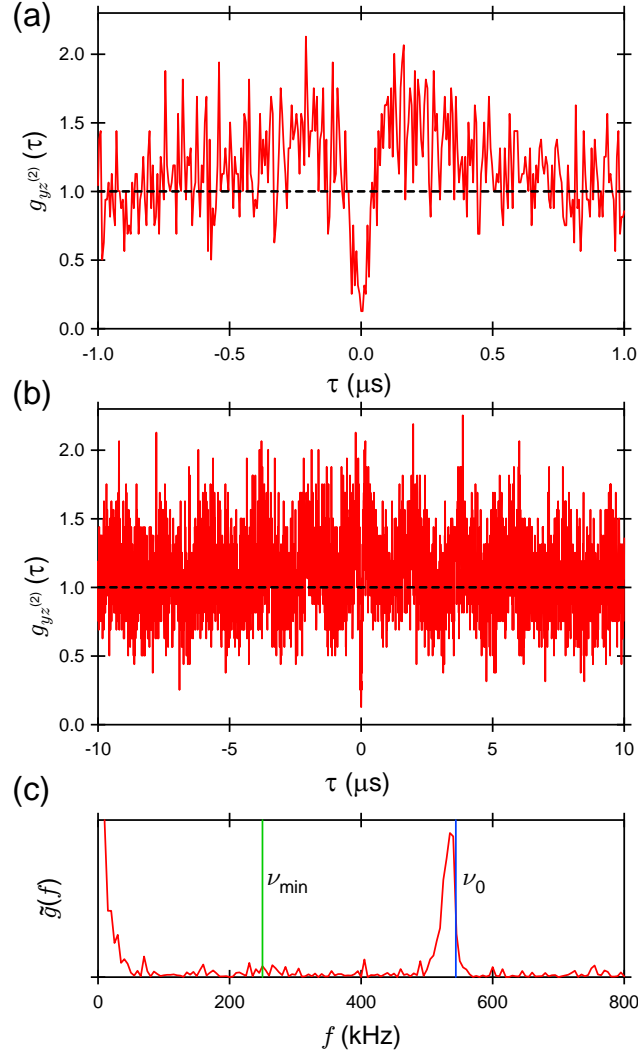
Figure 4.3: Intensity correlation function $g_{yz}^{(2)}(\tau)$ for incident excitation with polarization along $\hat{y}$ and detection with orthogonal polarization $\hat{z}$. (a) $g_{yz}^{(2)}(\tau)$ over the interval $|\tau| \leq 1.0$ μs demonstrates that the transmitted field exhibits both sub-Poissonian photon statistics $g_{yz}^{(2)}(0) = (0.13 \pm 0.11) < 1$ and photon antibunching $g_{yz}^{(2)}(0) < g_{yz}^{(2)}(\tau)$ [49]. (b) $g_{yz}^{(2)}(\tau)$ over longer intervals $|\tau| \leq 10$ μs displays a pronounced modulation due to axial motion of the trapped atom. (c) The Fourier transform $\tilde{g}(f)$ of $g_{yz}^{(2)}(\tau)$ with the independently determined minimum and maximum frequencies ν_{min} and ν_0 for axial motion in a FORT well indicated by the dotted lines.

transmitted field, and with $g_{yz}^{(2)}(0) < g_{yz}^{(2)}(\tau)$ as a manifestation of photon antibunching. $g_{yz}^{(2)}(\tau)$ displayed in Fig. 4.3, shown with a 6 ns resolution, has been corrected for background counts due to detector dark counts and scattered light from the repumping beam. Absent this correction, $g_{yz}^{(2)}(0) \simeq (0.18 \pm 0.10)$ is directly derived from the

recorded counts. We find that $g^{(2)}(\tau)$ rises to unity at a time $\tau = \tau_B \simeq 45$ns, which is consistent with a simple estimate $\tau_- = 2/(\gamma + \kappa) = 48$ ns based upon the lifetime for the state $|1, -\rangle$.

Although for small $|\tau|$ our observations of $g^{(2)}_{yz}(\tau)$ are in reasonable accord with the predictions from our theoretical model, there are significant deviations on longer time scales. Evident in Fig. 4.3(b) is modulation that is not present in the model which arises from the center-of-mass motion of the trapped atom. In support of this assertion, Fig. 4.3(c) displays the Fourier transform $\tilde{g}(f)$ of $g^{(2)}_{yz}(\tau)$ which exhibits a narrow peak at frequency $f_0 \simeq 535$ kHz just below the independently determined frequency $\nu_0 \simeq 544$ kHz for harmonic motion of a trapped atom about an antinode of the FORT in the axial direction x. This modulation is analogous to that observed in Ref. [53] for $g^{(2)}(\tau)$ for the light from a single ion, which arose from micro-motion of the ion in the RF trap.

Here, $U(\vec{r}) = U_0 \sin^2(2\pi x/\lambda_{C_2}) \exp(-2\rho^2/w_{C_2}^2)$ is the FORT potential, which gives rise to an anharmonic ladder of vibrational states with energies $\{E_m\}$. There are $\simeq 100$ bound states in the axial dimension for radial coordinate $\rho \equiv \sqrt{y^2 + z^2} = 0$. The anharmonicity leads to the observed offset $f_0 < \nu_0$ due to the distribution of energies for axial motion in the FORT well. Indeed, the frequency $\nu_{\min} = (E_{m_{\max}} - E_{m_{\max}-1})/h$ at the top of the well is approximately half that at the bottom of the well, $\nu_0 = (E_1 - E_0)/h$. By comparing the measured distribution of frequencies exhibited by $\tilde{g}(f)$ with the calculated axial frequencies $\{\nu_m\}$, we estimate that those atoms from which data was obtained are trapped in the lowest lying axial states $m \lesssim 10$, which corresponds to a maximum energy $E/k_B \sim 250$ μK. This energy estimate is consistent with other measurements of $g^{(2)}_{yz}(\tau)$ that we have made, as well as the Fourier transform of the record of the transmitted intensity and the transmission spectra of Ref. [11].

We have demonstrated photon blockade for the transmission of an optical cavity strongly coupled to a single trapped atom [38, 39, 40, 41, 45, 46, 8]. The observed nonclassical photon statistics for the transmitted field result from strong nonlinear interactions at the single-photon level, in analogy with the phenomena of Coulomb

blockade for electron transport [36, 37, 54]. Extensions of our work include operation in a pulsed mode as was analyzed in Ref. [38], thereby realizing a source for single photons "on demand." As we improve the effectiveness of our cooling procedure, we should be able to explore the dependence of $g_{yz}^{(2)}(\tau)$ on probe detuning, $\omega_p - \omega_0$, as well as to move to higher levels of excitation to increase the output flux.

Chapter 5

Detailed Theory of Photon Blockade

In Chapter 4, we employ a model of a two-mode cavity coupled to an atom with multiple internal states. In this chapter, we make explicit the coupling used in the model Hamiltonian to determine the eigenvalues displayed in Fig. 4.1(b). This Hamiltonian was also incorporated into the master equation for the damped, driven system used to compute the theoretical results in Fig. 4.2(b). We compare the effects of a two-mode cavity to the effect of driving the atom (rather than the cavity) in a Jaynes-Cummings system. We also present an extension to our atom-cavity model which includes the effect of cavity birefringence and FORT induced ac-Stark shifts in the atomic states. The modified cavity transmission and intensity correlation function are presented for comparison. Finally, we present a theoretical result for the time dependence of the intensity correlation function.

5.1 Eigenvalues

This section is adapted from Ref. [55].

We approximate the atom-cavity coupling to be a dipole interaction. We define the atomic dipole transition operators for the $6S_{1/2}, F = 4 \rightarrow 6P_{3/2}, F' = 5'$ transition

in atomic Cesium as

$$D_q = \sum_{m_F=-4}^{4} |F = 4, m_F\rangle\langle F = 4, m_F|\mu_q|F' = 5', m_F + q\rangle\langle F' = 5', m_F + q|, \quad (5.1)$$

where $q = \{-1, 0, 1\}$ and μ_q is the dipole operator for $\{\sigma_-, \pi, \sigma_+\}$-polarization, respectively, normalized such that for the cycling transition $\langle F = 4, m_F = 4|\mu_1|F' = 5', m_F = 5\rangle = 1$. The matrix element of the dipole operator $\langle F = 4, m_F|\mu_q|F' = 5', m'_F\rangle$ is equivalent to the Clebsch-Gordan coefficient for adding spin 1 to spin 4 to reach total spin 5, namely $\langle j_1 = 4, j_2 = 1; m_1 = m_F, m_2 = q|j_{total} = 5; m_{total} = m'_F\rangle$.

The Hamiltonian of a single atom coupled to a cavity with two degenerate orthogonal linear modes is

$$\begin{aligned} H_{4\to5'} &= \hbar\omega_A \sum_{m'_F=-5}^{5} |F' = 5', m'_F\rangle\langle F' = 5', m'_F| + \hbar\omega_{C_1}(a^\dagger a + b^\dagger b) \quad (5.2) \\ &+ \hbar g_0 (a^\dagger D_0 + D_0^\dagger a + b^\dagger D_y + D_y^\dagger b) \end{aligned}$$

where $D_y = \frac{i}{\sqrt{2}}(D_{-1} + D_{+1})$ is the dipole operator for linear polarization along the y-axis. We are using coordinates where the cavity supports $\hat{y}$ and $\hat{z}$ polarizations and $\hat{x}$ is along the cavity axis. The annihilation operator for the $\hat{z}$ ($\hat{y}$) polarized cavity mode is a (b).

Assuming $\omega_A = \omega_{C_1} \equiv \omega_0$, we find that the lowest eigenvalues of $H_{4\to5'}$ have a relatively simple structure. In the manifold of zero excitations, all nine eigenvalues are zero. In manifolds with n excitations, the eigenvalues are of the form $E_{n,k} = n\hbar\omega_0 + \hbar g_0 \varepsilon_k^{(n)}$, where $\varepsilon_k^{(n)}$ is a numerical factor and k is an index for distinct eigenvalues. There are 29 states in the $n = 1$ manifold, but due to degeneracy k has only 13 distinct values, $k \in \{-6, \ldots 6\}$; in the $n = 2$ manifold there are 49 states but $k \in \{-11, \ldots 11\}$. The number of states in any manifold can be understood by considering how the excitations can be distributed among the atom and the two cavity modes. For example, in the $n = 1$ manifold, the atom can be in one of its 9 ground states ($m_F \in \{-4, \ldots 4\}$) and either cavity mode l_y or mode l_z can have one photon (giving 18 possible states), or the atom can be in one of its 11 excited states ($m'_F \in \{-5, \ldots 5\}$)

k	$\varepsilon_k^{(1)}$	$\eta_k^{(1)}$	$\varepsilon_k^{(2)}$	$\eta_k^{(2)}$
0	0	7	0	5
1	0.667	1	0.516	1
2	0.683	2	0.556	2
3	0.730	2	0.662	2
4	0.803	2	0.805	2
5	0.894	2	0.966	3
6	1	2	0.978	2
7			1.014	2
8			1.073	2
9			1.155	2
10			1.265	2
11			1.414	2

Table 5.1: Numerical factors $\varepsilon_k^{(n)}$ for the eigenvalues of the Hamiltonian $H_{4\to5'}$ in Eq. 5.2, together with their degeneracies $\eta_k^{(n)}$.

while both cavity modes are in the vacuum state, yielding a total of 29 states. Table 5.1 lists numerical values for $\varepsilon_k^{(1,2)}$ as well as their respective degeneracies $\eta_k^{(1,2)}$. The numerical factors and degeneracies have the symmetries $\varepsilon_{-k}^{(n)} = -\varepsilon_k^{(n)}$ and $\eta_{-k}^{(n)} = \eta_k^{(n)}$. The resulting eigenvalues $E_{n,k}$ for $n = \{0, 1, 2\}$ are displayed in Fig. 4.1(b).

Although these eigenvalues are certainly not sufficient for understanding the complex dynamics associated with the full master equation, they do provide some insight into some structural aspects of the atom-cavity system. For example, the eigenvalues $\varepsilon_{\pm6}^{(1)} = \pm1$ correspond to the vacuum-Rabi splitting for the states $|1, \pm\rangle$ for a two-state atom coupled to a single cavity mode [cf., Fig. 4.1(a)]. The one-photon detunings for transitions from the $n = 1 \to n' = 2$ manifold are largest for the eigenstates associated with $\varepsilon_{\pm6}^{(1)}$. Indeed, just as for the two-state atom with one cavity mode, transitions from the eigenstates at $\pm g_0$ have frequency detunings $\pm(2-\sqrt{2})g_0$ relative to the nearest states in the $n' = 2$ manifold (at $\varepsilon_{\pm11}^{(2)} = \pm\sqrt{2}$, respectively). Hence, as a function of probe frequency ω_p, the eigenvalue structure in Table 5.1 suggests that the ratio of two-photon to one-photon excitation would exhibit a minimum around $\omega_p = \omega_0 \pm g_0$, resulting in reduced values $g^{(2)}(0) < 1$, which the full calculation verifies in Fig. 4.2(b).
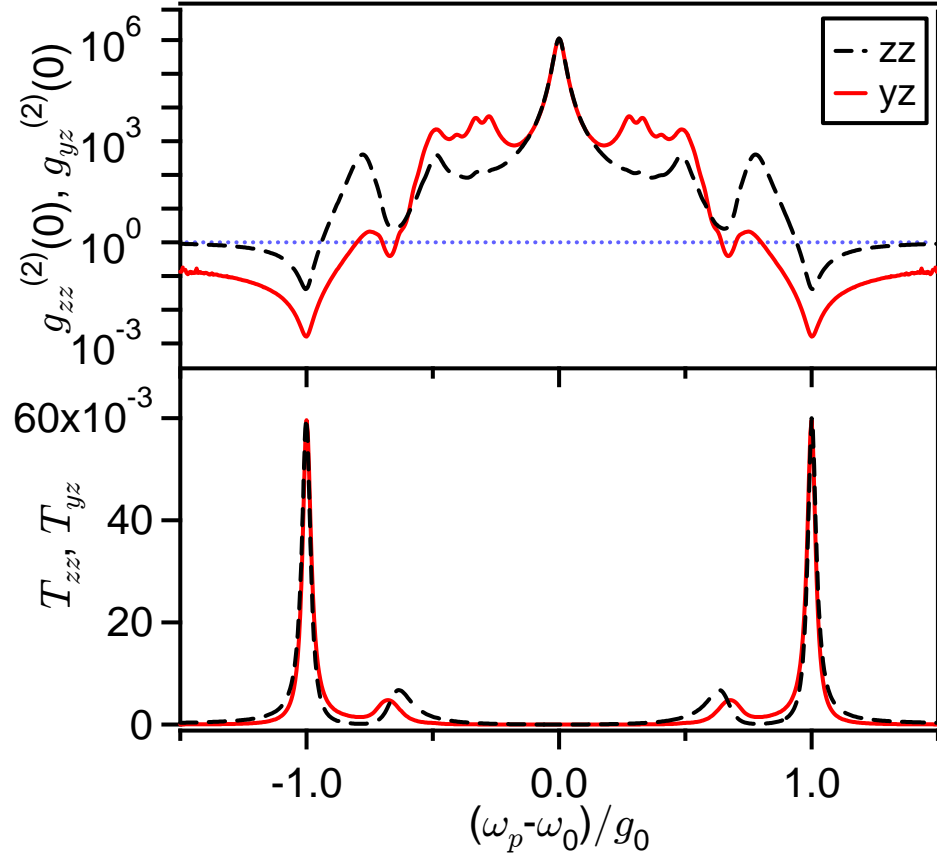
Figure 5.1: T_{zz} and $g_{zz}^{(2)}(0)$ (dashed), and T_{yz} and $g_{yz}^{(2)}(0)$ (red) versus normalized probe detuning (see Chapter 4 for definition of variables). We consider an $F = 4 \rightarrow F' = 5'$ transition driven by linearly polarized light in a cavity containing two modes of orthogonal polarization that are frequency degenerate. Parameters are $(g_0, \kappa, \gamma)/2\pi = (50, 1, 1)$ MHz. The probe strength is such that the intracavity photon number on resonance without an atom is 0.05. The blue dotted line indicates $g^{(2)}(0) = 1$ for Poissonian statistics.

For excitation to the other eigenstates in the $n = 1$ manifold, such blockade is not evidenced in Fig. 4.2(b). A contributing factor suggested by the structure of eigenvalues in Table 5.1 is interference of one and two-photon excitation processes. For example, excitation at $\omega_p \simeq \omega_0 \pm g_0/4$ results in two-photon resonance for the eigenstates associated with $\varepsilon_{\pm 1}^{(2)} \simeq \pm 0.5$, and to photon bunching with $g^{(2)}(0) \gg 1$ as confirmed by our full calculation of photon statistics.

Fig. 5.1 provides a global perspective of these various effects. Here, we calculate transmission spectra and intensity correlation functions analogous to those shown

in Fig. 4.2(b), but now with coherent coupling g_0 much larger than the dissipative rates (κ, γ) and well beyond what we have achieved in our experiments, $g_0/\kappa = g_0/\gamma = 50$. At $\omega_p = \omega_0 \pm g_0$, $g_{yz}^{(2)}(0) \simeq 0.002$ in evidence of the previously discussed photon blockade suggested by the eigenvalue structure in Table 5.1. As anticipated, large photon bunching results near $\omega_p \simeq \omega_0 \pm g_0/4$ associated with the two-photon resonance to reach the eigenstates with $\varepsilon_{\pm 1}^{(2)} \simeq \pm 0.5$. Between these two extremes for the eigenvalues with the largest and smallest nonzero magnitudes ($\omega_0 \pm g_0 \leq \omega_p \leq \omega_0 \pm g_0/4$), $g_{yz}^{(2)}(0)$ displays a complex structure involving multiple excitation pathways through states in the $n = 1$ manifold to reach states in the $n' = 2$ manifold. The extremely large peak at $\omega_p = \omega_0$ is discussed in Refs. [50, 46].

5.2 Driven Atom

In Section 4.3, we describe the difference in the photon statistics when driving the detected cavity mode ($\hat{z}$) or the other mode ($\hat{y}$). The driven cavity mode has photon statistics which are less strongly sub-Poissonian, an effect we hypothesize to be caused by interference between the atomic dipole radiation and the coherent drive. In this section, we will further explore this hypothesis by considering atom-cavity systems where the driving field is directly coupled to the atom, not the cavity mode.

We will first study the familiar Jaynes-Cummings system, a two-state atom coupled to a single mode cavity. We assume a coherent drive field made of many photons which we will treat classically. In Fig. 5.2, we compare the intracavity fields [51] when driving the cavity (a) and the atom (b) for $g_0/\kappa = g_0/\gamma = 50$. $T, \tilde{T}$ are proportional to the intracavity photon number, with T normalized to the bare-cavity on-resonance photon number for the driven cavity and $\tilde{T}$ normalized to the bare-atom excited-state population for the driven atom. The intensity correlation function $\tilde{g}^{(2)}(0)$ of the system when driving the atom is much lower than $g^{(2)}(0)$ (the correlation function of the system when driving the cavity) at $\omega_p = \omega_0 \pm g_0$, with $\tilde{g}^{(2)}(0) \simeq 0.002$ and $g^{(2)}(0) \simeq 0.02$. $\tilde{g}^{(2)}(0)$ is super-Poissonian at $\omega_p = \omega_0 \pm g_0/\sqrt{2}$ due to the two-photon resonance discussed above, but lacks the large peak at $\omega_p = \omega_0$ evident in $g^{(2)}(0)$. At
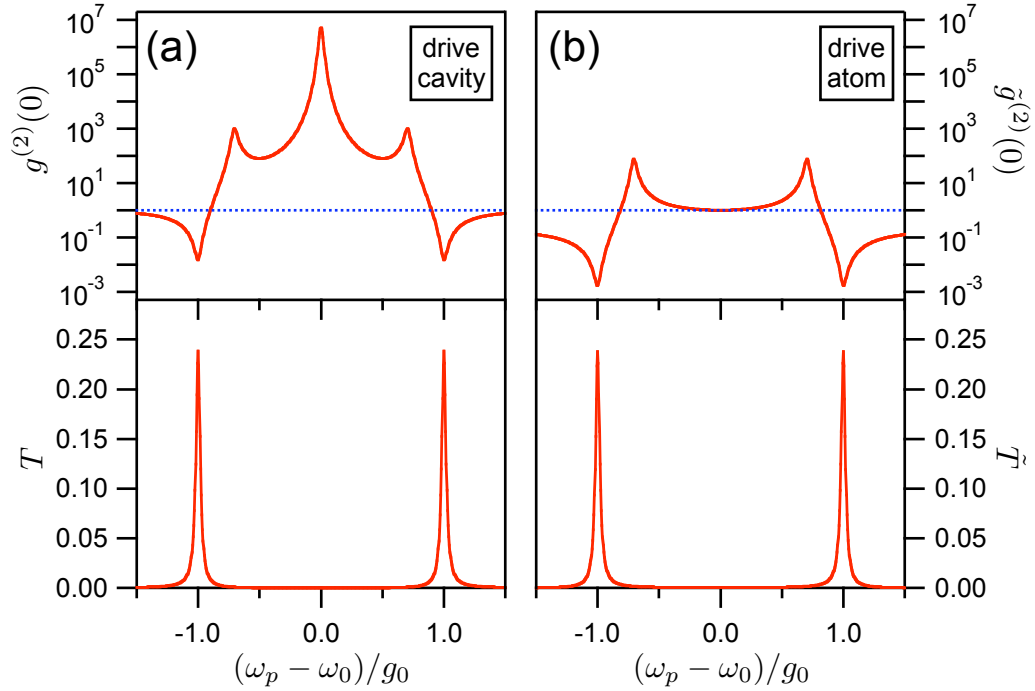
Figure 5.2: T and $g^{(2)}(0)$ (a), and $\tilde{g}^{(2)}(0)$ and $\tilde{T}$ (b) versus normalized probe detuning. Parameters are $(g_0, \kappa, \gamma)/2\pi = (50, 1, 1)$ MHz. The probe strength is such that the intracavity photon number on resonance without an atom is 0.05 for (a), and the atomic excited state population on resonance without a cavity is 0.05 for (b). The blue dotted lines indicates $g^{(2)}(0) = 1$ for Poissonian statistics.

$\omega_p = \omega_0$ we have $\tilde{g}^{(2)}(0) \simeq 1$.

We now consider a two-mode cavity coupled to the Zeeman states of the $F = 4 \rightarrow F' = 5'$ transition of a single atom, as above. We will take the probe field driving the atom to be polarized along $\hat{z}$ and calculate the intracavity photon number $\tilde{T}_{zz}, \tilde{T}_{yz}$ in the $\hat{z}, \hat{y}$ modes, respectively (normalized to the drive strength as above), and the corresponding intensity correlation functions $\tilde{g}_{zz}^{(2)}(0), \tilde{g}_{yz}^{(2)}(0)$. Results of the calculations are plotted in Fig. 5.3 for $g_0/\kappa = g_0/\gamma = 50$. At $\omega_p = \omega_0 \pm g_0$, both $\tilde{g}_{zz}^{(2)}(0)$ and $\tilde{g}_{yz}^{(2)}(0)$ are close to $g_{yz}^{(2)}(0)$ as in Fig. 5.1. This supports our hypothesis that the somewhat higher value of $g_{zz}^{(2)}(0)$ at $\omega_p = \omega_0 \pm g_0$ is caused by interference with the drive field. Interestingly, though the central peak at $\omega_p = \omega_0$ is absent in $\tilde{g}_{zz}^{(2)}(0)$, as we expect in correspondence with the Jaynes-Cummings case and as implied by the usual explanation of the phenomenon as resulting from the interference of the drive
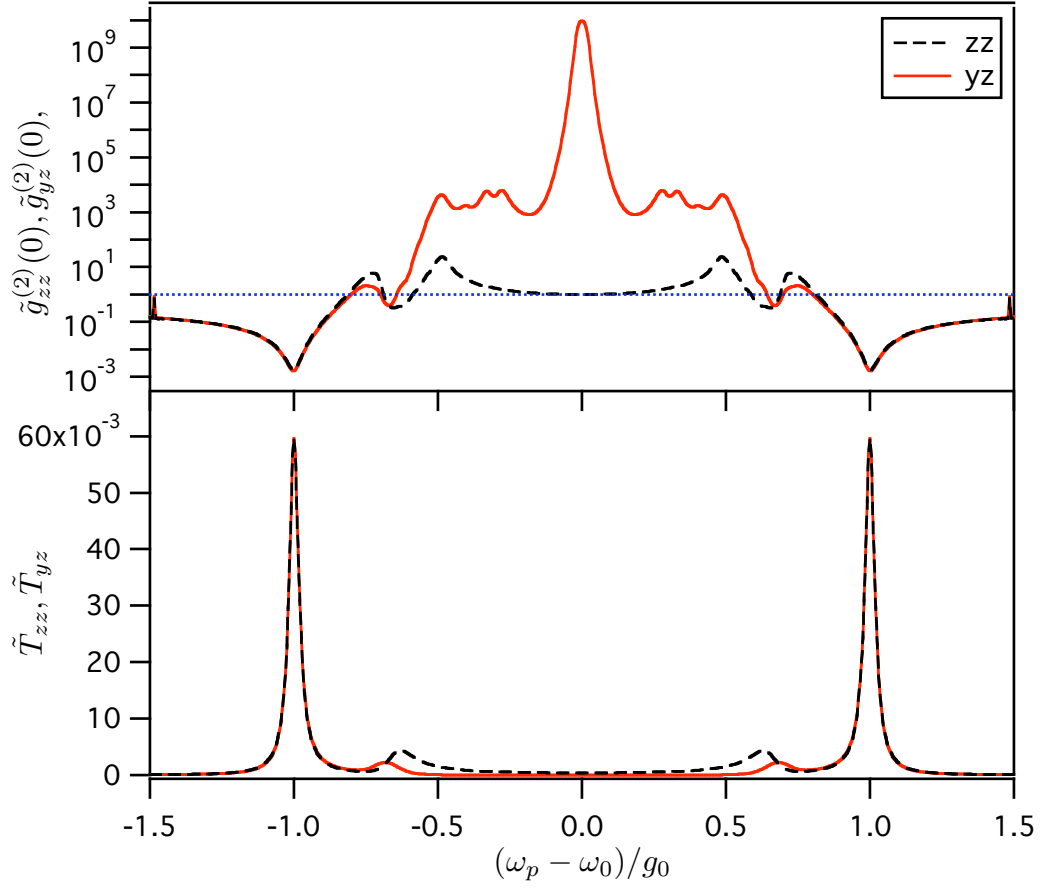
Figure 5.3: $\tilde{T}_{zz}$ and $\tilde{g}^{(2)}_{zz}(0)$ (dashed), and $\tilde{T}_{yz}$ and $\tilde{g}^{(2)}_{yz}(0)$ (red) versus normalized probe detuning. Parameters are $(g_0, \kappa, \gamma)/2\pi = (50, 1, 1)$ MHz. The probe strength is such that the atomic excited state population on resonance without a cavity is 0.05. The blue dotted line indicates $g^{(2)}(0) = 1$ for Poissonian statistics.

field with the atomic dipole radiation, the peak in $\tilde{g}^{(2)}_{yz}(0)$ is even greater than that of $g^{(2)}_{zz}(0), g^{(2)}_{yz}(0)$. This effect may be of interest in future studies.

5.3 Birefringence and Stark Shifts

This section is an expanded adaptation from Ref. [55].

We now consider the effects of cavity birefringence and m'_F-dependent ac-Stark
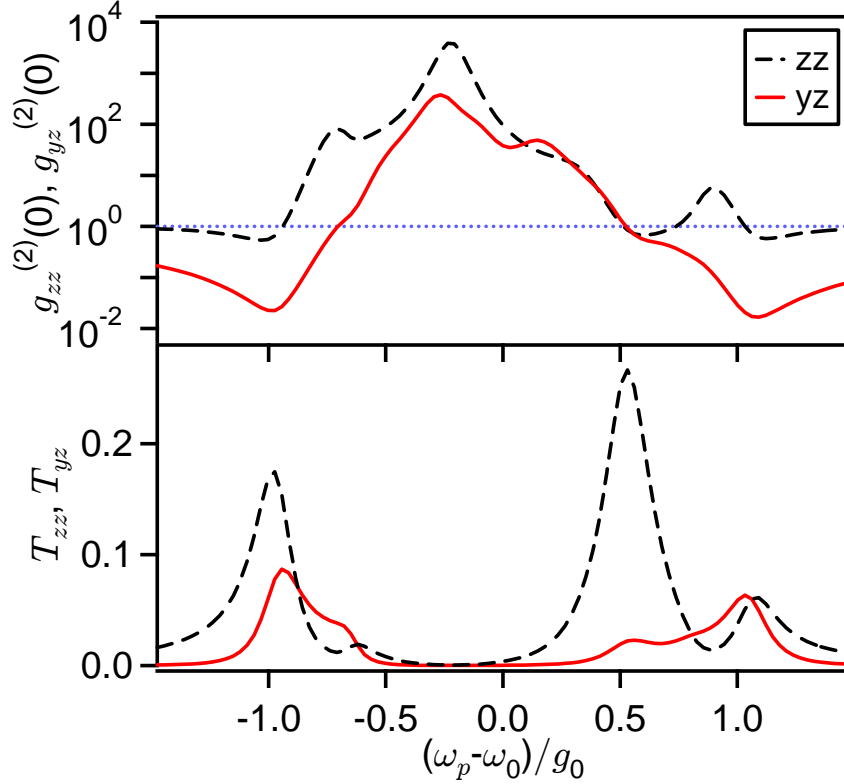
Figure 5.4: T_{zz} and $g_{zz}^{(2)}(0)$ (dashed), and T_{yz} and $g_{yz}^{(2)}(0)$ (red) versus normalized probe detuning (see Chapter 4 for definition of variables). We consider an $F = 4 \rightarrow F' = 5'$ transition driven by linearly polarized light in a cavity containing two nondegenerate modes of orthogonal polarization. Parameters are $(g_0, \kappa, \gamma, \Delta\omega_{C_1}, U_0)/2\pi = (33.9, 4.1, 2.6, 4.4, -43)$ MHz, and $\omega_{C_1^z} = \omega_A \equiv \omega_0$. The probe strength is such that the intracavity photon number on resonance without an atom is 0.05. The blue dotted line indicates $g^{(2)}(0) = 1$ for Poissonian statistics.

shifts. These modify the Hamiltonian $H_{4 \rightarrow 5'}$ in Eq. 5.2 to

$$
\begin{aligned}
H_{full} &= \sum_{m_F'=-5}^{5} \hbar\omega_{m_F'}|F' = 5', m_F'\rangle\langle F' = 5', m_F'| + \hbar\omega_{C_1^z}a^\dagger a + \hbar\omega_{C_1^y}b^\dagger b \quad (5.3) \\
&+ \hbar g_0(a^\dagger D_0 + D_0^\dagger a + b^\dagger D_y + D_y^\dagger b)
\end{aligned}
$$

The birefringent splitting $\Delta\omega_{C_1}$ is the difference of the resonant frequencies of the two polarization modes, $\Delta\omega_{C_1} = \omega_{C_1^z} - \omega_{C_1^y}$. The atomic excited state frequencies are given by $\omega_{m_F'} = \omega_A + U_0\beta_{m_F'}$, where ω_A is the unshifted frequency of the $F = 4 \rightarrow F' = 5'$ transition in free space, U_0 is the FORT potential, and $\beta_{m_F'}$ for the
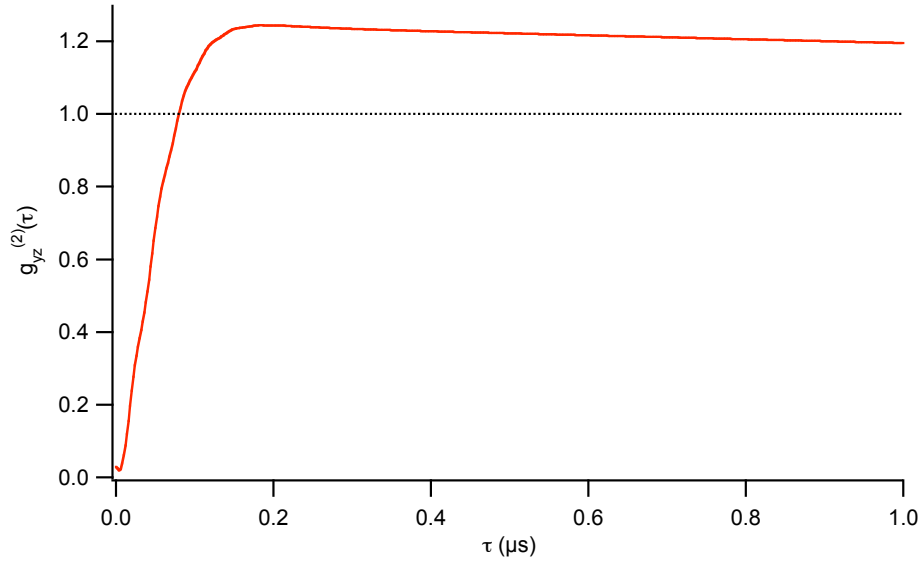
Figure 5.5: Theoretical result for $g_{yz}^{(2)}(\tau)$ versus τ with parameters as in Fig. 5.4. The probe strength is such that the resonant intracavity photon number of the bare cavity would be 0.21 as in the experiment. The blue dotted line indicates $g^{(2)}(0) = 1$ for Poissonian statistics. This calculation was performed with a Fock basis of $\{0, 1, 2\}$ photons in the $\hat{z}$ polarized mode and $\{0, 1\}$ photons in the $\hat{y}$ polarized mode.

FORT wavelength of the experiment is given by $\{m'_F, \beta_{m'_F}\} = \{\pm 5, 0.18\}, \{\pm 4, 0.06\}$, $\{\pm 3, -0.03\}, \{\pm 2, -0.10\}, \{\pm 1, -0.14\}, \{0, -0.15\}$ [4].

The effect of these corrections to the Hamiltonian on the transmitted field from the steady-state solutions to the master equation are displayed in Fig. 5.4. The heights and shapes of the multiplets in $T_{yz,zz}$ are modified, but the basic structure is unaffected relative to Fig. 4.2(b). The structure of $g_{yz,zz}^{(2)}(0)$ is also qualitatively unchanged. The value of $g_{yz}^{(2)}(0)$ for $\omega_p = \omega_0 - g_0$ is 0.02 (ignoring the above corrections yields $g_{yz}^{(2)}(0) \simeq$ 0.03). These values are consistent with the experimental result $g_{yz}^{(2)}(0) = 0.13 \pm 0.11$.

In Fig. 5.5, we present the theoretical prediction for $g_{yz}^{(2)}(\tau)$ including the effects of Stark shifts and birefringence. We find that $g_{yz}^{(2)}(\tau)$ rises to unity at $\tau \simeq 80$ ns, well above the experimental result of $\tau \simeq 45$ ns. The theory, however, does not take in to account atomic motion, but rather assumes the atom to be fixed at a place of optimal coupling. Since atomic motion clearly has a large effect on $g_{yz}^{(2)}(\tau)$, as is evident in Fig. 4.3(b), we believe that this is the dominant cause of the discrepancy.

Chapter 6

Cavity QED with Multiple Hyperfine Levels

We calculate the weak-driving transmission of a linearly polarized cavity mode strongly coupled to the D2 transition of a single Cs atom. Results are relevant to future experiments with microtoroid cavities [5], where the single-photon Rabi frequency g exceeds the excited-state hyperfine splittings, and photonic bandgap resonators [6], where g is greater than both the excited- and ground-state splitting.

The Jaynes-Cummings model of cavity QED treats an atom as a two-level system. This is appropriate when the atom has a cycling transition, typically reached by optical pumping with circularly polarized light [3, 7]. However, new types of optical resonators such as microtoroids [5] and photonic band gap cavities [6] do not support circularly polarized modes. Though these structures with extremely low critical atom and photon numbers show great promise for strong coupling, a more detailed model of the atom must be employed when calculating the properties of these atom-cavity systems. A linearly polarized mode may couple multiple Zeeman states of the atom. Additionally, for these very small resonators, the single photon Rabi frequency $(2g)$ can be comparable to or larger than the hyperfine splitting of the atom, so that multiple hyperfine levels must be considered when calculating the excitations of the system. We will consider a linearly polarized single-mode resonator coupled to the D2 $(6S_{1/2} \to 6P_{3/2})$ transition of a single Cesium atom. However, this may also give some intuition for other multilevel scatterers, such as molecules and excitons [56, 57].

In order to describe the interaction of the atom with various light fields, it is useful to define the atomic dipole transition operators

$$D_q(F, F') = \sum_{m_F=-F}^{F} |F, m_F\rangle\langle F, m_F|\mu_q|F', m_F + q\rangle\langle F', m_F + q| \qquad (6.1)$$

where $q = \{-1, 0, 1\}$ and μ_q is the dipole operator for $\{\sigma_-, \pi, \sigma_+\}$-polarization, normalized such that for a cycling transition $\langle\mu\rangle = 1$. We will approximate all atom-field interactions to be dipole interactions.

6.1   Coupling to Multiple Excited Levels

First, let us consider the case when g is comparable to the hyperfine splitting of the excited states, but still small compared to the ground-state splitting. This limit is appropriate for the proposed parameters of microtoroid resonators [5] and small Fabry-Perot cavities [34]. If the cavity is tuned near the $F = 4 \rightarrow F'$ transitions, then the Hamiltonian for the atom cavity system can be written using the rotating wave approximation as

$$
\begin{aligned}
H_0 &= \omega_c a^\dagger a + \sum_{F'=3}^{5} \omega_{F'}|F'\rangle\langle F'| \\
&+ g\Big(\sum_{F'=3}^{5} a^\dagger D_0(4, F') + D_0^\dagger(4, F')a\Big),
\end{aligned}
\qquad (6.2)
$$

where $\omega_{F'}$ is the frequency of the $F = 4 \rightarrow F'$ transition, ω_c is the frequency of the cavity, and a is the annihilation operator for the cavity mode. The operator $|F'\rangle\langle F'|$ projects onto the manifold of excited states with hyperfine number F', and may be written more explicitly as $|F'\rangle\langle F'| = \sum_{m'_F} |F', m'_F\rangle\langle F', m'_F|$. We use units such that $\hbar = 1$ and energy has the same dimensions as frequency. Note that we are treating the cavity as a single-mode resonator with linear polarization. Fabry-Perot cavities have two modes with orthogonal polarizations, so this model is only appropriate if there is a birefringent splitting which makes one of the modes greatly detuned (compared

Figure 6.1: Eigenfrequencies of excitations in the first manifold $\{\epsilon_k^{(1)}\}$ versus cavity detuning. Color represents $\langle a^\dagger a \rangle$ for each corresponding eigenvector. Here $\omega_{4\to4'} - \omega_{4\to5'} = -251$ MHz, $\omega_{4\to3'} - \omega_{4\to5'} = -452$ MHz [58], and $g = 450$ MHz [5]. Although there are 36 eigenvectors in the manifold, there are only 20 unique eigenvalues due to symmetry.

to g) from the atomic resonance.

In the weak-driving limit of an atom-cavity system in the regime of strong coupling, we expect that high transmission will occur when the probe light is resonant with a transition from a ground state of the system to a state in the $N = 1$ lowest excitation manifold. Furthermore, we expect a higher transmission when resonantly exciting an eigenstate which is "cavity-like," i.e., an eigenstate which has larger weight in the field excitation rather than the atomic dipole.

In Fig. 6.1, we plot the eigenfrequencies $\{\epsilon_k^{(1)}\}$ of H_0 determined by the equation $H_0|\psi_k^{(N)}\rangle = \epsilon_k^{(N)}|\psi_k^{(N)}\rangle$. Here N is the excitation manifold, where $\epsilon_k^{(N+1)} - \epsilon_k^{(N)} \sim \omega_c$ and $\epsilon_k^{(0)} = 0$. Also displayed is $\langle \psi_k^{(1)}|a^\dagger a|\psi_k^{(1)}\rangle$ for each eigenstate $|\psi_k^{(1)}\rangle$ corresponding to each eigenfrequency $\epsilon_k^{(1)}$, which is a measure of how "cavity-like" that state is. This should give some indication of what cavity and probe detunings yield high

transmission.

In order to study the system properties more precisely, we can find the Hamiltonian of the driven system, write the Liouvillian that describes the time-evolution including damping, and calculate the steady state of the system. We will assume that the cavity resonance is tuned near the $F = 4 \rightarrow F'$ atomic transitions. We expect that, absent any repumping fields, atomic decays to the $F = 3$ ground state will leave the atom uncoupled to the resonator. To avoid this, we will assume a classical (coherent-state) driving field tuned near the $F = 3 \rightarrow F'$ transitions is applied to the atom in addition to the probe field which drives the cavity. In the rotating wave approximation, the Hamiltonian of this driven atom-cavity system in the frame rotating with the cavity probe is

$$
\begin{aligned}
H_1 &= \sum_{F'=2}^{5} \Delta_{F'} |F'\rangle\langle F'| + \Delta_r |F = 3\rangle\langle F = 3| + \Delta_c a^\dagger a \\
&+ g \sum_{F'=2}^{5} \left(a^\dagger D_0(4, F') + D_0^\dagger(4, F')a \right) \\
&+ \Omega_r \sum_{F'=2}^{5} \left(D_0(3, F') + D_0^\dagger(3, F') \right) \\
&+ \varepsilon a^\dagger + \varepsilon^* a,
\end{aligned}
\tag{6.3}
$$

where $\Delta_{F'} = \omega_{4 \rightarrow F'} - \omega_p$, $\Delta_r = \omega_r - \omega_{GSS} - \omega_p$. Here ω_p is the probe frequency, ω_r is the repump frequency, and $\omega_{GSS} \approx 9.2$ GHz is the ground-state splitting of Cs. The cavity is driven at a rate ε so that in the absence of an atom the intracavity photon number would be $N_{no\ atom} = |\varepsilon|^2/(\kappa^2 + \Delta_c^2)$, and the atom is driven by the repump field with Rabi frequency $2\Omega_r$. Here, we have assumed that there is no off-resonant coupling of the cavity mode to the $F = 3$ ground states, nor is there off-resonant coupling of the repump light to the $F = 4$ states. We expect that corrections due to those terms will be small when $g, \Omega_r \ll \omega_{GSS}$.

The time evolution of the density matrix ρ of the atom-cavity system is given by

Figure 6.2: Transmission (intracavity photon number, normalized to the empty cavity on resonance) versus probe and cavity detunings in the weak-driving limit (calculated in a Fock basis of {0,1} photons) from Eq. 6.4. Red dotted lines indicate resonances for uncoupled atomic and cavity transitions. The blue dashed line indicates the cavity detuning in Fig. 6.3. Rates are $(g, \kappa, \gamma) = (450, 1.75, 2.6)$MHz [5], $\varepsilon = \kappa\gamma/g$, and $\Omega_r = \gamma$. The repump beam is resonant with the $F = 3 \rightarrow F' = 4'$ transition, i.e., $\Delta_r = \Delta_{4'}$.

the master equation,

$$\dot{\rho} = -i[H_1, \rho] + \kappa\mathcal{D}[a]\rho + \gamma\sum_{q,F}\mathcal{D}\left[\sum_{F'}D_q(F, F')\right]\rho \qquad (6.4)$$

where the zero-temperature decay superoperator $\mathcal{D}$ acts on the density matrix such that $\mathcal{D}[c]\rho \equiv 2c\rho c^\dagger - c^\dagger c\rho - \rho c^\dagger c$ for any operator c. Note that in the term proportional to γ, we have assumed that the environment provides a common reservoir for photons with frequencies varying over the excited-state hyperfine splittings, but that photons separated in frequency by the ground-state splitting are emitted into independent reservoirs. This is consistent with our assumption that there is no off-resonant coupling between transitions from different hyperfine ground-state manifolds. From the
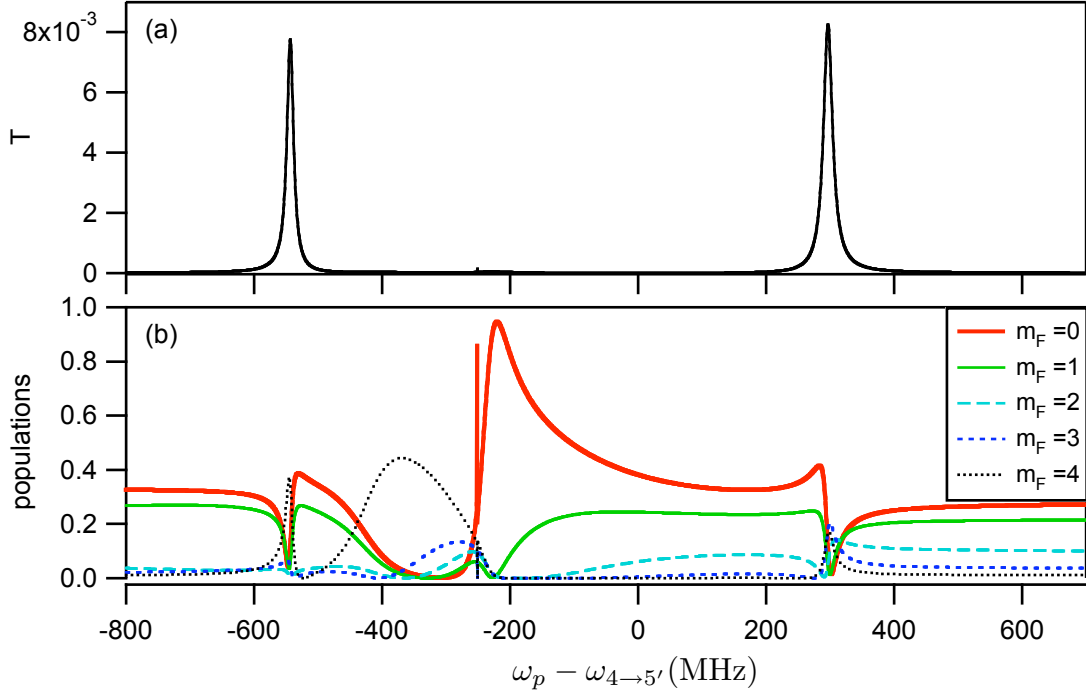
Figure 6.3: (a) Normalized transmission T and (b) populations in various Zeeman ground states of the $F = 4$ manifold as a function of probe detuning, with the cavity frequency fixed at $\omega_c = \omega_{4\to5'} - 100\text{MHz}$. Parameters are the same as in Fig. 6.2. By symmetry, populations are the same in Zeeman level m_F as in level $-m_F$. The sharp feature at $\omega_p = \omega_{4\to5'} - 251$ is caused by a coherent Raman effect between the probe and the repump light. Note that because of the weak cavity drive and the strong repump light, nearly all of the population is in the $F = 4$ manifold.

steady-state solution to Eq. 6.4, $\dot{\rho}_{ss} = 0$, we can compute steady-state expectation values of an operator c by evaluating $\text{Tr}(\rho_{ss}c)$. We define the normalized cavity transmission $T = \text{Tr}(\rho_{ss}a^\dagger a)\kappa^2/|\varepsilon|^2$, where $T = 1$ for an empty cavity on resonance. T is plotted in Fig. 6.2 versus cavity and probe detunings. Notice the similarity to Fig. 6.1, which demonstrates that the qualitative features of the transmission are indeed determined by the eigenvalues and eigenstates of the Hamiltonian.

Fig. 6.3 shows T as a function of probe detuning for fixed cavity frequency along with atomic ground-state populations $\langle F = 4, m_F | \rho_{ss} | F = 4, m_F \rangle$. The large swings in the relative populations of various Zeeman states demonstrate the importance of optical pumping in understanding the steady-state behavior of the transmission. The rapid variation of the populations that occurs near the transmission peaks can be un-
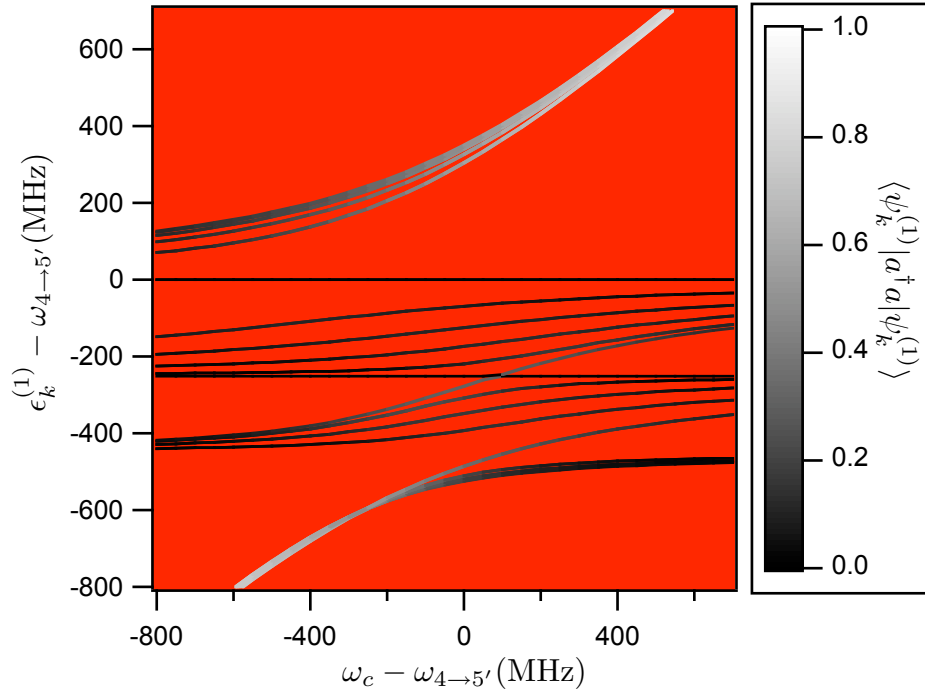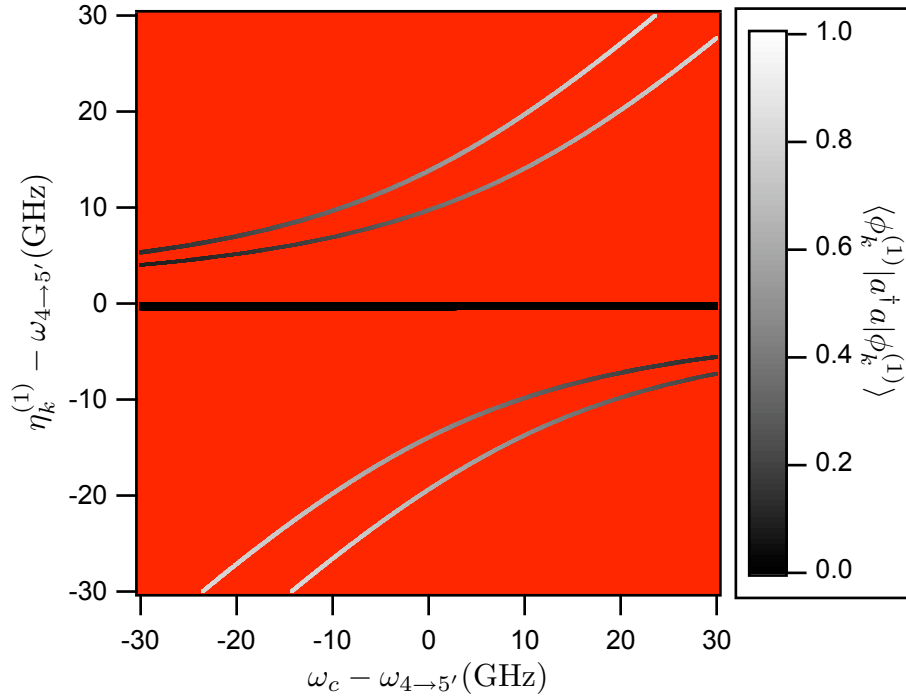
Figure 6.4: Eigenfrequencies of excitations in the first manifold $\{\eta_k^{(1)}\}$ versus cavity detuning. Color represents $\langle a^\dagger a \rangle$ for each corresponding eigenvector. The coupling $g = 17$ GHz [6]. Although there are 48 eigenvectors in the manifold, there are only 27 unique eigenvalues due to symmetry. These eigenvalues are clustered in 5 bands.

derstood by noting in Fig. 6.1 that each transmission peak is associated with multiple eigenstates with similar eigenvalues. These eigenstates have different amplitudes of the Zeeman states and therefore lead to different optical pumping effects. It should be noted that the width of the transmission peaks are therefore not simply determined by κ and γ but also by the separation of the various eigenvalues contributing to each peak, making the peaks wider than would be naively expected.

6.2   Coupling to the Entire D2 Transition

Now we will turn to the regime where g is larger than both the ground- and excited-state hyperfine splittings. This case is applicable for the expected parameters of cavity QED with photonic band gap cavities. In this regime, the cavity mode couples to both ground-state hyperfine manifolds, and the Hamiltonian of the atom-cavity
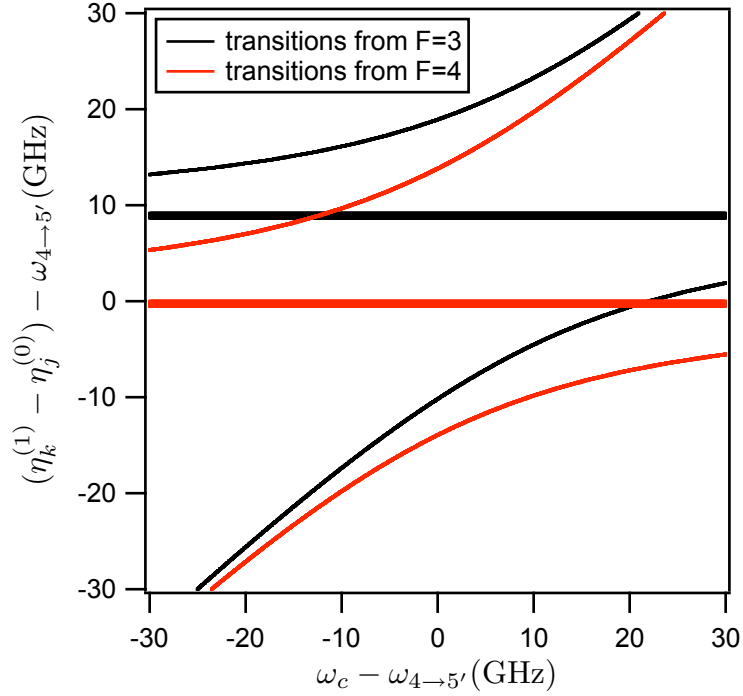
Figure 6.5: Difference frequencies for allowed single-quanta transitions between ground and first excited states, $\eta_k^{(1)} - \eta_j^{(0)}$, versus cavity detuning. Eigenfrequencies are the same as in Fig. 6.4. Black (red) lines indicate transitions from ground states with the atom in the $F = 3$ ($F = 4$) manifold.

system in the absence of a driving field can be written

$$
\begin{aligned}
H_2 &= \sum_{F'} \omega_{F'} |F'\rangle\langle F'| - \omega_{GSS} |F=3\rangle\langle F=3| + \omega_c a^\dagger a \\
&+ g \sum_{F,F'} \left(a^\dagger D_0(F, F') + D_0^\dagger(F, F') a \right)
\end{aligned}
\tag{6.5}
$$

As we did earlier for H_0, we find the eigenvalues and eigenvectors of this Hamiltonian determined by the condition $H_2 |\phi_k^{(N)}\rangle = \eta_k^{(N)} |\phi_k^{(N)}\rangle$. In Fig. 6.4, we plot the the frequencies $\eta_k^{(1)}$ of the lowest lying excitations, as well as how "cavity-like" the corresponding eigenmodes are, $\langle \phi_k^{(1)} | a^\dagger a | \phi_k^{(1)} \rangle$. The eigenvalues in the first excitation manifold separate into five bands. The lowest and second-highest of these bands have eigenstates which are superpositions of $F = 3$ atomic ground states with one photon in the cavity and $F' = \{2', 3', 4'\}$ atomic excited states with zero photons; the highest
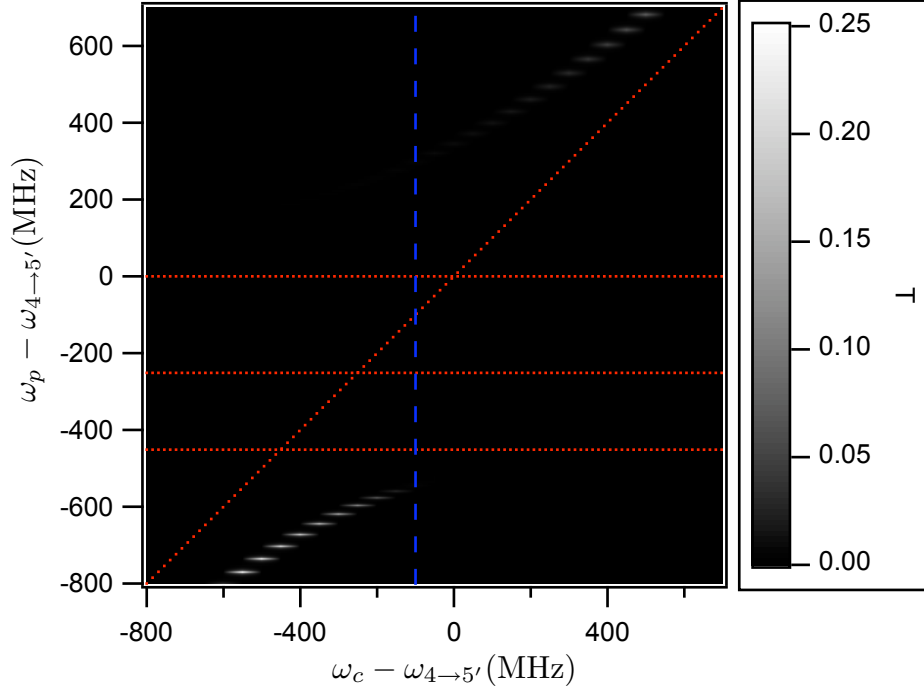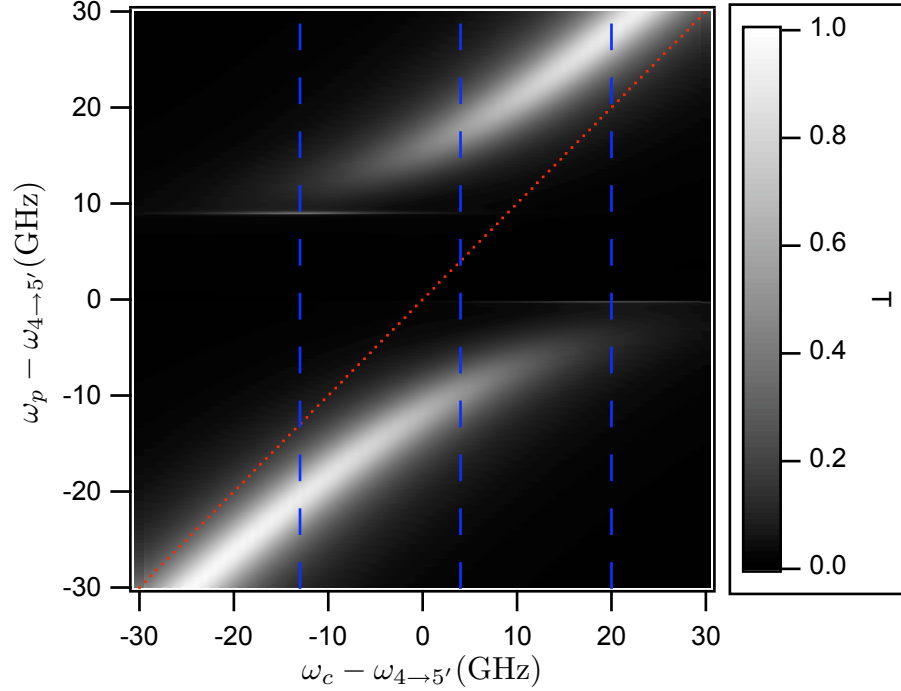
Figure 6.6: Transmission (intracavity photon number, normalized to the empty cavity on resonance) versus probe and cavity detunings in the weak-driving limit (calculated in a Fock basis of $\{0,1\}$ photons) from Eq. 6.7. The red dotted line indicates resonance for the uncoupled cavity. The blue dashed lines indicates the cavity detunings in Figs. 6.7, 6.8 and 6.9. Rates are $(g, \kappa, \gamma) = (17, 4.4, 0.0026)$GHz [6], $\varepsilon = 100\kappa\gamma/g$.

and second-lowest bands have eigenstates which are superpositions of $F = 4$ states with one photon and $F' = \{3', 4', 5'\}$ states with zero photons. The central band is dominated by atomic excited states.

We expect high transmission when a probe is tuned to be resonant with a transition from a ground state of the atom-cavity system to one of the states in the first excitation manifold. The eigenvalues of the ground states are $\eta^{(0)} = 0$ for states with the atom in the $F = 4$ manifold and $\eta^{(0)} = -\omega_{GSS}$ for states with the atom in $F = 3$. In Fig. 6.5, we plot the difference frequencies for transitions between ground and first excited states, $\eta_k^{(1)} - \eta_j^{(0)}$, where k, j are restricted to allowed single-quanta transitions. Notice that although the eigenvalues of the Hamiltonian do not cross, the differences of eigenvalues between the ground and first excitation manifolds do have crossings. These crossings correspond to a dual resonance condition, in which
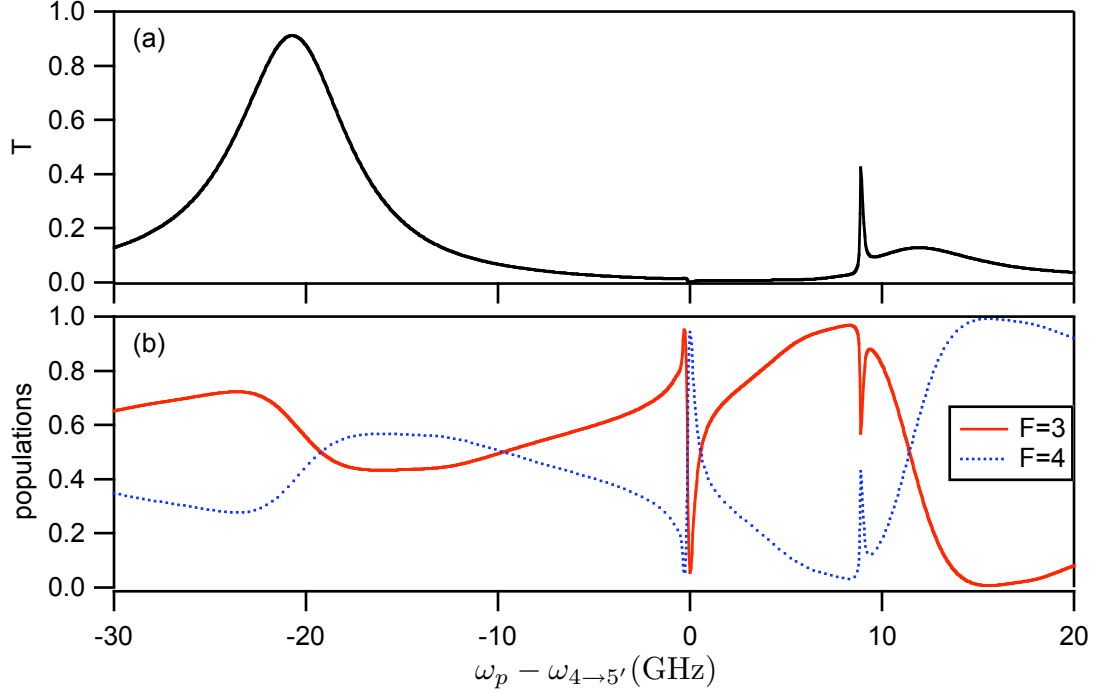
Figure 6.7: Normalized transmission T (a) and atomic populations in the hyperfine ground states (b) as a function of probe detuning, with the cavity frequency fixed at $\omega_c = \omega_{4\to5'} - 13\text{GHz}$. Parameters are the same as in Fig. 6.6. Note that because the cavity drive is weak, nearly all of the population is in the ground states.

a transition from one ground state to an excited state is resonant with a transition from another ground state to a different excited state.

We will now calculate the steady state of the driven, damped system. We will consider the cavity to be driven by a single coherent-state field at the frequency ω_p. Since the cavity can couple to all of the atomic ground states, a repump field is not needed. The Hamiltonian of the driven atom-cavity system under the rotating wave approximation, in the frame rotating with the probe, is

$$
\begin{aligned}
H_3 &= \sum_{F'} \Delta_{F'} |F'\rangle\langle F'| - \omega_{GSS}|F=3\rangle\langle F=3| + \Delta_c a^\dagger a \\
&+ g\sum_{F,F'} \left(a^\dagger D_0(F,F') + D_0^\dagger(F,F')a \right) \\
&+ \varepsilon a^\dagger + \varepsilon^* a
\end{aligned}
\tag{6.6}
$$
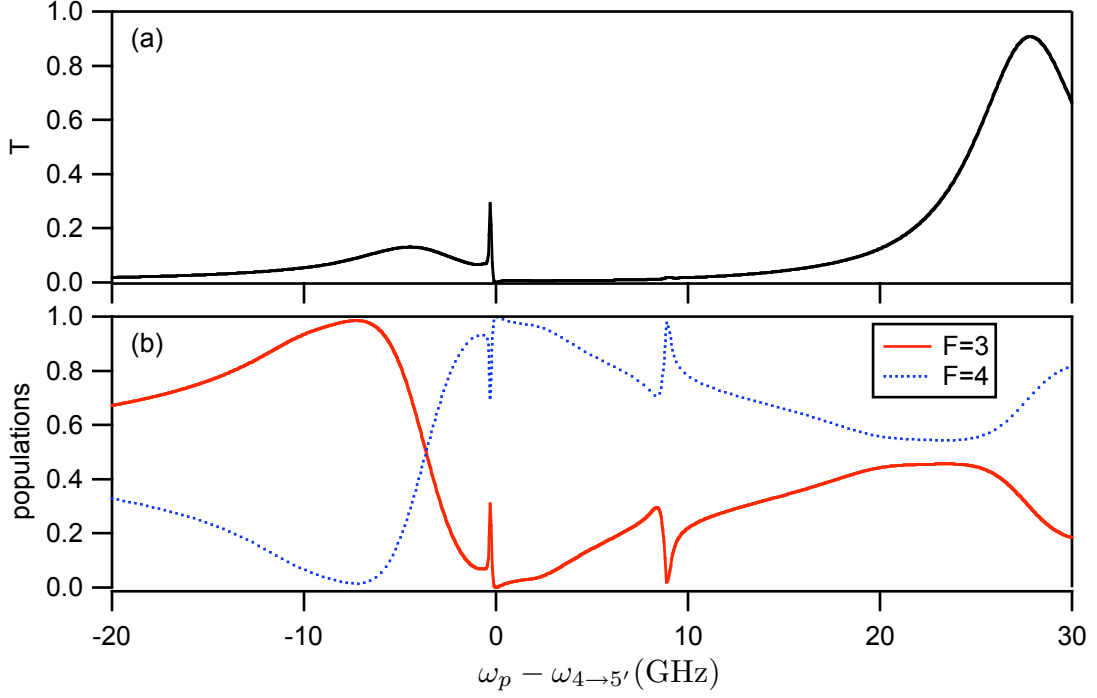
Figure 6.8: Normalized transmission T (a) and atomic populations in the hyperfine ground states (b) as a function of probe detuning, with the cavity frequency fixed at $\omega_c = \omega_{4\to5'} + 20\text{GHz}$. Parameters are the same as in Fig. 6.6. Note that because the cavity drive is weak, nearly all of the population is in the ground states.

and the master equation for the evolution of the density matrix is

$$\dot{\rho} = -i[H_3, \rho] + \kappa \mathcal{D}[a]\rho + \gamma \sum_q \mathcal{D}\Big[\sum_{F,F'} D_q(F, F')\Big]\rho \qquad (6.7)$$

Note that in this limit, we assume that all atomic decays of a given polarization are into a common reservoir (without regard for the initial F and final F'). From this master equation, we find the steady-state density matrix $\dot{\rho}_{ss}$ and the steady-state normalized transmission T, plotted versus probe and cavity detunings in Fig. 6.6.

These transmission spectra reflect the structure of the eigenvalues plotted in Fig. 6.5. Of particular interest are the sharp transmission peaks at $\omega_p \approx \omega_{4\to5'} - 0.3$ GHz and $\omega_p \approx \omega_{4\to5'} + 8.9$ GHz, which appear to correspond to a dual resonance condition. These transmission features are particularly strong at the cavity detunings where transition frequencies of H_2 cross, which for the parameters
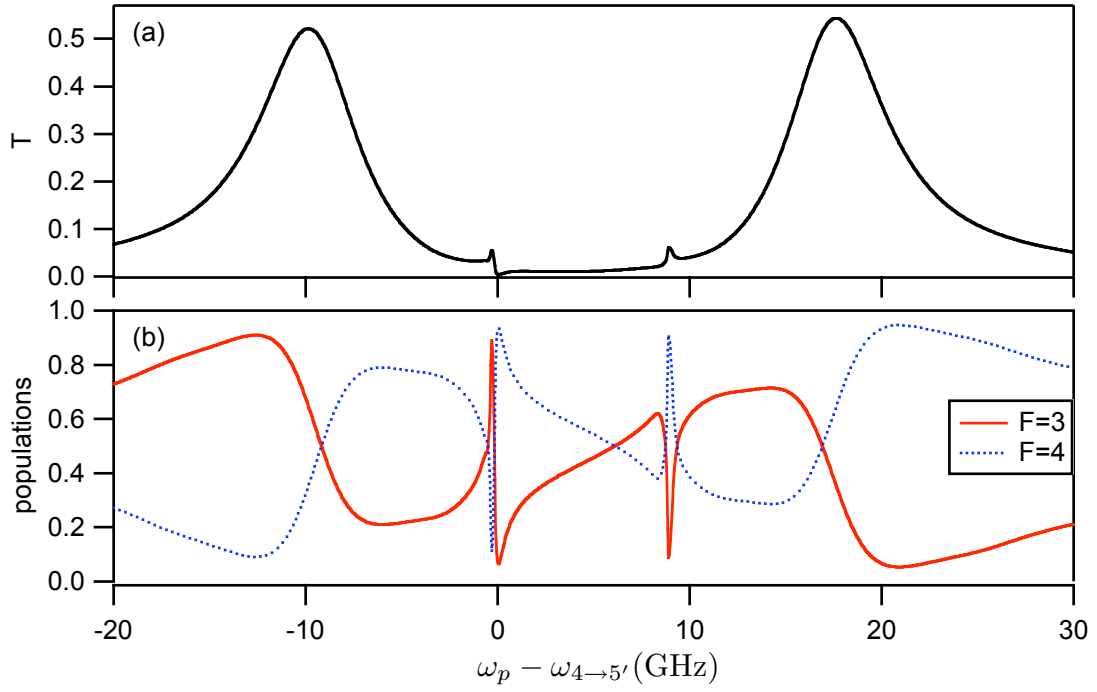
Figure 6.9: Normalized transmission T (a) and atomic populations in the hyperfine ground states (b) as a function of probe detuning, with the cavity frequency fixed at $\omega_c = \omega_{4\to5'} + 4\text{GHz}$. Parameters are the same as in Fig. 6.6. Note that because the cavity drive is weak, nearly all of the population is in the ground states.

$(g, \kappa, \gamma) = (17, 4.4, 0.0026)\text{GHz}$ are $\omega_c \approx \omega_{4\to5'} + 20$ GHz and $\omega_c \approx \omega_{4\to5'} - 13$ GHz. The steady-state transmission at these cavity detunings is plotted in Figs. 6.7 and 6.8 versus probe detuning.

The sharp peaks in cavity transmission are associated with strong optical pumping between the ground-state hyperfine manifolds. In Fig. 6.9(a), we plot the normalized steady-state transmission versus probe detuning with the cavity frequency fixed between the frequencies of the $F = 3 \to F'$ and $F = 4 \to F'$ transitions. In addition to the large peaks associated with single transitions are two smaller narrow peaks associated with the dual resonances. In Fig. 6.9(b), we show the populations in the $F = 3$ and $F = 4$ ground-state manifolds. The atomic population is strongly pumped into the $F = 3$ manifold at the $\omega_p \approx \omega_{4\to5'} - 0.3$ GHz peak, and strongly pumped into $F = 4$ at the peak near $\omega_p \approx \omega_{4\to5'} + 8.9$ GHz.

Future experiments with single atoms coupled to photonic band gap cavities should

be able to study these sharp features. They should be relatively easy to measure because although they are narrow in probe frequency (which is easily controlled), they are fairly wide in cavity frequency (which is harder to control experimentally).

Chapter 7

Computer Code

This chapter describes the computer code used to perform the calculations in this thesis. Representative samples of the code are reproduced in `this typeface`. Unless otherwise noted, all of the code is built upon the Quantum Optics Toolbox (Version 0.15) [59, 60] written by Sze Tan for use for use with the MATLAB® language. This code evolved with major contributions from Dave Boozer, Scott Parkins, and John Stockton.

7.1   Basics

It is important to note that as of Version 0.15 of the Quantum Optics Toolbox, there are some bugs in the routines which calculate Wigner symbols. The remedy is to define the following functions:

```
function D = ddelta(a,b,c)
    D = factorial(a+b-c)*factorial(b+c-a)*factorial(c+a-b)/factorial(a+b+c+1);


function b = fact(a)
    b=factorial(a);
```

It is also highly useful to add the following function to the Toolbox:

```
function super = decay(lower) % The decay superoperator
    super = 2*spre(lower)*spost(lower')-spre(lower'*lower)-spost(lower'*lower);
```

This function takes a lowering operator as an argument and constructs the corresponding zero-temperature decay superoperator. Once these functions are saved in

m-files in the Toolbox directory, we are ready to perform our calculations.

We begin with the Jaynes-Cummings system described in Section 3.1. The following function calculates the steady state:

```
function [rhoss, a, d, H]=jaynescummings(g,kappa,gamma,cavfreq,probe,E,W,N)
% g is half the single-photon Rabi frequency
% kappa is the cavity linewidth (half width half max)
% gamma is the atom HWHM
% cavfreq is the cavity-atom detuning = (cavity frequency)-(atom frequency)
% probe is the probe-atom detuning
% E is the amplitude of the cavity drive field.  E*E'/(kappa^2) is the empty
%    cavity on resonance photon number
% W is the Rabi frequency of the classical field driving the atom.  W=gamma at
%    saturation intensity
% Either E or W should be zero, depending on whether the probe drives the atom
%    or the cavity.
% N is the size of the Fock space for the cavity field, i.e. the maximum number
%    of photons within the basis is (N-1)

atomfreq = 0;           % the atom-atom detuning is of course zero
dc = cavfreq - probe;   % cavity-probe detuning
d0 = atomfreq - probe;  % atom-probe detuning

% Define operators
ida = identity(N);      % identity for the cavity field
idatom = identity(2);   % identity for the atom
a = tensor(destroy(N), idatom); % the cavity annihilation operator
d = tensor(ida, sigmam);        % lowering operator for the atom

% The Hamiltonian
H = dc*a'*a + d0*d'*d + g*(d'*a + a'*d) + E*a + E'*a' + W*d + W'*d';

% The Liouvillian
L = -i*(spre(H) - spost(H)) + kappa*decay(a) + gamma*decay(d);

% Calculate the steady-state
rhoss = steady(L);      % steady state density matrix
```

This function is similar to the Toolbox example contained in `probss.m`. Instead of returning expectation values of operators, however, it returns the operators themselves. Typically, a script would call this function many times over, varying some parameters each time. The script would calculate any desired expectation values and store them in a file, from which they could be recalled for further analysis or plotting. For example, here is a script that could be used to calculate various properties of the Jaynes-Cummings system:

```
tic % initialize timer
% all frequencies in MHz
g = 33.9;
kappa = 4.1;
gamma = 2.6;
cavfreq = 0;
Nempty = 0.01;  % empty cavity on resonance photon number
E = kappa*sqrt(Nempty);  % we will drive the cavity
W = 0;
N = 3;


% We will vary probe detuning
first = -50;    % first probe detuning to calculate
step = 1;     % step size
Numsteps = 101; % how many points we will calculate
last = first + step*(Numsteps-1); % last detuning we will calculate


% initialize output variables
ada = zeros(Numsteps,1);    % photon number ("a-dagger a")
g2 = zeros(Numsteps,1);     % intensity correlation at zero time delay ("g2 of
                            %    zero")
comm = zeros(Numsteps,1);   % commutator of annihilation and creation operators
inv = zeros(Numsteps,1);    % population in atomic excited state ("inversion")
rholight = zeros(N,N,Numsteps); % density matrix of cavity field, tracing over
                            %    the atom


for k=1:Numsteps
    probe = first + step*(k-1);
    [rhoss, a, d, H]=jaynescummings(g,kappa,gamma,cavfreq,probe,E,W,N);
```

```
        ada(k) = expect(a'*a, rhoss)/Nempty;    % normalize to empty cavity

        g2(k) = expect(a'*a'*a*a, rhoss)/(expect(a'*a, rhoss)^2);

        comm(k) = expect(a*a'-a'*a, rhoss);

        inv(k) = expect(d'*d, rhoss);

        rholight(1:N,1:N,k) = full(double(ptrace(rhoss,1)));

end

toc % print elapsed time on timer

% save results to a file

     ada_suffix = real(ada);

      g2_suffix = real(g2);

    comm_suffix = real(comm);

     inv_suffix = real(inv);

rholight_suffix = rholight;

    save filename_suffix ...

        *suffix;
```

This script would be saved to an m-file, which by convention would be named `jaynescummings_w_suffix.m`. Typically, the core function would be rigorously tested and then used (unmodified) many times, while the script would be frequently altered to calculate different properties as a function of different parameters. Each time, the suffix would change, so that saved data would not be overwritten. The script associated with each file would also be saved as a record of what parameters were used to generate the data.

In the above script, one of the computed values is $\langle [a, a^\dagger] \rangle$. This might seem like a strange thing to calculate since we expect that $[a, a^\dagger] = 1$. While this is true for an infinite Fock basis, in our finite basis where the photon number is $\{0, \dots N - 1\}$, we have $[a, a^\dagger] = 1 - |N - 1\rangle N \langle N - 1|$. We use this operator to check how much population is in the highest Fock state of our basis. If that population gets too large, then we suspect that a bigger basis is needed for an accurate calculation. Note that due to the multiple-photon resonance effects discussed in Section 4.3, it is possible for the population in a higher Fock state to be larger than the population in a lower Fock state even when the empty cavity on resonance photon number is less than one, so care is needed.

Besides the finite basis, other problems can arise when solving for the steady state. The Toolbox uses the inverse power method to find the null space of the Liouvillian (the steady-state density matrix). This method is stochastic and sometimes fails without warning. Anecdotally, this is more likely when solving problems with large Hilbert spaces and very weak excitation. If the Liouvillian does not have a unique steady state, the method will generally fail. It is a good idea to check the density matrix returned from the `steady` routine to see that it is physically reasonable. For example, the matrix must be Hermitian, and diagonal elements should always be between 0 and 1. Most scripts we have used have a few different checks on the density matrix to find when `steady` has failed, though these tests are by no means exhaustive.

One way to reduce the number of failures of the inverse power method is to make its tolerance more strict. This can be done by modifying the Toolbox file `steady.m`, changing the line

```
tol = 1e-6;
```

to, for example,

```
tol = eps;
```

This sets the tolerance to the level of machine precision. It may be necessary to increase `maxiter`, the maximum number of iterations that `steady.m` allows, when reducing the tolerance. Tightening the tolerance will generally increase the time it takes to perform the calculations, so this should be done only when necessary.

7.2 Vacuum Rabi Calculations

Now we will present code for calculations of the more complex models described in Chapter 3. In these models, the atom has nine ground states corresponding to $F = 4, m_F \in \{-4, \ldots + 4\}$, and eleven excited states representing $F' = 5, m'_F \in \{-5, \ldots + 5\}$. It is useful to create index functions to keep track of which atomic states correspond to which rows and columns of the matrices we will use to describe our operators.

```
function n = index_g_45(F,m)
if ((m <= F) & (m >= -F))
    switch (F)
        case 4, n = 5 + m;
        otherwise, error('F out of range in index_g_45');
    end
else
    error('m out of range in index_g_45');
end


function n = index_e_45(F,m)
if ((m <= F) & (m >= -F))
    switch (F)
        case 5, n = 15 + m;
        otherwise, error('F out of range in index_e_45');
    end
else
    error('m out of range in index_e_45');
end
```

With the indices defined, we now present the code for a single mode cavity coupled to the $F = 4 \rightarrow F' = 5$ transition of one atom:

```
function [rhoss, a, H, g4_m4, g4_m3, g4_m2, g4_m1, g4_p0, g4_p1, g4_p2, ...
    g4_p3, g4_p4] = kmb_Cs133_4_to_5prime(gamma, kappa, g, Na, cavity_freq,...
    probe_freq, eps_p, p_xi, p_psi,depth)
% steady state of one atom with a 4->5' transition coupled to a single mode
%    cavity.
%
% gamma is atomic HWHM
% kappa is cavity HWHM
% g is half the single photon Rabi frequency for 4,4->5'5' (cycling transition)
% Na is number of Fock states for cavity mode
% cavity_freq is cavity frequency relative to F'=5->F=4 transition
% probe_freq is probe frequency relative to F'=5->F=4 transition
% eps_p is strength of probe.  Empty cavity on resonance photon number is
%    |eps_p|^2/kappa^2
```

```
% p_xi, p_psi are angles that set the cavity polarization

%xi = 0 for 0 polarization, pi/2 for p or m polarization

%psi = 0 for p polarization , pi/2 for m polarization

% depth is the FORT depth (should be a positive number).  Used for Stark shifts.


f_5 = 0;


d5 = f_5 - probe_freq;

dc = cavity_freq - probe_freq;            % (cavity freq) - (probe freq)


Ng4 = 2*4 + 1;                            % number of ground states

Ne5 = 2*5 + 1;                            % number of excited states

Natomic = Ng4+Ne5;                        % total number of atomic states


%-------------------- Atomic lowering operators -----------------------

%    [Am,A0,Ap] = murelf(Fg,Fe,Jg,Je,I)

%    Calculate the sparse dipole operator lowering matrices for a Fg to Fe

%     transition using the "murelf" routine. Returned matrix is of size

%     (2*Fg+1) by (2*Fe+1).

%    Change minus sign for 0-polarized transitions to be consistent with

%    Steck notes.

% lowering operators for 5' --> 4

Fg=4; Fe=5;

[cg_m,cg_0,cg_p] = murelf(Fg,Fe,1/2,3/2,7/2);


g_m_e = sparse(Natomic, Natomic);

g_0_e = sparse(Natomic, Natomic);

g_p_e = sparse(Natomic, Natomic);


g_m_e(index_g_45(4,-4):index_g_45(4,4),index_e_45(5,-5):index_e_45(5,5)) = cg_m;

g_0_e(index_g_45(4,-4):index_g_45(4,4),index_e_45(5,-5):index_e_45(5,5)) =-cg_0;

g_p_e(index_g_45(4,-4):index_g_45(4,4),index_e_45(5,-5):index_e_45(5,5)) = cg_p;


g4_m_e5 = tensor(qo(g_m_e),identity(Na));

g4_0_e5 = tensor(qo(g_0_e),identity(Na));

g4_p_e5 = tensor(qo(g_p_e),identity(Na));
```

```
%-------------------- Atomic projection operators ---------------------
%project onto F = 4 ground state subspace
g4_g4 = sparse(Natomic, Natomic);
g4_g4(index_g_45(4,-4):index_g_45(4,4), index_g_45(4,-4):index_g_45(4,4))...
    =eye(Ng4);
g4_g4 = tensor(qo(g4_g4),identity(Na));


%project onto F' = 5 excited state subspace
e5_e5 = sparse(Natomic, Natomic);
e5_e5(index_e_45(5,-5):index_e_45(5,5), index_e_45(5,-5):index_e_45(5,5))...
    =eye(Ne5);
e5_e5 = tensor(qo(e5_e5),identity(Na));


%project onto different mF's of F'=5
e5_m5 = sparse(Natomic, Natomic);
e5_m5(index_e_45(5,-5), index_e_45(5,-5))=1;
e5_m5 = tensor(q0(e5_m5),identity(Na));


e5_m4 = sparse(Natomic, Natomic);
e5_m4(index_e_45(5,-4), index_e_45(5,-4))=1;
e5_m4 = tensor(q0(e5_m4),identity(Na));


e5_m3 = sparse(Natomic, Natomic);
e5_m3(index_e_45(5,-3), index_e_45(5,-3))=1;
e5_m3 = tensor(q0(e5_m3),identity(Na));


e5_m2 = sparse(Natomic, Natomic);
e5_m2(index_e_45(5,-2), index_e_45(5,-2))=1;
e5_m2 = tensor(q0(e5_m2),identity(Na));


e5_m1 = sparse(Natomic, Natomic);
e5_m1(index_e_45(5,-1), index_e_45(5,-1))=1;
e5_m1 = tensor(q0(e5_m1),identity(Na));


e5_p0 = sparse(Natomic, Natomic);
```

```
e5_p0(index_e_45(5, 0), index_e_45(5, 0))=1;
e5_p0 = tensor(q0(e5_p0),identity(Na));


e5_p1 = sparse(Natomic, Natomic);
e5_p1(index_e_45(5, 1), index_e_45(5, 1))=1;
e5_p1 = tensor(q0(e5_p1),identity(Na));


e5_p2 = sparse(Natomic, Natomic);
e5_p2(index_e_45(5, 2), index_e_45(5, 2))=1;
e5_p2 = tensor(q0(e5_p2),identity(Na));


e5_p3 = sparse(Natomic, Natomic);
e5_p3(index_e_45(5, 3), index_e_45(5, 3))=1;
e5_p3 = tensor(q0(e5_p3),identity(Na));


e5_p4 = sparse(Natomic, Natomic);
e5_p4(index_e_45(5, 4), index_e_45(5, 4))=1;
e5_p4 = tensor(q0(e5_p4),identity(Na));


e5_p5 = sparse(Natomic, Natomic);
e5_p5(index_e_45(5, 5), index_e_45(5, 5))=1;
e5_p5 = tensor(q0(e5_p5),identity(Na));


%-------------------- Photon annhilation operator ---------------------
a = tensor(identity(Natomic), destroy(Na));

%-------------------- Hamiltonian -------------------------------------
H0 = d5*e5_e5 + dc*a'*a;


H1 = g*(a'*g4_p_e5 + g4_p_e5'*a)*sin(p_xi)*cos(p_psi) ...
    +g*(a'*g4_0_e5 + g4_0_e5'*a)*cos(p_xi) ...
    +g*(a'*g4_m_e5 + g4_m_e5'*a)*sin(p_xi)*sin(p_psi);


H3 = eps_p*a + eps_p'*a';


%stark shifts from FORT
```

```
H4 = -0.1751*(e5_m5 + e5_p5)*depth ...
    + -0.0586*(e5_m4 + e5_p4)*depth ...
    +  0.0319*(e5_m3 + e5_p3)*depth ...
    +  0.0966*(e5_m2 + e5_p2)*depth ...
    +  0.1354*(e5_m1 + e5_p1)*depth ...
    +  0.1484*(         e5_p0)*depth;


H = H0 + H1 + H3 + H4;


%-------------------- Liouvillian ------------------------------------
% Hamiltonian
L0 = -i*(spre(H) - spost(H));


% cavity decay
L1  = kappa*decay(a);


% 5'->4 decays
L2  = gamma*decay(g4_m_e5) ...
     +gamma*decay(g4_0_e5) ...
     +gamma*decay(g4_p_e5);


L =  L0 + L1 + L2;


%-------------------- Steady State ------------------------------------
rhoss = steady(L);


%project onto F = 4 ground state with various mF's
g4_m4 = sparse(Natomic, Natomic);
g4_m4(index_g_45(4,-4), index_g_45(4,-4))=1;
g4_m4 = tensor(qo(g4_m4),identity(Na));


g4_m3 = sparse(Natomic, Natomic);
g4_m3(index_g_45(4,-3), index_g_45(4,-3))=1;
g4_m3 = tensor(qo(g4_m3),identity(Na));


g4_m2 = sparse(Natomic, Natomic);
```

```
g4_m2(index_g_45(4,-2), index_g_45(4,-2))=1;
g4_m2 = tensor(qo(g4_m2),identity(Na));


g4_m1 = sparse(Natomic, Natomic);
g4_m1(index_g_45(4,-1), index_g_45(4,-1))=1;
g4_m1 = tensor(qo(g4_m1),identity(Na));


g4_p0 = sparse(Natomic, Natomic);
g4_p0(index_g_45(4, 0), index_g_45(4, 0))=1;
g4_p0 = tensor(qo(g4_p0),identity(Na));


g4_p1 = sparse(Natomic, Natomic);
g4_p1(index_g_45(4, 1), index_g_45(4, 1))=1;
g4_p1 = tensor(qo(g4_p1),identity(Na));


g4_p2 = sparse(Natomic, Natomic);
g4_p2(index_g_45(4, 2), index_g_45(4, 2))=1;
g4_p2 = tensor(qo(g4_p2),identity(Na));


g4_p3 = sparse(Natomic, Natomic);
g4_p3(index_g_45(4, 3), index_g_45(4, 3))=1;
g4_p3 = tensor(qo(g4_p3),identity(Na));


g4_p4 = sparse(Natomic, Natomic);
g4_p4(index_g_45(4, 4), index_g_45(4, 4))=1;
g4_p4 = tensor(qo(g4_p4),identity(Na));
```

In this function, I have followed the sign conventions of Steck [58] for the Clebsch-Gordan elements. Upon further consideration, I believe that for future development of the code it would be simpler to use the conventions of the Toolbox itself. This would eliminate the need to insert factors of -1 in various places. Furthermore, Dave Boozer has written a very clear set of notes on angular momentum in his thesis [61] which are consistent with the conventions of the Toolbox. These sign conventions do not represent real physics and do not affect the outcome provided that they are used consistently. Mixing conventions, however, could lead to errors.

Here is a function for finding the steady state of a single atom with a $F = 4 \rightarrow F' = 5$ transition coupled to a two-mode cavity:

```
function [rhoss, a, b, H, H1, g4_m4, g4_m3, g4_m2, g4_m1, g4_p0, g4_p1, ...
    g4_p2, g4_p3, g4_p4] = kmb_Cs133_4_to_5prime_twomode(gamma, kappa_c, ...
    kappa_d, g, Nc, Nd, cavity_freq, probe_freq, splitting, eps_a, eps_b, depth)
% steady state of one atom with a 4->5' transition coupled to a cavity with two
%    orthogonal linear modes
% mode "a" (sometimes called "c" -- sorry) is polarized along z
% mode "b" (sometimes called "d" -- sorry) is polarized along y
%
% gamma is atomic HWHM
% kappa_c is cavity HWHM for z mode
% kappa_d is cavity HWHM for y mode
% g is half the single photon Rabi frequency for 4,4->5'5'
% Nc is the number of Fock states for z cavity mode
% Nd is the number of Fock states for y cavity mode
% cavity_freq is AVERAGE cavity frequency relative to F'=5->F=4 transition
% probe_freq is probe frequency relative to F'=5->F=4 transition
% splitting is HALF of the difference of the two cavity frequencies
%    splitting = ((freq of y mode)-(freq of z mode))/2
% eps_c is the drive of the z mode
% eps_d is the drive of the y mode
% depth is the FORT depth used for calculating stark shifts. Should be positive.
% the FORT is assumed to have the polarization of the z mode


f_5 = 0;
d5 = f_5 - probe_freq;
dc = cavity_freq - splitting - probe_freq;
dd = cavity_freq + splitting - probe_freq;


Ng4 = 2*4 + 1;                          % number of states in g4 manifold
Ne5 = 2*5 + 1;                          % number of states in e5 manifold


Natomic = Ng4+Ne5;


%-------------------- Atomic lowering operators ----------------------
```

```
%   Change minus sign for 0-polarized transitions to be consistent with
%   Steck notes.
% lowering operators for 5' --> 4
Fg=4; Fe=5;
[cg_m,cg_0,cg_p] = murelf(Fg,Fe,1/2,3/2,7/2);


g_m_e = sparse(Natomic, Natomic);
g_0_e = sparse(Natomic, Natomic);
g_p_e = sparse(Natomic, Natomic);


g_m_e(index_g_45(4,-4):index_g_45(4,4),index_e_45(5,-5):index_e_45(5,5)) = cg_m;
g_0_e(index_g_45(4,-4):index_g_45(4,4),index_e_45(5,-5):index_e_45(5,5)) =-cg_0;
g_p_e(index_g_45(4,-4):index_g_45(4,4),index_e_45(5,-5):index_e_45(5,5)) = cg_p;


g4_m_e5 = tensor(qo(g_m_e),identity(Nc), identity(Nd));
g4_0_e5 = tensor(qo(g_0_e),identity(Nc), identity(Nd));
g4_p_e5 = tensor(qo(g_p_e),identity(Nc), identity(Nd));


g4_d_e5 = i*sqrt(0.5)*(g4_p_e5 + g4_m_e5); % corresponds to y-polarization


%-------------------- Atomic projection operators ----------------------
%project onto F = 4 ground state subspace
g4_g4 = sparse(Natomic, Natomic);
g4_g4(index_g_45(4,-4):index_g_45(4,4), index_g_45(4,-4):index_g_45(4,4))...
    =eye(Ng4);
g4_g4 = tensor(qo(g4_g4),identity(Nc), identity(Nd));


%project onto F' = 5 excited state subspace
e5_e5 = sparse(Natomic, Natomic);
e5_e5(index_e_45(5,-5):index_e_45(5,5), index_e_45(5,-5):index_e_45(5,5))...
    =eye(Ne5);
e5_e5 = tensor(qo(e5_e5),identity(Nc), identity(Nd));


%project onto different mF's of F'=5
e5_m5 = sparse(Natomic, Natomic);
e5_m5(index_e_45(5,-5), index_e_45(5,-5))=1;
```

```
e5_m5 = tensor(qo(e5_m5),identity(Nc), identity(Nd));


e5_m4 = sparse(Natomic, Natomic);
e5_m4(index_e_45(5,-4), index_e_45(5,-4))=1;
e5_m4 = tensor(qo(e5_m4),identity(Nc), identity(Nd));


e5_m3 = sparse(Natomic, Natomic);
e5_m3(index_e_45(5,-3), index_e_45(5,-3))=1;
e5_m3 = tensor(qo(e5_m3),identity(Nc), identity(Nd));


e5_m2 = sparse(Natomic, Natomic);
e5_m2(index_e_45(5,-2), index_e_45(5,-2))=1;
e5_m2 = tensor(qo(e5_m2),identity(Nc), identity(Nd));


e5_m1 = sparse(Natomic, Natomic);
e5_m1(index_e_45(5,-1), index_e_45(5,-1))=1;
e5_m1 = tensor(qo(e5_m1),identity(Nc), identity(Nd));


e5_p0 = sparse(Natomic, Natomic);
e5_p0(index_e_45(5, 0), index_e_45(5, 0))=1;
e5_p0 = tensor(qo(e5_p0),identity(Nc), identity(Nd));


e5_p1 = sparse(Natomic, Natomic);
e5_p1(index_e_45(5, 1), index_e_45(5, 1))=1;
e5_p1 = tensor(qo(e5_p1),identity(Nc), identity(Nd));


e5_p2 = sparse(Natomic, Natomic);
e5_p2(index_e_45(5, 2), index_e_45(5, 2))=1;
e5_p2 = tensor(qo(e5_p2),identity(Nc), identity(Nd));


e5_p3 = sparse(Natomic, Natomic);
e5_p3(index_e_45(5, 3), index_e_45(5, 3))=1;
e5_p3 = tensor(qo(e5_p3),identity(Nc), identity(Nd));


e5_p4 = sparse(Natomic, Natomic);
e5_p4(index_e_45(5, 4), index_e_45(5, 4))=1;
```

```
e5_p4 = tensor(qo(e5_p4),identity(Nc), identity(Nd));


e5_p5 = sparse(Natomic, Natomic);
e5_p5(index_e_45(5, 5), index_e_45(5, 5))=1;
e5_p5 = tensor(qo(e5_p5),identity(Nc), identity(Nd));


%-------------------- Photon annhilation operator ---------------------
a = tensor(identity(Natomic), destroy(Nc), identity(Nd));
b = tensor(identity(Natomic), identity(Nc), destroy(Nd));


%------------------- Hamiltonian -------------------------------------
H0 = d5*e5_e5 + dc*a'*a + dd*b'*b;


H1 = g*(a'*g4_0_e5 + g4_0_e5'*a)...
    + g*(b'*g4_d_e5 + g4_d_e5'*b);


H3 = eps_a*a + eps_a'*a' + eps_b*b + eps_b'*b';


%stark shifts from FORT
H4 = -0.1751*(e5_m5 + e5_p5)*depth ...
    + -0.0586*(e5_m4 + e5_p4)*depth ...
    +  0.0319*(e5_m3 + e5_p3)*depth ...
    +  0.0966*(e5_m2 + e5_p2)*depth ...
    +  0.1354*(e5_m1 + e5_p1)*depth ...
    +  0.1484*(        e5_p0)*depth;


H = H0 + H1 + H3 + H4;


%-------------------- Liouvillian ------------------------------------
% Hamiltonian
L0 = -i*(spre(H) - spost(H));


% cavity decay
L1  = kappa_c*decay(a) + kappa_d*decay(b);


% 5'->4 decays
```

```
L2  = gamma*decay(g4_m_e5) ...
     +gamma*decay(g4_0_e5) ...
     +gamma*decay(g4_p_e5);


L =  L0 + L1 + L2;


%-------------------- Steady State ------------------------------------
rhoss = steady(L);


%project onto F = 4 ground state with various mF's
g4_m4 = sparse(Natomic, Natomic);
g4_m4(index_g_45(4,-4), index_g_45(4,-4))=1;
g4_m4 = tensor(qo(g4_m4),identity(Nc),identity(Nd));


g4_m3 = sparse(Natomic, Natomic);
g4_m3(index_g_45(4,-3), index_g_45(4,-3))=1;
g4_m3 = tensor(qo(g4_m3),identity(Nc),identity(Nd));


g4_m2 = sparse(Natomic, Natomic);
g4_m2(index_g_45(4,-2), index_g_45(4,-2))=1;
g4_m2 = tensor(qo(g4_m2),identity(Nc),identity(Nd));


g4_m1 = sparse(Natomic, Natomic);
g4_m1(index_g_45(4,-1), index_g_45(4,-1))=1;
g4_m1 = tensor(qo(g4_m1),identity(Nc),identity(Nd));


g4_p0 = sparse(Natomic, Natomic);
g4_p0(index_g_45(4, 0), index_g_45(4, 0))=1;
g4_p0 = tensor(qo(g4_p0),identity(Nc),identity(Nd));


g4_p1 = sparse(Natomic, Natomic);
g4_p1(index_g_45(4, 1), index_g_45(4, 1))=1;
g4_p1 = tensor(qo(g4_p1),identity(Nc),identity(Nd));


g4_p2 = sparse(Natomic, Natomic);
g4_p2(index_g_45(4, 2), index_g_45(4, 2))=1;
```

```
g4_p2 = tensor(qo(g4_p2),identity(Nc),identity(Nd));


g4_p3 = sparse(Natomic, Natomic);
g4_p3(index_g_45(4, 3), index_g_45(4, 3))=1;
g4_p3 = tensor(qo(g4_p3),identity(Nc),identity(Nd));


g4_p4 = sparse(Natomic, Natomic);
g4_p4(index_g_45(4, 4), index_g_45(4, 4))=1;
g4_p4 = tensor(qo(g4_p4),identity(Nc),identity(Nd));
```

7.3   Photon Blockade

Here is an example of a script which calls `kmb_Cs133_4_to_5prime_twomode`. This script,
`kmb_Cs133_4_to_5prime_twomode_w_149.m`, generated the data plotted in Fig. 4.2(b).

```
addpath(genpath('/home/Kevin/qotoolboxV015'));% put the Toolbox in the path
tic


gamma = 2.6;
kappa_a = 4.1;
kappa_b = 4.1;
kappa_avg = (kappa_a + kappa_b)/2;
g = 33.9;
splitting = 0;
Na = 3; %size of Fock basis
Nb = 3;


N = 101;        %number of points in probe detuning
Ng = 1;         %number of points in coupling
Nd = 1;         %number of points in FORT depth
start = -50;   %start freq
stepsize = 1;      %stepsize for probe
endfreq = start + stepsize*(N-1)


ada   = 13*ones(N, Ng, Nd); % "a-dagger a"
bdb   = 13*ones(N, Ng, Nd); % "b-dagger b"
```

```
g2a    = 13*ones(N, Ng, Nd); % "g-2 of zero for mode a"

g2b    = 13*ones(N, Ng, Nd); % "g-2 of zero for mode b"

cdc    = 13*ones(N, Ng, Nd); % "c-dagger c" (rotated polarization mode)

ddd    = 13*ones(N, Ng, Nd); % "d-dagger d" (rotated polarization mode)

comma = 13*ones(N, Ng, Nd); % "commutator of a and a-dagger"

commb = 13*ones(N, Ng, Nd); % "commutator of b and b-dagger"

m4     = 13*ones(N, Ng, Nd); % population in ground state F=4, mF=-4

m3     = 13*ones(N, Ng, Nd); % population in ground state F=4, mF=-3

m2     = 13*ones(N, Ng, Nd); % population in ground state F=4, mF=-2

m1     = 13*ones(N, Ng, Nd); % population in ground state F=4, mF=-1

p0     = 13*ones(N, Ng, Nd); % population in ground state F=4, mF=0

p1     = 13*ones(N, Ng, Nd); % population in ground state F=4, mF=1

p2     = 13*ones(N, Ng, Nd); % population in ground state F=4, mF=2

p3     = 13*ones(N, Ng, Nd); % population in ground state F=4, mF=3

p4     = 13*ones(N, Ng, Nd); % population in ground state F=4, mF=4

force = 13*ones(N, Ng, Nd); % interaction term, useful for calculating force
                           %    on the atom

trace_of_rhoss_squared = 0*ones(N, Ng, Nd); % should be less than 1

max_dif_of_rhoss_and_rhoss_dagger = 0*ones(N, Ng, Nd); % should be 0

max_diag_element_of_rhoss = 0*ones(N, Ng, Nd); % should be less than 1

max_imag_of_diag_of_rhoss = 0*ones(N, Ng, Nd); % should be zero


Nempty = 0.05;

theta_in = 0;   % cavity drive field is linearly polarized and at an angle
                %    theta_in with respect to the z axis

eps_a = kappa_a*sqrt(Nempty)*cos(theta_in);

eps_b = kappa_b*sqrt(Nempty)*sin(theta_in);

theta_out = pi/4;   % if we were detecting linearly polarized photons
                    %    at the output at theta_out with respect to z.
                    %    These modes are "c" and "d"


cavity_freq = splitting;

depth = 0;

numberofpoints = 0;

for m=1:Nd
    %depth = (m-1)*38.5/20;
```

```
for j=1:Ng,
    %g = (j-1)*33.9/20;
for k=1:N,
    probe_freq = start + stepsize*(k-1);
    numberofpoints = numberofpoints+1;

    [rhoss, a, b, H, H1, g4_m4, g4_m3, g4_m2, g4_m1, g4_p0, g4_p1, g4_p2,...
     g4_p3, g4_p4] = kmb_Cs133_4_to_5prime_twomode(gamma, kappa_a, kappa_b,...
      g, Na, Nb, cavity_freq, probe_freq, splitting, eps_a, eps_b, depth);

    c = cos(theta_out)*a*sqrt(kappa_a) - sin(theta_out)*b*sqrt(kappa_b);
    d = sin(theta_out)*a*sqrt(kappa_a) + cos(theta_out)*b*sqrt(kappa_b);
    ada(k,j,m) = kappa_a*expect(a'*a, rhoss)/(Nempty*kappa_avg);
    bdb(k,j,m) = kappa_b*expect(b'*b, rhoss)/(Nempty*kappa_avg);
    cdc(k,j,m) = expect(c'*c, rhoss)/(Nempty*kappa_avg);
    ddd(k,j,m) = expect(d'*d, rhoss)/(Nempty*kappa_avg);
    g2a(k,j,m) = expect(a'*a'*a*a, rhoss)/(expect(a'*a, rhoss)^2);
    g2b(k,j,m) = expect(b'*b'*b*b, rhoss)/(expect(b'*b, rhoss)^2);
    comma(k,j,m) = expect(a*a'-a'*a, rhoss);
    commb(k,j,m) = expect(b*b'-b'*b, rhoss);
    m4(k,j,m) = expect(g4_m4, rhoss);
    m3(k,j,m) = expect(g4_m3, rhoss);
    m2(k,j,m) = expect(g4_m2, rhoss);
    m1(k,j,m) = expect(g4_m1, rhoss);
    p0(k,j,m) = expect(g4_p0, rhoss);
    p1(k,j,m) = expect(g4_p1, rhoss);
    p2(k,j,m) = expect(g4_p2, rhoss);
    p3(k,j,m) = expect(g4_p3, rhoss);
    p4(k,j,m) = expect(g4_p4, rhoss);
    force(k,j,m) = expect(H1, rhoss);
    trace_of_rhoss_squared(k,j,m) = abs(trace(rhoss*rhoss));
    max_dif_of_rhoss_and_rhoss_dagger(k,j,m) = ...
        full(max(max(abs(double(rhoss - rhoss')))));
    max_diag_element_of_rhoss(k,j,m) = full(max(abs(diag(double(rhoss)))));
    max_imag_of_diag_of_rhoss(k,j,m) = full(max(imag(diag(double(rhoss)))));
end
```

```
end

end


                        ada_149 = real(ada);
                        bdb_149 = real(bdb);
                        cdc_149 = real(cdc);
                        ddd_149 = real(ddd);
                        g2a_149 = real(g2a);
                        g2b_149 = real(g2b);
                      comma_149 = real(comma);
                      commb_149 = real(commb);
                         m4_149 = real(m4);
                         m3_149 = real(m3);
                         m2_149 = real(m2);
                         m1_149 = real(m1);
                         p0_149 = real(p0);
                         p1_149 = real(p1);
                         p2_149 = real(p2);
                         p3_149 = real(p3);
                         p4_149 = real(p4);
                      force_149 = real(force);
                        trs_149 = trace_of_rhoss_squared;
                      mdrrd_149 = max_dif_of_rhoss_and_rhoss_dagger;
                       mder_149 = max_diag_element_of_rhoss;
                       midr_149 = max_imag_of_diag_of_rhoss;
save              tempfile_149 ...
                        *_149;


toc
max_imag_ada = max(max(max(abs(imag(ada)))));
disp(['max_imag_ada = ' num2str(max_imag_ada)]);
max_imag_bdb = max(max(max(abs(imag(bdb)))));
disp(['max_imag_bdb = ' num2str(max_imag_bdb)]);
max_diff_ab_cd = max(max(max(abs(ada+bdb-cdc-ddd))));
disp(['max_diff_ab_cd = ' num2str(max_diff_ab_cd)]);
min_sum_of_4ground_states = min(min(min(real(m4+m3+m2+m1+p0+p1+p2+p3+p4))));
```

```
disp(['min_sum_of_4ground_states = ' num2str(min_sum_of_4ground_states)]);

max_sum_of_4ground_states = max(max(max(real(m4+m3+m2+m1+p0+p1+p2+p3+p4)))));

disp(['max_sum_of_4ground_states = ' num2str(max_sum_of_4ground_states)]);

pop_in_max_a = (1-min(min(min(real(comma))))))/Na;

disp(['pop_in_max_a = ' num2str(pop_in_max_a)]);

pop_in_max_b = (1-min(min(min(real(commb))))))/Nb;

disp(['pop_in_max_b = ' num2str(pop_in_max_b)]);

max_trace_of_rhoss_squared = max(max(max(trace_of_rhoss_squared)));

disp(['max_trace_of_rhoss_squared = ' num2str(max_trace_of_rhoss_squared)]);

violation_of_hermiticity = max(max(max(max_dif_of_rhoss_and_rhoss_dagger)));

disp(['violation_of_hermiticity = ' num2str(violation_of_hermiticity)]);

max_diag_element_of_all_rhoss = max(max(max(max_diag_element_of_rhoss)));

disp(['max_diag_element_of_all_rhoss = '...

    num2str(max_diag_element_of_all_rhoss)]);

max_imag_of_diag_of_all_rhoss = max(max(max(max_imag_of_diag_of_rhoss)));

disp(['max_imag_of_diag_of_all_rhoss = '...

    num2str(max_imag_of_diag_of_all_rhoss)]);

disp(['numberofpoints = ' num2str(numberofpoints)]);
```

The above script varies only the probe detuning, but it can be easily modified to also vary the coupling and FORT depth by changing `Ng` and `Nd`, and replacing the lines `%depth = (m-1)*38.5/20;` and `%g = (j-1)*33.9/20;` as appropriate. This is useful when calculating an averaged cavity transmission, as described in Section 3.4.

7.4   Thermal Averaging

The average transmissions were computed by using a mixture of MATLAB® and Igor Pro®. First, a matrix containing the transmission as a function of probe detuning, coupling strength, and Stark shifts was calculated as described above. Then, it was imported into an Igor experiment, where the wave was appropriately scaled. Wave scaling in Igor allows one to associate what parameters go with each data point. It furthermore allows one to perform linear interpolation between data points in a completely transparent manner by simply asking for the value of the data for a set of parameters which is inside the parameter range of the wave.

The Igor code which calculates the averaged cavity transmission from the pre-computed matrix is

```
Function GaussianDistributePosition3D(kbT, xnum, well,g0, depth, trans, ada)
//this function calculates the T spectrum averaged over one well
Variable kbT //actually this is kbT/U0
Variable xnum //how many steps to take in along axis
Variable well //registration number
Variable g0 //max value of g
Variable depth  //max FORT depth
Wave trans //wave which will have transmission spectrum (output wave)
Wave ada  //matrix containing T as a function of detuning, g, FORT


Variable lp = 852.358 //probe wavelength
Variable lf = 935.586 //FORT wavelength
Variable wf = 24.54 //FORT waist
Variable wp = 23.43 //probe waist
Variable xstep = lf*0.5 /xnum //integrates over one well
Variable i, j
Variable xv, g, fort , rv
Variable xm = 0.5*lf*(well + 0.5)
Variable denom=0
Variable sigmasq = kbT*lf*lf/(8*pi*pi)
Variable sigsqr = kbT*wf*wf/4
Variable rstep = 4*sqrt(sigsqr)/xnum
trans = 0
for(i=0;i<=xnum;i+=1)
for(j=0;j<=xnum;j+=1)
rv = j*rstep
xv = i*xstep +0.5*lf*(well)
g = abs(g0*cos(2*pi*xv/lp)*exp(-rv*rv/(wp*wp)) )
fort = depth*(sin(2*pi*xv/lf)^2)*exp(-2*rv*rv/(wf*wf) )
trans+=ada(x)(g)(fort)*exp(-(xv-xm)*(xv-xm)/(2*sigmasq))*rv*exp(-rv*rv/(2*sigsqr))
denom += exp(-(xv-xm)*(xv-xm)/(2*sigmasq) )*rv*exp(-rv*rv/(2*sigsqr))
endfor
endfor
```

```
trans /=denom

denom *= xstep*rstep/(sqrt(2*pi*sigmasq)*sigsqr)

return denom //this should be close to one

//it is the "integral" of the

//probability distribution function

End


Function UseGaussianPosition3D(kbT, xnum, numwells, g0, depth, trans, ada)

//this function calculates a T average over many wells

Variable kbT //(temperature)/(FORT depth)

Variable xnum //how many steps to take in along axis

Variable numwells //how many wells to use

//(starting with the best and working down)

// should be between 1 and 90.

Variable g0 //max value of g

Variable depth  //max FORT depth

Wave trans //wave which will have transmission spectrum

Wave ada  //matrix containing T as a function of detuning, g, FORT


Variable well

Variable i

Variable denom = 0

Duplicate/o trans trans_temp

trans =0

wave bestwells = root:bestwells   //this is a precomputed wave which

                                  //is a sorted list of the best wells

for(i=0;i<numwells;i+=1)

well = bestwells[i]

denom += GaussianDistributePosition3D(kbT,xnum,well,g0,depth,trans_temp,ada)

trans += trans_temp

endfor

trans /= numwells

denom /= numwells

return(denom)

End
```

```
Function MakeBestwells()
//this generates the wave bestwells,
//which holds an ordered list of which wells
//have the strongest coupling
Variable lf = 935.586 //FORT wavelength
Variable lc = 852.358 //probe wavelength
Make/d/o/n=90 wellgoodness
SetScale/P x -45,1,"",wellgoodness
Duplicate/o wellgoodness, bestwells
bestwells = x
wellgoodness = abs(cos(pi*(x+0.5)*lf/lc))
Sort/R wellgoodness bestwells, wellgoodness
End
```

7.5   Coupling to Multiple Excited Hyperfine Levels

We now present the code used to calculate atom-cavity interactions that involve multiple hyperfine levels as in Section 6.1. Again, it will be useful to define index functions to help keep track of the atomic states:

```
function n = index_g_Cs(F,m)
if ((m <= F) & (m >= -F))
    switch (F)
        case 3, n = 4 + m;
        case 4, n = 12 + m;
        otherwise, error('F out of range in index_g_Cs');
    end
else
    error('m out of range in index_g_Cs');
end

function n = index_e_Cs(F,m)
if ((m <= F) & (m >= -F))
    switch (F)
        case 2, n = 19 + m;
        case 3, n = 25 + m;
```

```
        case 4, n = 33 + m;

        case 5, n = 43 + m;

        otherwise, error('F out of range in index_e_Cs');

    end

else

    error('m out of range in index_e_Cs');

end
```

With the atomic basis thus defined, we present the code which calculates a single atom coupled to a one-mode resonator, appropriate when g is comparable to the excited state hyperfine splittings, but still much less than the ground state splitting:

```
function [rhoss, a, H, g4_m4, g4_m3, g4_m2, g4_m1, g4_p0, g4_p1, g4_p2,...
    g4_p3, g4_p4] = kmb_Cs133_scott(gamma, kappa, g, Na, cavity_freq,...
    probe_freq, eps_p, repump_freq, Wrp, p_xi, p_psi, r_xi, r_psi)
% One Cesium atom (D2 transition) coupled to cavity with one mode.
% Atom's 4->N' transitions are all coupled to cavity.
% A classical beam repumps from 3 ground state.
% This routine calculates the steady state density matrix of the system.
% All 4-> N' transitions (of the same polarization) couple to the same
%    environmental reservoir. All 3->N' also couple to one reservoir,
%    but this is NOT the same reservoir as 4->N'.  Thanks to Scott for
%    working out this rather subtle point in the derivation of the master
%    equation.

% gamma is atomic HWHM
% kappa is cavity HWHM
% g is half the single photon Rabi frequency for 4,4->5'5'
% Na is number of Fock states for cavity mode
% cavity_freq is cavity frequency relative to F'=5->F=4 transition
% probe_freq is probe frequency relative to F'=5->F=4 transition
% eps_p is strength of probe.  Empty cavity on resonance photon number
%    is eps_p^2/kappa^2.  eps_p must be real
% repump_freq is relative to F'=4->F=3
% Wrp is half of the Rabi freq for repump (Wrp=gamma at saturation)
%    Wrp must be real
% p_xi, p_psi are angles that set the cavity polarization
```

```
% r_xi, r_psi are angles that set the repump polarization

%xi = 0 for 0 polarization, pi/2 for p or m polarization

%psi = 0 for p polarization , pi/2 for m polarization


f_5 = 0;                    % excited state frequencies

f_4 = -251;

f_3 = -251-201;

f_2 = -251-201-151;


dr = f_4 - probe_freq + repump_freq; % (repump freq) - (probe freq) -

                                     %    (groundstate splitting)

d2 = f_2 - probe_freq;               % (F=2'->F=4 freq) - (probe freq)

d3 = f_3 - probe_freq;               % (F=3'->F=4 freq) - (probe freq)

d4 = f_4 - probe_freq;               % (F=4'->F=4 freq) - (probe freq)

d5 = f_5 - probe_freq;               % (F=5'->F=4 freq) - (probe freq)

dc = cavity_freq - probe_freq;       % (cavity freq) - (probe freq)


phi = 0;                             % phase of repump relative to probe


Ng3 = 2*3 + 1;                       % number of states in g3 manifold

Ng4 = 2*4 + 1;                       % number of states in g4 manifold


Ne2 = 2*2 + 1;                       % number of states in e2 manifold

Ne3 = 2*3 + 1;                       % number of states in e3 manifold

Ne4 = 2*4 + 1;                       % number of states in e4 manifold

Ne5 = 2*5 + 1;                       % number of states in e5 manifold


Natomic = Ng3 + Ng4 + Ne2 + Ne3 + Ne4 + Ne5;    % number of atomic states


%-------------------- Atomic lowering operators -----------------------

%   Change minus sign for 0-polarized transitions to be consistent with

%   Steck notes.

% lowering operators for 5' --> 4

Fg=4; Fe=5;

[cg_m,cg_0,cg_p] = murelf(Fg,Fe,1/2,3/2,7/2);
```

```
g_m_e = sparse(Natomic, Natomic);
g_0_e = sparse(Natomic, Natomic);
g_p_e = sparse(Natomic, Natomic);


g_m_e(index_g_Cs(4,-4):index_g_Cs(4,4),index_e_Cs(5,-5):index_e_Cs(5,5)) = cg_m;
g_0_e(index_g_Cs(4,-4):index_g_Cs(4,4),index_e_Cs(5,-5):index_e_Cs(5,5)) =-cg_0;
g_p_e(index_g_Cs(4,-4):index_g_Cs(4,4),index_e_Cs(5,-5):index_e_Cs(5,5)) = cg_p;


g4_m_e5 = tensor(qo(g_m_e),identity(Na));
g4_0_e5 = tensor(qo(g_0_e),identity(Na));
g4_p_e5 = tensor(qo(g_p_e),identity(Na));


% lowering operators for 4' --> 4
Fg=4; Fe=4;
[cg_m,cg_0,cg_p] = murelf(Fg,Fe,1/2,3/2,7/2);


g_m_e = sparse(Natomic, Natomic);
g_0_e = sparse(Natomic, Natomic);
g_p_e = sparse(Natomic, Natomic);


g_m_e(index_g_Cs(4,-4):index_g_Cs(4,4),index_e_Cs(4,-4):index_e_Cs(4,4)) = cg_m;
g_0_e(index_g_Cs(4,-4):index_g_Cs(4,4),index_e_Cs(4,-4):index_e_Cs(4,4)) =-cg_0;
g_p_e(index_g_Cs(4,-4):index_g_Cs(4,4),index_e_Cs(4,-4):index_e_Cs(4,4)) = cg_p;


g4_m_e4 = tensor(qo(g_m_e),identity(Na));
g4_0_e4 = tensor(qo(g_0_e),identity(Na));
g4_p_e4 = tensor(qo(g_p_e),identity(Na));


% lowering operators for 3' --> 4
Fg=4; Fe=3;
[cg_m,cg_0,cg_p] = murelf(Fg,Fe,1/2,3/2,7/2);


g_m_e = sparse(Natomic, Natomic);
g_0_e = sparse(Natomic, Natomic);
g_p_e = sparse(Natomic, Natomic);
```

```
g_m_e(index_g_Cs(4,-4):index_g_Cs(4,4),index_e_Cs(3,-3):index_e_Cs(3,3)) = cg_m;
g_0_e(index_g_Cs(4,-4):index_g_Cs(4,4),index_e_Cs(3,-3):index_e_Cs(3,3)) =-cg_0;
g_p_e(index_g_Cs(4,-4):index_g_Cs(4,4),index_e_Cs(3,-3):index_e_Cs(3,3)) = cg_p;


g4_m_e3 = tensor(qo(g_m_e),identity(Na));
g4_0_e3 = tensor(qo(g_0_e),identity(Na));
g4_p_e3 = tensor(qo(g_p_e),identity(Na));


% lowering operators for 4' --> 3
Fg=3; Fe=4;
[cg_m,cg_0,cg_p] = murelf(Fg,Fe,1/2,3/2,7/2);


g_m_e = sparse(Natomic, Natomic);
g_0_e = sparse(Natomic, Natomic);
g_p_e = sparse(Natomic, Natomic);


g_m_e(index_g_Cs(3,-3):index_g_Cs(3,3),index_e_Cs(4,-4):index_e_Cs(4,4)) = cg_m;
g_0_e(index_g_Cs(3,-3):index_g_Cs(3,3),index_e_Cs(4,-4):index_e_Cs(4,4)) =-cg_0;
g_p_e(index_g_Cs(3,-3):index_g_Cs(3,3),index_e_Cs(4,-4):index_e_Cs(4,4)) = cg_p;


g3_m_e4 = tensor(qo(g_m_e),identity(Na));
g3_0_e4 = tensor(qo(g_0_e),identity(Na));
g3_p_e4 = tensor(qo(g_p_e),identity(Na));


% lowering operators for 3' --> 3
Fg=3; Fe=3;
[cg_m,cg_0,cg_p] = murelf(Fg,Fe,1/2,3/2,7/2);


g_m_e = sparse(Natomic, Natomic);
g_0_e = sparse(Natomic, Natomic);
g_p_e = sparse(Natomic, Natomic);


g_m_e(index_g_Cs(3,-3):index_g_Cs(3,3),index_e_Cs(3,-3):index_e_Cs(3,3)) = cg_m;
g_0_e(index_g_Cs(3,-3):index_g_Cs(3,3),index_e_Cs(3,-3):index_e_Cs(3,3)) =-cg_0;
g_p_e(index_g_Cs(3,-3):index_g_Cs(3,3),index_e_Cs(3,-3):index_e_Cs(3,3)) = cg_p;
```

```
g3_m_e3 = tensor(qo(g_m_e),identity(Na));
g3_0_e3 = tensor(qo(g_0_e),identity(Na));
g3_p_e3 = tensor(qo(g_p_e),identity(Na));


% lowering operators for 2' --> 3
Fg=3; Fe=2;
[cg_m,cg_0,cg_p] = murelf(Fg,Fe,1/2,3/2,7/2);


g_m_e = sparse(Natomic, Natomic);
g_0_e = sparse(Natomic, Natomic);
g_p_e = sparse(Natomic, Natomic);


g_m_e(index_g_Cs(3,-3):index_g_Cs(3,3),index_e_Cs(2,-2):index_e_Cs(2,2)) = cg_m;
g_0_e(index_g_Cs(3,-3):index_g_Cs(3,3),index_e_Cs(2,-2):index_e_Cs(2,2)) =-cg_0;
g_p_e(index_g_Cs(3,-3):index_g_Cs(3,3),index_e_Cs(2,-2):index_e_Cs(2,2)) = cg_p;


g3_m_e2 = tensor(qo(g_m_e),identity(Na));
g3_0_e2 = tensor(qo(g_0_e),identity(Na));
g3_p_e2 = tensor(qo(g_p_e),identity(Na));


%-------------------- Atomic projection operators ----------------------
%project onto F = 3 ground state subspace
g3_g3 = sparse(Natomic, Natomic);
g3_g3(index_g_Cs(3,-3):index_g_Cs(3,3), index_g_Cs(3,-3):index_g_Cs(3,3))...
    =eye(Ng3);
g3_g3 = tensor(qo(g3_g3),identity(Na));


%project onto F = 4 ground state subspace
g4_g4 = sparse(Natomic, Natomic);
g4_g4(index_g_Cs(4,-4):index_g_Cs(4,4), index_g_Cs(4,-4):index_g_Cs(4,4))...
    =eye(Ng4);
g4_g4 = tensor(qo(g4_g4),identity(Na));


%project onto F' = 2 excited state subspace
e2_e2 = sparse(Natomic, Natomic);
e2_e2(index_e_Cs(2,-2):index_e_Cs(2,2), index_e_Cs(2,-2):index_e_Cs(2,2))...
```

```
        =eye(Ne2);
e2_e2 = tensor(qo(e2_e2),identity(Na));


%project onto F' = 3 excited state subspace
e3_e3 = sparse(Natomic, Natomic);
e3_e3(index_e_Cs(3,-3):index_e_Cs(3,3), index_e_Cs(3,-3):index_e_Cs(3,3))...
        =eye(Ne3);
e3_e3 = tensor(qo(e3_e3),identity(Na));


%project onto F' = 4 excited state subspace
e4_e4 = sparse(Natomic, Natomic);
e4_e4(index_e_Cs(4,-4):index_e_Cs(4,4), index_e_Cs(4,-4):index_e_Cs(4,4))...
        =eye(Ne4);
e4_e4 = tensor(qo(e4_e4),identity(Na));


%project onto F' = 5 excited state subspace
e5_e5 = sparse(Natomic, Natomic);
e5_e5(index_e_Cs(5,-5):index_e_Cs(5,5), index_e_Cs(5,-5):index_e_Cs(5,5))...
        =eye(Ne5);
e5_e5 = tensor(qo(e5_e5),identity(Na));


%-------------------- Photon annhilation operator ---------------------
a = tensor(identity(Natomic), destroy(Na));


%------------------- Hamiltonian --------------------------------------
H0 = dr*g3_g3 + d2*e2_e2 + d3*e3_e3 + d4*e4_e4 + d5*e5_e5 + dc*a'*a;


H1 = g*(a'*g4_p_e3 + g4_p_e3'*a + ...
        a'*g4_p_e4 + g4_p_e4'*a + ...
        a'*g4_p_e5 + g4_p_e5'*a)*sin(p_xi)*cos(p_psi) ...
    +g*(a'*g4_0_e3 + g4_0_e3'*a + ...
        a'*g4_0_e4 + g4_0_e4'*a + ...
        a'*g4_0_e5 + g4_0_e5'*a)*cos(p_xi) ...
    +g*(a'*g4_m_e3 + g4_m_e3'*a + ...
        a'*g4_m_e4 + g4_m_e4'*a + ...
        a'*g4_m_e5 + g4_m_e5'*a)*sin(p_xi)*sin(p_psi);
```

```
H2 = Wrp*(exp(i*phi)*(g3_p_e2 + g3_p_e3 + g3_p_e4) + ...
          exp(-i*phi)*(g3_p_e2' + g3_p_e3' + g3_p_e4'))*sin(r_xi)*cos(r_psi) ...
    +Wrp*(exp(i*phi)*(g3_0_e2 + g3_0_e3 + g3_0_e4) + ...
          exp(-i*phi)*(g3_0_e2' + g3_0_e3' + g3_0_e4'))*cos(r_xi) ...
    +Wrp*(exp(i*phi)*(g3_m_e2 + g3_m_e3 + g3_m_e4) + ...
          exp(-i*phi)*(g3_m_e2' + g3_m_e3' + g3_m_e4'))*sin(r_xi)*sin(r_psi);


H3 = eps_p*(a + a');


H = H0 + H1 + H2 + H3;


%------------------- Liouvillian -------------------------------------
% Hamiltonian
L0 = -i*(spre(H) - spost(H));


% cavity decay
L1  = kappa*decay(a);


%Coupling 4->N' (where N' = 3', 4', 5') by various polarizations
g4_m_n = g4_m_e5 + g4_m_e4 + g4_m_e3;
g4_0_n = g4_0_e5 + g4_0_e4 + g4_0_e3;
g4_p_n = g4_p_e5 + g4_p_e4 + g4_p_e3;


%Coupling 3->N' (where N' = 2', 3', 4') by various polarizations
g3_m_n = g3_m_e4 + g3_m_e3 + g3_m_e2;
g3_0_n = g3_0_e4 + g3_0_e3 + g3_0_e2;
g3_p_n = g3_p_e4 + g3_p_e3 + g3_p_e2;


L9 = gamma*decay(g4_m_n) ...
   + gamma*decay(g4_0_n) ...
   + gamma*decay(g4_p_n);


L11= gamma*decay(g3_m_n) ...
   + gamma*decay(g3_0_n) ...
   + gamma*decay(g3_p_n);
```

```
L = L0 + L1 + L9 + L11;


%-------------------- Steady State -------------------------------------
rhoss = steady(L);


%project onto F = 4 ground state with various mF's
g4_m4 = sparse(Natomic, Natomic);
g4_m4(index_g_Cs(4,-4), index_g_Cs(4,-4))=1;
g4_m4 = tensor(qo(g4_m4),identity(Na));


g4_m3 = sparse(Natomic, Natomic);
g4_m3(index_g_Cs(4,-3), index_g_Cs(4,-3))=1;
g4_m3 = tensor(qo(g4_m3),identity(Na));


g4_m2 = sparse(Natomic, Natomic);
g4_m2(index_g_Cs(4,-2), index_g_Cs(4,-2))=1;
g4_m2 = tensor(qo(g4_m2),identity(Na));


g4_m1 = sparse(Natomic, Natomic);
g4_m1(index_g_Cs(4,-1), index_g_Cs(4,-1))=1;
g4_m1 = tensor(qo(g4_m1),identity(Na));


g4_p0 = sparse(Natomic, Natomic);
g4_p0(index_g_Cs(4, 0), index_g_Cs(4, 0))=1;
g4_p0 = tensor(qo(g4_p0),identity(Na));


g4_p1 = sparse(Natomic, Natomic);
g4_p1(index_g_Cs(4, 1), index_g_Cs(4, 1))=1;
g4_p1 = tensor(qo(g4_p1),identity(Na));


g4_p2 = sparse(Natomic, Natomic);
g4_p2(index_g_Cs(4, 2), index_g_Cs(4, 2))=1;
g4_p2 = tensor(qo(g4_p2),identity(Na));


g4_p3 = sparse(Natomic, Natomic);
g4_p3(index_g_Cs(4, 3), index_g_Cs(4, 3))=1;
```

```
g4_p3 = tensor(qo(g4_p3),identity(Na));


g4_p4 = sparse(Natomic, Natomic);
g4_p4(index_g_Cs(4, 4), index_g_Cs(4, 4))=1;
g4_p4 = tensor(qo(g4_p4),identity(Na));
```

Note that since this calculation assumes that the cavity has only one mode, it is not appropriate for the typical Fabry-Perot cavity, which has two modes of orthogonal polarizations which are nearly degenerate. Some code was written to calculate the Fabry-Perot case, but it was never tested because we did not have available any computer with enough memory to hold the extremely large (even in sparse matrix form) Liouvillian. Nonetheless, the problem solved above is useful for resonators which have large splittings between the modes, such as microtoroid and photonic band gap resonators, where the TE and TM modes are separated by frequencies large compared to all hyperfine and coupling frequencies. In this limit, only one mode of the resonator can be close enough to the atomic resonance to interact with the atom.

There is a caveat, however, to assuming a single-mode resonator when modeling microtoroids. Microtoroids have two modes which propagate clockwise and counter-clockwise around the circumference. Each of these traveling waves will interact with an atom in the evanescent fields. On the other hand, we may decompose the two modes of the resonator into two standing waves such that the atom is at a node of one mode and an anti-node of the other. In this case, the single-mode assumption again seems valid, since the coupling to the atom is zero at a node. Surface irregularities, however, may cause scattering between the two standing wave modes, so that they may not be separable. This scattering is essentially equivalent to the microtoroid having two standing wave eigenmodes (not generally aligned with the atomic position) with a small separation in resonance frequencies (the scattering rate). Further investigation is needed to find the properties of this system.

7.6 Coupling to All Hyperfine Levels of D2

We now present the code appropriate for extremely small single-mode resonators which couples all states of the D2 transition of Cesium to an optical field as described in Section 6.2:

```
function [rhoss, a, H, g4_m4, g4_m3, g4_m2, g4_m1, g4_p0, g4_p1, g4_p2, ...
    g4_p3, g4_p4, g3_m3, g3_m2, g3_m1, g3_p0, g3_p1, g3_p2, g3_p3] = ...
    kmb_Cs133_scott_pbg_g(gamma, kappa, g, Na, cavity_freq, probe_freq, eps_p)
% One Cesium atom, entire D2 transition coupled to single linearly polarized
%    cavity mode.  Relevant for photonic band gap (pbg) cavities.  This
%    program calculates the steady state density matrix.  All atomic decays of
%    the same polarization are coupled to the same environmental reservoir.


% gamma is atomic HWHM
% kappa is cavity HWHM
% g is half the single photon Rabi frequency for 4,4->5'5'
% Na is number of Fock states for cavity mode
% cavity_freq is cavity frequency relative to F'=5->F=4 transition
% probe_freq is probe frequency relative to F'=5->F=4 transition
% eps_p is strength of probe.  Empty cavity on resonance photon number is
%    |eps_p|^2/kappa^2.
% p_xi, p_psi are angles that set the cavity polarization
% cavity is linearly polarized (pi polarized in this basis)

f_5 = 0;                              % excited state splittings
f_4 = -251;                           %    taken from Steck notes.
f_3 = -251-201;
f_2 = -251-201-151;

dr = -9192.6; % F=3 ground state energy in rotating frame
d2 = f_2 - probe_freq;                % (F=2'->F=4 freq) - (probe freq)
d3 = f_3 - probe_freq;                % (F=3'->F=4 freq) - (probe freq)
d4 = f_4 - probe_freq;                % (F=4'->F=4 freq) - (probe freq)
d5 = f_5 - probe_freq;                % (F=5'->F=4 freq) - (probe freq)
dc = cavity_freq - probe_freq;        % (cavity freq) - (probe freq)
```

```
phi = 0;


Ng3 = 2*3 + 1;                          % number of states in g3 manifold
Ng4 = 2*4 + 1;                          % number of states in g4 manifold


Ne2 = 2*2 + 1;                          % number of states in e2 manifold
Ne3 = 2*3 + 1;                          % number of states in e3 manifold
Ne4 = 2*4 + 1;                          % number of states in e4 manifold
Ne5 = 2*5 + 1;                          % number of states in e5 manifold


Natomic = Ng3 + Ng4 + Ne2 + Ne3 + Ne4 + Ne5;    % number of atomic states


%-------------------- Atomic lowering operators -----------------------
%   Change minus sign for 0-polarized transitions to be consistent with
%   Steck notes.
% lowering operators for 5' --> 4
Fg=4; Fe=5;
[cg_m,cg_0,cg_p] = murelf(Fg,Fe,1/2,3/2,7/2);


g_m_e = sparse(Natomic, Natomic);
g_0_e = sparse(Natomic, Natomic);
g_p_e = sparse(Natomic, Natomic);

g_m_e(index_g_Cs(4,-4):index_g_Cs(4,4),index_e_Cs(5,-5):index_e_Cs(5,5)) = cg_m;
g_0_e(index_g_Cs(4,-4):index_g_Cs(4,4),index_e_Cs(5,-5):index_e_Cs(5,5)) =-cg_0;
g_p_e(index_g_Cs(4,-4):index_g_Cs(4,4),index_e_Cs(5,-5):index_e_Cs(5,5)) = cg_p;


g4_m_e5 = tensor(qo(g_m_e),identity(Na));
g4_0_e5 = tensor(qo(g_0_e),identity(Na));
g4_p_e5 = tensor(qo(g_p_e),identity(Na));


% lowering operators for 4' --> 4
Fg=4; Fe=4;
[cg_m,cg_0,cg_p] = murelf(Fg,Fe,1/2,3/2,7/2);


g_m_e = sparse(Natomic, Natomic);
```

```
g_0_e = sparse(Natomic, Natomic);
g_p_e = sparse(Natomic, Natomic);


g_m_e(index_g_Cs(4,-4):index_g_Cs(4,4),index_e_Cs(4,-4):index_e_Cs(4,4)) = cg_m;
g_0_e(index_g_Cs(4,-4):index_g_Cs(4,4),index_e_Cs(4,-4):index_e_Cs(4,4)) =-cg_0;
g_p_e(index_g_Cs(4,-4):index_g_Cs(4,4),index_e_Cs(4,-4):index_e_Cs(4,4)) = cg_p;


g4_m_e4 = tensor(qo(g_m_e),identity(Na));
g4_0_e4 = tensor(qo(g_0_e),identity(Na));
g4_p_e4 = tensor(qo(g_p_e),identity(Na));


% lowering operators for 3' --> 4
Fg=4; Fe=3;
[cg_m,cg_0,cg_p] = murelf(Fg,Fe,1/2,3/2,7/2);


g_m_e = sparse(Natomic, Natomic);
g_0_e = sparse(Natomic, Natomic);
g_p_e = sparse(Natomic, Natomic);


g_m_e(index_g_Cs(4,-4):index_g_Cs(4,4),index_e_Cs(3,-3):index_e_Cs(3,3)) = cg_m;
g_0_e(index_g_Cs(4,-4):index_g_Cs(4,4),index_e_Cs(3,-3):index_e_Cs(3,3)) =-cg_0;
g_p_e(index_g_Cs(4,-4):index_g_Cs(4,4),index_e_Cs(3,-3):index_e_Cs(3,3)) = cg_p;


g4_m_e3 = tensor(qo(g_m_e),identity(Na));
g4_0_e3 = tensor(qo(g_0_e),identity(Na));
g4_p_e3 = tensor(qo(g_p_e),identity(Na));


% lowering operators for 4' --> 3
Fg=3; Fe=4;
[cg_m,cg_0,cg_p] = murelf(Fg,Fe,1/2,3/2,7/2);


g_m_e = sparse(Natomic, Natomic);
g_0_e = sparse(Natomic, Natomic);
g_p_e = sparse(Natomic, Natomic);


g_m_e(index_g_Cs(3,-3):index_g_Cs(3,3),index_e_Cs(4,-4):index_e_Cs(4,4)) = cg_m;
```

```
g_0_e(index_g_Cs(3,-3):index_g_Cs(3,3),index_e_Cs(4,-4):index_e_Cs(4,4)) =-cg_0;
g_p_e(index_g_Cs(3,-3):index_g_Cs(3,3),index_e_Cs(4,-4):index_e_Cs(4,4)) = cg_p;


g3_m_e4 = tensor(qo(g_m_e),identity(Na));
g3_0_e4 = tensor(qo(g_0_e),identity(Na));
g3_p_e4 = tensor(qo(g_p_e),identity(Na));


% lowering operators for 3' --> 3
Fg=3; Fe=3;
[cg_m,cg_0,cg_p] = murelf(Fg,Fe,1/2,3/2,7/2);


g_m_e = sparse(Natomic, Natomic);
g_0_e = sparse(Natomic, Natomic);
g_p_e = sparse(Natomic, Natomic);


g_m_e(index_g_Cs(3,-3):index_g_Cs(3,3),index_e_Cs(3,-3):index_e_Cs(3,3)) = cg_m;
g_0_e(index_g_Cs(3,-3):index_g_Cs(3,3),index_e_Cs(3,-3):index_e_Cs(3,3)) =-cg_0;
g_p_e(index_g_Cs(3,-3):index_g_Cs(3,3),index_e_Cs(3,-3):index_e_Cs(3,3)) = cg_p;


g3_m_e3 = tensor(qo(g_m_e),identity(Na));
g3_0_e3 = tensor(qo(g_0_e),identity(Na));
g3_p_e3 = tensor(qo(g_p_e),identity(Na));


% lowering operators for 2' --> 3
Fg=3; Fe=2;
[cg_m,cg_0,cg_p] = murelf(Fg,Fe,1/2,3/2,7/2);


g_m_e = sparse(Natomic, Natomic);
g_0_e = sparse(Natomic, Natomic);
g_p_e = sparse(Natomic, Natomic);


g_m_e(index_g_Cs(3,-3):index_g_Cs(3,3),index_e_Cs(2,-2):index_e_Cs(2,2)) = cg_m;
g_0_e(index_g_Cs(3,-3):index_g_Cs(3,3),index_e_Cs(2,-2):index_e_Cs(2,2)) =-cg_0;
g_p_e(index_g_Cs(3,-3):index_g_Cs(3,3),index_e_Cs(2,-2):index_e_Cs(2,2)) = cg_p;


g3_m_e2 = tensor(qo(g_m_e),identity(Na));
```

```
g3_0_e2 = tensor(qo(g_0_e),identity(Na));
g3_p_e2 = tensor(qo(g_p_e),identity(Na));


%-------------------- Atomic projection operators ----------------------
%project onto F = 3 ground state subspace
g3_g3 = sparse(Natomic, Natomic);
g3_g3(index_g_Cs(3,-3):index_g_Cs(3,3), index_g_Cs(3,-3):index_g_Cs(3,3))...
    =eye(Ng3);
g3_g3 = tensor(qo(g3_g3),identity(Na));


%project onto F = 4 ground state subspace
g4_g4 = sparse(Natomic, Natomic);
g4_g4(index_g_Cs(4,-4):index_g_Cs(4,4), index_g_Cs(4,-4):index_g_Cs(4,4))...
    =eye(Ng4);
g4_g4 = tensor(qo(g4_g4),identity(Na));


%project onto F' = 2 excited state subspace
e2_e2 = sparse(Natomic, Natomic);
e2_e2(index_e_Cs(2,-2):index_e_Cs(2,2), index_e_Cs(2,-2):index_e_Cs(2,2))...
    =eye(Ne2);
e2_e2 = tensor(qo(e2_e2),identity(Na));


%project onto F' = 3 excited state subspace
e3_e3 = sparse(Natomic, Natomic);
e3_e3(index_e_Cs(3,-3):index_e_Cs(3,3), index_e_Cs(3,-3):index_e_Cs(3,3))...
    =eye(Ne3);
e3_e3 = tensor(qo(e3_e3),identity(Na));


%project onto F' = 4 excited state subspace
e4_e4 = sparse(Natomic, Natomic);
e4_e4(index_e_Cs(4,-4):index_e_Cs(4,4), index_e_Cs(4,-4):index_e_Cs(4,4))...
    =eye(Ne4);
e4_e4 = tensor(qo(e4_e4),identity(Na));


%project onto F' = 5 excited state subspace
e5_e5 = sparse(Natomic, Natomic);
```

```
e5_e5(index_e_Cs(5,-5):index_e_Cs(5,5), index_e_Cs(5,-5):index_e_Cs(5,5))...
    =eye(Ne5);
e5_e5 = tensor(qo(e5_e5),identity(Na));


%-------------------- Photon annhilation operator ---------------------
a = tensor(identity(Natomic), destroy(Na));


%-------------------- Hamiltonian -------------------------------------
H0 = dr*g3_g3 + d2*e2_e2 + d3*e3_e3 + d4*e4_e4 + d5*e5_e5 + dc*a'*a;


Hint = g*a'*(g4_0_e3 + g4_0_e4 + g4_0_e5 + g3_0_e2 + g3_0_e3 + g3_0_e4);


Hdrive = eps_p*a;


H = H0 + Hint + Hint' + Hdrive + Hdrive';


%-------------------- Liouvillian -------------------------------------
% Hamiltonian
L0 = -i*(spre(H) - spost(H));


% cavity decay
L1  = kappa*decay(a);


%Coupling 4->N' (where N' = 3', 4', 5') by various polarizations
g4_m_n = g4_m_e5 + g4_m_e4 + g4_m_e3;
g4_0_n = g4_0_e5 + g4_0_e4 + g4_0_e3;
g4_p_n = g4_p_e5 + g4_p_e4 + g4_p_e3;


%Coupling 3->N' (where N' = 2', 3', 4') by various polarizations
g3_m_n = g3_m_e4 + g3_m_e3 + g3_m_e2;
g3_0_n = g3_0_e4 + g3_0_e3 + g3_0_e2;
g3_p_n = g3_p_e4 + g3_p_e3 + g3_p_e2;


%Coupling the entire D2 transition by various polarizations
g_m_e = g3_m_n + g4_m_n;
g_0_e = g3_0_n + g4_0_n;
```

```
g_p_e = g3_p_n + g4_p_n;


L10 = gamma*decay(g_m_e) ...
    + gamma*decay(g_0_e) ...
    + gamma*decay(g_p_e);


L = L0 + L1 + L10;


%-------------------- Steady State -------------------------------------
rhoss = steady(L);


%project onto F = 4 ground state with various mF's
g4_m4 = sparse(Natomic, Natomic);
g4_m4(index_g_Cs(4,-4), index_g_Cs(4,-4))=1;
g4_m4 = tensor(qo(g4_m4),identity(Na));


g4_m3 = sparse(Natomic, Natomic);
g4_m3(index_g_Cs(4,-3), index_g_Cs(4,-3))=1;
g4_m3 = tensor(qo(g4_m3),identity(Na));


g4_m2 = sparse(Natomic, Natomic);
g4_m2(index_g_Cs(4,-2), index_g_Cs(4,-2))=1;
g4_m2 = tensor(qo(g4_m2),identity(Na));


g4_m1 = sparse(Natomic, Natomic);
g4_m1(index_g_Cs(4,-1), index_g_Cs(4,-1))=1;
g4_m1 = tensor(qo(g4_m1),identity(Na));


g4_p0 = sparse(Natomic, Natomic);
g4_p0(index_g_Cs(4, 0), index_g_Cs(4, 0))=1;
g4_p0 = tensor(qo(g4_p0),identity(Na));


g4_p1 = sparse(Natomic, Natomic);
g4_p1(index_g_Cs(4, 1), index_g_Cs(4, 1))=1;
g4_p1 = tensor(qo(g4_p1),identity(Na));
```

```
g4_p2 = sparse(Natomic, Natomic);
g4_p2(index_g_Cs(4, 2), index_g_Cs(4, 2))=1;
g4_p2 = tensor(qo(g4_p2),identity(Na));


g4_p3 = sparse(Natomic, Natomic);
g4_p3(index_g_Cs(4, 3), index_g_Cs(4, 3))=1;
g4_p3 = tensor(qo(g4_p3),identity(Na));


g4_p4 = sparse(Natomic, Natomic);
g4_p4(index_g_Cs(4, 4), index_g_Cs(4, 4))=1;
g4_p4 = tensor(qo(g4_p4),identity(Na));


%project onto F = 3 ground state with various mF's
g3_m3 = sparse(Natomic, Natomic);
g3_m3(index_g_Cs(3,-3), index_g_Cs(3,-3))=1;
g3_m3 = tensor(qo(g3_m3),identity(Na));


g3_m2 = sparse(Natomic, Natomic);
g3_m2(index_g_Cs(3,-2), index_g_Cs(3,-2))=1;
g3_m2 = tensor(qo(g3_m2),identity(Na));


g3_m1 = sparse(Natomic, Natomic);
g3_m1(index_g_Cs(3,-1), index_g_Cs(3,-1))=1;
g3_m1 = tensor(qo(g3_m1),identity(Na));


g3_p0 = sparse(Natomic, Natomic);
g3_p0(index_g_Cs(3, 0), index_g_Cs(3, 0))=1;
g3_p0 = tensor(qo(g3_p0),identity(Na));


g3_p1 = sparse(Natomic, Natomic);
g3_p1(index_g_Cs(3, 1), index_g_Cs(3, 1))=1;
g3_p1 = tensor(qo(g3_p1),identity(Na));


g3_p2 = sparse(Natomic, Natomic);
g3_p2(index_g_Cs(3, 2), index_g_Cs(3, 2))=1;
g3_p2 = tensor(qo(g3_p2),identity(Na));
```

```
g3_p3 = sparse(Natomic, Natomic);
g3_p3(index_g_Cs(3, 3), index_g_Cs(3, 3))=1;
g3_p3 = tensor(qo(g3_p3),identity(Na));
```

7.7   Beyond the Steady State Density Matrix

We will now show how to extend these routines to go beyond the steady state solution. We will give example code for modifying `kmb_Cs133_4_to_5prime_twomode.m`, but similar code can be used with the other routines.

Often, it is useful to find not just the steady state of the system, but the full time dependence. This can be easily computed within the framework of the Toolbox, which has functions for numerically integrating the master equation to find the density matrix as a function of time. In order to perform this integration, we must first define an initial state of the system, for example,

```
psi0 = sparse(Natomic, Natomic);
psi0(index_g_45(4,-4):index_g_45(4,4),index_g_45(4,-4):index_g_45(4,4))...
    =eye(Ng4)/Ng4; % atomic state is an equal mixture of all ground states
psi0 = qo(psi0);

nophotonsa = sparse(Nc,Nc);
nophotonsa(1,1)=1; % the vacuum state of the z mode
nophotonsa = qo(nophotonsa);

nophotonsb = sparse(Nd,Nd);
nophotonsb(1,1)=1; % the vacuum state of the y mode
nophotonsb = qo(nophotonsb);

rho0 = tensor(psi0, nophotonsa, nophotonsb);
```

The above code defines a density matrix where the cavity modes are both in the vacuum state and the atom is in an equal mixture of all Zeeman ground states. To put the atom in one particular ground state with $m_F =$`initmF`, use

```
psi0 = sparse(Natomic, Natomic);
```

```
psi0(index_g_45(4, initmF), index_g_45(4, initmF))=1;
psi0 = qo(psi0);
```

Once an initial state has been defined, we can compute the density matrix at a predetermined list of times `tlist` by using

```
options.mxstep = 1000000;% used to prevent ODE solver from giving up too easily
options.mxhnil = 100;    % used to prevent ODE solver from giving up too easily
ode2file('file1.dat',L,rho0,tlist,options); % write equations to a file
odesolve('file1.dat','file2.dat'); % call external ODE solver
fid = fopen('file2.dat','rb'); % open file with results
rho = qoread(fid, dims(rho0),size(tlist)); % read in results to variable
fclose(fid); % close file
```

The resulting variable `rho` contains the density matrix at each time specified in `tlist`. Note that if the input variables, such as `kappa, gamma, g,` etc. are in MHz, then the Liouvillian should be multiplied by 2π to convert to angular frequencies, e.g., `L = 2*pi*(L0 + L1 + L2);` and `tlist` should be in microseconds.

In the Toolbox, there is an alternative method to perform time evolution using exponential series. It allows one to compute the state of the system at any time without the need to compute the state at intervening times. It is therefore very useful when there is a large separation of time scales, which makes an ODE integrator take very many steps to calculate change on the longest time scale. The problems discussed above typically have this separation of time scales, with fast dynamics at a rate g and slower dynamics associated with optical pumping times. However, the exponential series calculation requires that the Liouvillian be diagonalized, and we do not have a computer with enough memory to perform this calculation. The integration technique is therefore our only option at this time.

Integration of the master equation is also useful for calculating some steady state properties of the system. For example, the intensity correlation function $g^{(2)}(\tau)$ of the system in steady state cannot be calculated from the steady state density matrix alone (although $g^{(2)}(0)$ can be). Using the quantum regression theorem [49], we find

$$g^{(2)}(\tau) = \frac{\text{Tr}(a^\dagger a \int_0^\tau \mathcal{L}(a\rho_{ss}a^\dagger)dt)}{(\text{Tr}(a^\dagger a\rho_{ss}))^2} \tag{7.1}$$

Thus, $g^{(2)}(\tau)$ can be calculated at a number of times specified by `tlist` by computing

```
rhoss = steady(L);          % find the steady state density matrix
a_rhoss_ad = a*rhoss*a';    % construct the operator that we will time evolve
options.mxstep = 10000000;
options.mxhnil = 100;
ode2file('file1.dat',L,a_rhoss_ad,tlist,options);
odesolve('file1.dat','file2.dat');   % integrate the ODE
fid = fopen('file2.dat','rb');
rho_out = qoread(fid, dims(rhoss),size(tlist));
fclose(fid);
numerator = expect(a'*a, rho_out);   % calculate expectation (Trace with a'*a)
denominator = expect(a'*a, rhoss)^2; % normalize
g2_tau = numerator/denominator;
```

The resulting variable `g2_tau` is a vector whose length is equal to that of `tlist` and whose value is $g^{(2)}(\texttt{tlist})$.

The evolution of the density matrix under the master equation does not include all of the information that can be found in a measurement record. This is because the state of the system at one time is dependent on the measurement record before that time. This is sometimes called "quantum back-action," although there is a similar effect in classical statistical physics which comes from the use of Bayes rule for conditional probabilities. The master equation describes the ensemble properties of the system; it is not conditioned upon the measurement record, and therefore cannot be used to calculate certain types of correlations within the record.

In order to calculate those properties which are beyond the master equation, we must turn to quantum trajectory theory [62]. A trajectory is a description of the system as it evolves in time which takes into account the prior measurement record. This is most simply accomplished by use of the stochastic Schrödinger equation. In the stochastic Schrödinger equation, the system is described as a pure state (a ket, not an operator such as the density matrix) which evolves continuously under the effect of a (non-Hermitian) Hamiltonian, punctuated by instantaneous transformations ("quantum jumps") that occur at random times corresponding to detection events.

In this framework, it is assumed that there is no part of the environment that is outside of the observer, and thus, no information is lost and the state of the system remains pure. More complicated environments involving both an observed part and an unobserved component can be simulated by simply throwing away part of the measurement record.

We will use the stochastic Schrödinger equation to calculate how well the "photon blockade" effect of Chapter 4 should work in pulse mode as a method to create single photon on demand. We imagine changing the probe from a continuous drive to a field which is in the vacuum state, except for a short period of time (the pulse) when it is in a coherent state. We expect that for pulses of an appropriate duration and intensity, the "photon blockade" effect should make the cavity transmit only one photon. We wish to calculate the probability P of getting a total of k clicks on a detector measuring the transmitted field. We desire a large $P(1)$ and a small $P(k)$ for $k \geq 2$.

We perform this calculation by first specifying an initial state for the system. We imagine that the atom has been prepared in the Zeeman state $m_F =$`initmF`, and that the cavity contains no photons.

```
psi0_atom = basis(Natomic, index_g_45(4,initmF));
nophotonsa = basis(Nc, 1);
nophotonsb = basis(Nd, 1);
psi0 = tensor(psi0_atom, nophotonsa, nophotonsb);
```

Notice that `psi0` is a ket, not an operator as in our previous examples.

Now we must define the effective Hamiltonian of the system, including the time-dependent drive, and the collapse operators corresponding to the environment (measurements).

```
H0 = d5*e5_e5 + dc*a'*a + dd*b'*b;


H1 = g*(a'*g4_0_e5 + g4_0_e5'*a)...
   + g*(b'*g4_d_e5 + g4_d_e5'*b);


% eps_a and eps_b will give peak drive amplitude
H3 = eps_a*a + eps_a'*a' + eps_b*b + eps_b'*b';  % drive term
```

```
%stark shifts from FORT
H4 = -0.1751*(e5_m5 + e5_p5)*depth ...
    + -0.0586*(e5_m4 + e5_p4)*depth ...
    +  0.0319*(e5_m3 + e5_p3)*depth ...
    +  0.0966*(e5_m2 + e5_p2)*depth ...
    +  0.1354*(e5_m1 + e5_p1)*depth ...
    +  0.1484*(         e5_p0)*depth;


Hconst = H0 + H1 + H4;   % this part of the Hamiltonian is constant


%Collapse operators
C = [
    sqrt(kappa_c)*a
    sqrt(kappa_d)*b
    sqrt(gamma)*g4_m_e5
    sqrt(gamma)*g4_0_e5
    sqrt(gamma)*g4_p_e5
    ]*sqrt(2*pi)*sqrt(2);  % 2*pi changes from cycles/second to angular
                           %    frequencies


C_cell_array = cell(1, length(C));
for k=1:length(C) C_cell_array{k} = C{k}; end;


% we take drive pulse to be gaussian in time with width pulsesigma
% the middle of the pulse is at time = 4*pulsesigma
Heff = 2*pi*Hconst + 2*pi*H3*fn('gauss', 4*pulsesigma, pulsesigma)...
        - 0.5*i*sum(C'*C);
```

Now we specify the time interval, perform the time evolution `ntraj` times (compute `ntraj` trajectories), and perform a histogram of the measurement records to find the probabilities of getting k clicks.

```
% calculate over a time interval that starts at zero and goes until we expect
%    the fields have all decayed away
tlist = [0, 8*pulsesigma+4*kappa_c];
% call the external Monte Carlo solver
```

```
mc2file('test.dat', -i*Heff, C_cell_array, {}, psi0, tlist, ntraj);
mcsolve('test.dat', 'out.dat', 'clix.dat');


% read in classical record from external MC solver
fid = fopen('clix.dat','rb');
clix = clread(fid);
fclose(fid);


clicktype = 1;  % we will look at photons emitted in the "a" mode
noc = zeros(100,1); % number of trajectories that had (index-1) number
                    %    of clicks of type clicktype
for k = 1:ntraj
    noc(sum(clix(k).channels==clicktype)+1) = ...
    noc(sum(clix(k).channels==clicktype)+1) + 1;
end
poc = noc/ntraj;    % probability of getting (index-1) number of clicks
```

The output, poc, should approach poc(k)$\approx P(k-1)$ for large values of ntraj.

7.8   Cavity QED with $1 \to 2'$

We will now present programs which solve problems not discussed elsewhere in this thesis. They may prove useful in future studies.

We begin with calculations of a single atom with a $F = 1 \to F' = 2$ transition coupled to a two-mode cavity. This problem is qualitatively similar to that discussed in Section 3.3, but is faster to compute and easier to understand because of the reduced number of atomic states.

```
function n = index_g_12(F,m)
if ((m <= F) & (m >= -F))
    switch (F)
        case 1, n = 2 + m;
        otherwise, error('F out of range in index_g_12');
    end
else
    error('m out of range in index_g_12');
```

```
end


function n = index_e_12(F,m)
if ((m <= F) & (m >= -F))
    switch (F)
        case 2, n = 6 + m;
        otherwise, error('F out of range in index_e_12');
    end
else
    error('m out of range in index_e_12');
end


function [rhoss, a, b, H, H1] = ...
    kmb_one_to_twoprime_twomode(gamma, kappa_c, kappa_d, g, Nc, Nd, ...
    cavity_freq, probe_freq, splitting, eps_a, eps_b, depth)
% steady state of one atom with a 1->2' transition coupled to a cavity with two
%    orthogonal linear modes
% mode "a" (sometimes called "c" -- sorry) is polarized along z
% mode "b" (sometimes called "d" -- sorry) is polarized along y
%
% gamma is atomic HWHM
% kappa_c is cavity HWHM for z mode
% kappa_d is cavity HWHM for y mode
% g is half the single photon Rabi frequency for 1,1->2',2'
% Nc is the number of Fock states for z cavity mode
% Nd is the number of Fock states for y cavity mode
% cavity_freq is AVERAGE cavity frequency relative to F'=2->F=1 transition
% probe_freq is probe frequency relative to F'=2->F=1 transition
% splitting is HALF of the difference of the two cavity frequencies
%    splitting = ((freq of y mode)-(freq of z mode))/2
% eps_c is the drive of the z mode
% eps_d is the drive of the y mode
% depth is the FORT depth used for calculating stark shifts. Should be positive.
% the FORT is assumed to have the polarization of the z mode
% These Stark shifts are not accurate for any real atom, but their magnitude
%    is similar to those for the Cs 4->5' transition in a FORT at 935nm
```

```
f_2 = 0;
d2 = f_2 - probe_freq;
dc = cavity_freq - splitting - probe_freq;
dd = cavity_freq + splitting - probe_freq;


Ng1 = 2*1 + 1;                              % number of states in g1 manifold
Ne2 = 2*2 + 1;                              % number of states in e2 manifold


Natomic = Ng1+Ne2;                          % total number of atomic states
%-------------------- Atomic lowering operators -----------------------
%   Change minus sign for 0-polarized transitions to be consistent with
%   Steck notes.
% lowering operators for 2' --> 1
Fg=1; Fe=2;
[cg_m,cg_0,cg_p] = murelf(Fg,Fe,1/2,3/2,1/2);


g_m_e = sparse(Natomic, Natomic);
g_0_e = sparse(Natomic, Natomic);
g_p_e = sparse(Natomic, Natomic);


g_m_e(index_g_12(1,-1):index_g_12(1,1),index_e_12(2,-2):index_e_12(2,2)) = cg_m;
g_0_e(index_g_12(1,-1):index_g_12(1,1),index_e_12(2,-2):index_e_12(2,2)) =-cg_0;
g_p_e(index_g_12(1,-1):index_g_12(1,1),index_e_12(2,-2):index_e_12(2,2)) = cg_p;


g1_m_e2 = tensor(qo(g_m_e),identity(Nc), identity(Nd));
g1_0_e2 = tensor(qo(g_0_e),identity(Nc), identity(Nd));
g1_p_e2 = tensor(qo(g_p_e),identity(Nc), identity(Nd));


g1_d_e2 = i*sqrt(0.5)*(g1_p_e2 + g1_m_e2);


%-------------------- Atomic projection operators ---------------------
%project onto F = 1 ground state subspace
g1_g1 = sparse(Natomic, Natomic);
g1_g1(index_g_12(1,-1):index_g_12(1,1), index_g_12(1,-1):index_g_12(1,1))...
    =eye(Ng1);
```

```
g1_g1 = tensor(qo(g1_g1),identity(Nc), identity(Nd));


%project onto F' = 2 excited state subspace
e2_e2 = sparse(Natomic, Natomic);
e2_e2(index_e_12(2,-2):index_e_12(2,2), index_e_12(2,-2):index_e_12(2,2))...
    =eye(Ne2);
e2_e2 = tensor(qo(e2_e2),identity(Nc), identity(Nd));


%project onto different mF's of F'=2
e2_m2 = sparse(Natomic, Natomic);
e2_m2(index_e_12(2,-2), index_e_12(2,-2))=1;
e2_m2 = tensor(qo(e2_m2),identity(Nc), identity(Nd));


e2_m1 = sparse(Natomic, Natomic);
e2_m1(index_e_12(2,-1), index_e_12(2,-1))=1;
e2_m1 = tensor(qo(e2_m1),identity(Nc), identity(Nd));


e2_p0 = sparse(Natomic, Natomic);
e2_p0(index_e_12(2, 0), index_e_12(2, 0))=1;
e2_p0 = tensor(qo(e2_p0),identity(Nc), identity(Nd));


e2_p1 = sparse(Natomic, Natomic);
e2_p1(index_e_12(2, 1), index_e_12(2, 1))=1;
e2_p1 = tensor(qo(e2_p1),identity(Nc), identity(Nd));


e2_p2 = sparse(Natomic, Natomic);
e2_p2(index_e_12(2, 2), index_e_12(2, 2))=1;
e2_p2 = tensor(qo(e2_p2),identity(Nc), identity(Nd));


%-------------------- Photon annhilation operator ----------------------
a = tensor(identity(Natomic), destroy(Nc), identity(Nd));
b = tensor(identity(Natomic), identity(Nc), destroy(Nd));


%-------------------- Hamiltonian -------------------------------------
H0 = d2*e2_e2 + dc*a'*a + dd*b'*b;
```

```
H1 = g*(a'*g1_0_e2 + g1_0_e2'*a)...
    + g*(b'*g1_d_e2 + g1_d_e2'*b);


H3 = eps_a*a + eps_a'*a' + eps_b*b + eps_b'*b';


% Stark shifts -- meant to be qualitatively similar to those for 4->5'
H4 = -0.1751*(e2_m2 + e2_p2)*depth ...
    +  0.0643*(e2_m1 + e2_p1)*depth ...
    +  0.1484*(         e2_p0)*depth;


H = H0 + H1 + H3 + H4;


%------------------- Liouvillian ------------------------------------
% Hamiltonian
L0 = -i*(spre(H) - spost(H));


% cavity decay
L1  = kappa_c*decay(a) + kappa_d*decay(b);


% 5'->4 decays
L2  = gamma*decay(g1_m_e2) ...
     +gamma*decay(g1_0_e2) ...
     +gamma*decay(g1_p_e2);


L =  L0 + L1 + L2;


%-------------------- Steady State ----------------------------------
rhoss = steady(L);
```

7.9   Atom Arrival Time

Finally, we present a program used to estimate how many atoms from the MOT should enter the mode of a Fabry-Perot cavity and calculate the distribution of arrival times. The user specifies the size and location of the cloud of atoms above the cavity, the
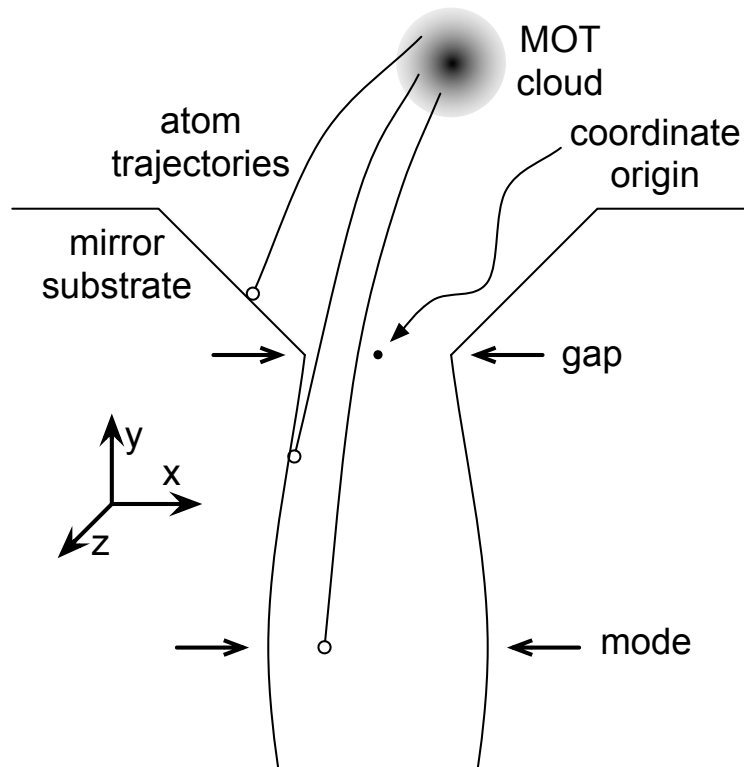
Figure 7.1: Diagram of basic cavity geometry (not to scale). After the MOT is switched off, atoms from the cloud trace out parabolas as they fall under the influence of gravity. Most atoms hit the top of the mirror substrates or the mirror faces; a few enter the mode at the center of the cavity.

cloud temperature, and the geometry of the cavity (see Fig. 7.1). The calculation randomly selects an initial position and velocity for the atom consistent with the input parameters and determines if (and when) the atom would enter the cavity mode. After many such calculations, it prints the probability of any individual atom entering the cavity mode and plots a histogram of expected arrival times (see Fig. 7.2).

The program, written as functions for Igor, is as follows:

```
Function TransitTime(alpha,vsdev,gap,modelength,cloud)
    //picks a random atom and decides if it makes it into the cavity
    //all units are SI.  x is horizontal (along cavity axis), y is vertical.
    //origin of coordinate system is at TOP of the cavity.
    Variable alpha    //tilt of cavity, in radians (must be a small angle)
    Variable vsdev     //Temperature of cloud, in Kelvin
```

```
Variable gap        //gap between mirrors at top of the cavity
Variable modelength    //distance between mirrors at the center
Wave cloud
//cloud is a wave which contains the position and size of the atomic cloud
//cloud[0] is the x displacement of the center (relative to top of cavity)
//cloud[1] is the y displacement of the center (relative to top of cavity)
//cloud[2] is the z displacement of the center
//cloud[3] is the standard deviation of x in the cloud
//cloud[4] is the standard deviation of y in the cloud
//cloud[5] is the standard deviation of z in the cloud


Variable x0, y0, vx, vy //initial position and velocity of atom
Variable s1=gap/2
Variable s2=modelength/2
Variable d=0.5e-3 //separation of top from mode (mirror face radius)
Variable g=9.8     //acceleration of gravity
Variable top=0     //1 if atom makes it through the top gap, 0 otherwise
Variable mode=0    //1 if atom makes it through the mode, 0 otherwise
Variable xtmp1, xtmp2
Variable arrivaltime  //time that the atom hits the mode.


x0 = cloud[0] + gnoise(cloud[3])
vx = gnoise(vsdev)
y0 = cloud[1] + gnoise(cloud[4])
vy = gnoise(vsdev)


arrivaltime = ( vy + sqrt(vy^2 + 2*g*(y0+d)) )/g


xtmp1 = x0 +vx*(vy+sqrt(vy^2 +2*y0*g))/g
if((xtmp1 > -s1) && (xtmp1< s1))
   top =1
endif


xtmp2 = x0 + vx*arrivaltime
if((xtmp2 > (-s2+alpha*d)) && (xtmp2<(s2+alpha*d)))//sin(alpha)=alpha
   mode=1
```

```
        endif


    if(top==1 && mode==1)

        return(arrivaltime)

    else

        return(-1)

    endif

End


Function N_arrival_times(N,alpha,temp,gap,modelength,waist,cloud)

    Variable N,alpha     //N is how many atoms to simulate

    Variable temp        //temperature of cloud, in Kelvin

    Variable gap,modelength

    Variable waist       //cavity mode waist in meters

    Wave cloud

    Variable i=0

    Variable j=0

    Variable prob=0      //probability of hitting mode

    Variable s           //standard deviation of cloud in z dimension at
                         //   arrival time.

    Variable mass = 132.9*1.66e-27  //mass of Cs in kg

    Variable kB = 1.38e-23   //Boltzmann constant

    Variable vsdev = sqrt(kB*temp/mass)


    make/o/d/n=(N) $("times_"+num2str(N))

    wave w = $("times_"+num2str(N))

    Do

        w[i] = TransitTime(alpha,vsdev,gap,modelength,cloud)

        If (w[i] != -1)

            s = sqrt(cloud[5]^2 + (w[i]*vsdev)^2)

            i+=1

            prob += 0.5*erf((cloud[2]+waist)/(sqrt(2)*s))

            prob -= 0.5*erf((cloud[2]-waist)/(sqrt(2)*s))

        Endif

        j+=1

    While(j<N)
```

```
    prob /= N
    Redimension/N=(i) w


    make/o/d/n=101  $("times_"+num2str(N)+"_hist")
    wave hist = $("times_"+num2str(N)+"_hist")
    Histogram/B=1 w, hist
    Display hist
    ModifyGraph mode=5
    K0 = 0;
    CurveFit/H="1000" gauss hist /D
    print "Probability of hitting mode = "+num2str(prob)
    print "hits = "+num2str(i)
End
```

This code has several uses. It is particularly helpful when designing a new cavity, as it gives a guide as to how many atoms can be expected for a given cavity geometry and number of atoms in the MOT, as well as finding sensitivity to tilt in the cavity. It also helps in optimizing the MOT, since it helps indicate whether, for example, it is better to make the MOT lower or tighter. In addition, if a histogram of transit times is measured experimentally, it can be compared to this theoretical result in order to estimate the MOT temperature.

•N_arrival_times(2e7,0,1.6e-5,6.02e-6,8.52e-6,14e-6,cloud)
Fit converged properly
'fit_times_2e+07_hist'= W_coef[0]+W_coef[1]*exp(-((x-W_coef[2])/W_coef[3])^2)
W_coef={0,414.86,0.024063,0.0046997}
V_chisq= 23003.5; V_npnts= 101; V_numNaNs= 0; V_numINFs= 0;
V_startRow= 0; V_endRow= 100; V_startCol= 0; V_endCol= 0;
W_sigma={0,3.92,3.63e-05,5.14e-05}
Coefficient values ± one standard deviation
    y0   = 0 ± 0
    A   = 414.86 ± 3.92
    x0   = 0.024063 ± 3.63e-05
    width   = 0.0046997 ± 5.14e-05
Probability of hitting mode = 9.5901e-06
hits = 13412

Point	cloud
0	0
1	0.0024
2	0
3	0.000174
4	0.000174
5	0.000174
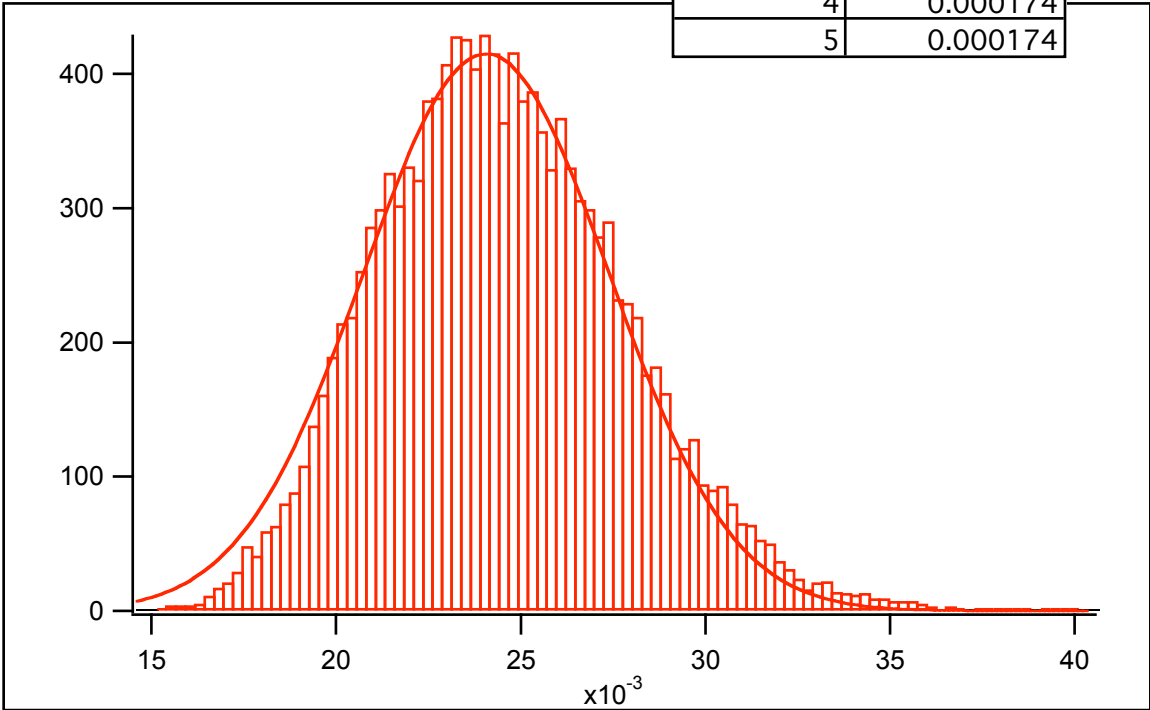
Figure 7.2: Sample input and output of program to calculate atom arrival times. Input parameters are for the cavity of Lab 1.

Chapter 8

Schemes for Improved Single Photon Generation

We outline a scheme for generating single photons using a single atom trapped in a cavity in the regime of strong coupling. This scheme efficiently produces polarized photons (even with a birefringent cavity) and reduces inhomogeneous pulse broadening by decreasing sensitivity to atomic motion. A variation on this scheme creates entanglement of the polarization of the single photon with the atomic Zeeman state.

A recent experiment [52] demonstrated that a cavity QED system can be used to generate single photons "on demand" with near-unit efficiency. This capability could enable diverse quantum information protocols [63, 18, 64, 65, 66, 16]. These protocals, however, require that the photon be emitted into a mode with a known temporal profile and polarization. The measurements of Ref. [52] indicated inhomogeneous temporal broadening, believed to be caused by variation in the atomic position and Zeeman state. The emitted photons were also believed to be an equal mixture of polarizations.

Ref. [67] outlines a technique for generating single photons which reduces sensitivity to atomic position within the cavity mode. The basic idea is to use adiabatic passage, which is sensitive to the ratio of two fields, but not to their absolute magnitudes. The two fields are overlapped since both are (different frequency) excitations of the same cavity mode, and as a result, there is little dependence on the atomic position.

A. Kuzmich further proposed [68] a method for optical pumping which would prepare the atom in a particular Zeeman state with high efficiency, reducing the inhomogeneous temporal broadening. The proposed method would also cause the photon to be preferentially generated with one polarization due to the ratio between Clebsch-Gordan coefficients.

In this chapter we will present schemes for preparing the initial atomic state and generating a single photon which use selection rules to completely control the photon polarization. These schemes also make use of the adiabatic passage technique of Ref. [67] to avoid sensitivity to atomic position.

8.1 Using $0 \nrightarrow 0$

The schemes discussed in this Section all rely on the dipole selection rule $|F, 0\rangle \nrightarrow |F' = F, 0\rangle$. This rule will allow us to use $m_F = 0$ states, which have the least sensitivity to magnetic fields, and linearly polarized beams, which are not affected by cavity birefringence. In addition, the SPG scheme below can be made "self-aligning" by having all critical beams polarized by the same optic.

We assume the capability to trap a single atom inside a cavity as in Ref [4]. We begin the protocol with optical pumping to an $m_F = 0$ state. This can be accomplished by illuminating the atom with a combination of coherent-state beams. Assuming that we are using Cesium atoms as in Ref [52], we can pump to the $|F = 4, m_F = 0\rangle$ state by using alternating pulses of linearly polarized $4 \rightarrow 4'$ light and any polarization of $3 \rightarrow 4'$ light. Of all the ground states, only $|F = 4, m_F = 0\rangle$ is dark to both beams, and hence, population will accumulate here. Note that the quantization axis is the polarization direction of the $4 \rightarrow 4'$ light. One must apply alternating pulses as opposed to using both beams continuously to avoid coherent effects which create another dark state [69]. Alternatively, one could instead use $4 \rightarrow 4'$ light continuously along with $3 \rightarrow 3'$ by introducing time variation into the polarization of the $3 \rightarrow 3'$ to avoid population accumulating in $|F = 3, m_F = 0\rangle$. If one wishes to pump into the $|F = 3, m_F = 0\rangle$ state, one can use linearly polarized $3 \rightarrow 3'$ light,

along with $4 \to 4'$ light of time-varying polarization, or alternating pulses of $3 \to 3'$ light with $4 \to 3'$ light of varying polarization.

Once an atom has been pumped into a state $|F, m_F = 0\rangle$, we can generate a single photon using adiabatic passage [67]. We apply a coherent-state beam which is π-polarized and tuned to $F \to F' \neq F$. This would drive the atom to the excited state $|F', m_F = 0\rangle$. However, the cavity is tuned to be resonant with the transition $F' \to F_{final} = F'$. By increasing the Rabi frequency Ω_R of the coherent-state beam slowly compared to g (the cavity coupling parameter) we adiabatically change the atomic state from the ground state $|F, m_F = 0\rangle$ to one of the ground states $|F_{final}, m_F = \pm 1\rangle$ while producing a single photon at the cavity frequency, with polarization to conserve angular momentum. The adiabatic condition avoids moving population to the excited state, from which there can be spontaneous emission. Note that the transition to the final state $|F_{final}, m_F = 0\rangle$ is not allowed by the selection rule since $F' = F_{final}$. Thus, the single photon generated cannot be π-polarized and will therefore be distinguishable from the coherent-state drive beam by polarization as well as by frequency.

The cavity geometry imposes additional constraints on the polarization of the single photon. The cavity supports only two polarizations, usually taken to be σ_+ and σ_- by quantizing along the cavity axis. However, birefringence in the cavity mirrors means that the eigenmodes of the cavity are linearly, not circularly, polarized [10]. If we quantize $\vec{z}$ along the direction of polarization of one of these birefringent modes, then that mode will be π-polarized. If we choose $\vec{y}$ to point along the other cavity mode polarization, then that polarization is $\frac{i}{\sqrt{2}}(\sigma_+ + \sigma_-)$. The remaining orthogonal linear mode, $\frac{-1}{\sqrt{2}}(\sigma_+ - \sigma_-)$, is not supported by the cavity because it is polarized along the cavity axis ($\vec{x}$). Therefore, if we use this basis, the single photon generated will be polarized along $\vec{y}$, and the final state of the atom will be $\frac{1}{\sqrt{2}}(|F_{final}, m_F = -1\rangle - |F_{final}, m_F = +1\rangle)$.

For example, this scheme could be implemented as illustrated in Fig. 8.1 by following these steps: Tune the cavity to $F = 4 \to F' = 4'$. After loading the atom into the trap, apply light near $F = 3 \to F' = 3'$ coupled to the cavity mode, aligned to
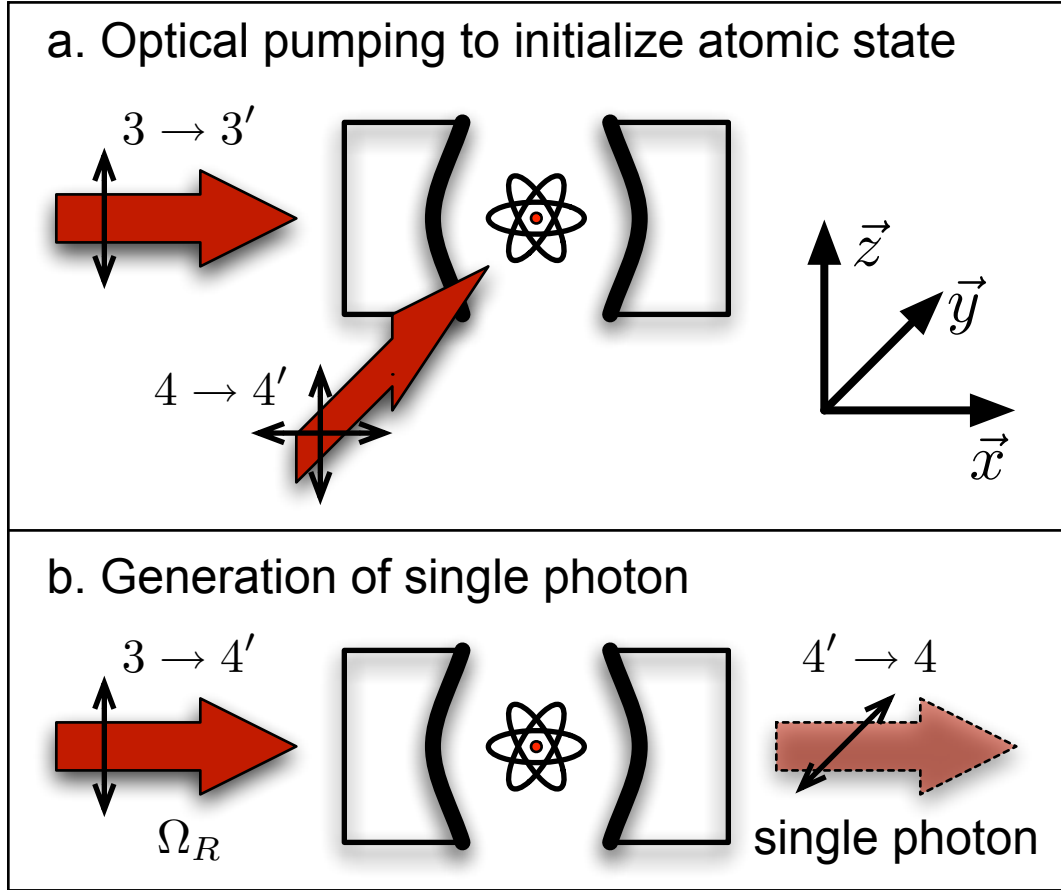
Figure 8.1: Beam placement, frequencies, and polarizations for one implementation of the (a) optical pumping and (b) single photon generation scheme.

a birefringent axis. Apply $F = 4 \rightarrow F' = 4'$ from the side, varying its polarization (this can be done, for example, by varying the relative amplitude or phase of different arms of a polarization gradient lattice). By using this implementation, it should be possible to also perform some cooling of atomic motion during this optical pumping phase [32]. In addition, the atom will transfer some light from the side beams into the cavity mode [70], which could be used to detect or count atoms [71], or to determine when the atom has reached the dark state. Once the atom has been pumped into the $|F = 3, m_F = 0\rangle$ dark state, shut off the optical pumping beams and turn on the coherent-state drive beam tuned near $F = 3 \rightarrow F' = 4'$, which is also coupled to the cavity and has the same polarization as the $F = 3 \rightarrow F' = 3'$ pumping light. This procedure is "self-aligning" in that the optical pumping light and the coherent-state

drive light can go through the same polarizer, and hence, are automatically aligned to each other in polarization. By aligning the polarizer to match the birefringent axes of the cavity, polarization errors can be minimized. Since the coherent-state drive field is also mode matched to the cavity, the ratio Ω_R/g does not depend on atomic position, reducing inhomogeneous temporal broadening [67]. The single photon generated is polarized perpendicular to the coherent-state drive field and ~ 9.2GHz detuned, which should make it easy to separate.

In a variation on this scheme, the optical pumping and coherent-state drive fields are linearly polarized along the cavity axis (they must come in the side of the cavity). In this case, the single photon can be in either cavity mode, and the polarization of the photon becomes entangled with the final state of the atom. Now choosing $\vec{z}$ to be along the cavity axis, we find that for a cavity with no birefringence, the final state of the light and atom is given by the maximally entangled state $\frac{1}{\sqrt{2}}(|\sigma_+\rangle \otimes |m_F = -1\rangle - |\sigma_-\rangle \otimes |m_F = +1\rangle)$, where the first ket gives the polarization of the photon and the second gives the Zeeman state of the atom. The relative sign of the two terms comes from the relative signs of the Clebsch-Gordan coefficients associated with the transitions. These photon states, however, are not robust with respect to cavity birefringence. More study is needed to determine the effect of birefringence on this scheme. It should also be noted that this scheme is not insensitive to atomic position, since the coherent-state drive field is not overlapped with the cavity mode.

8.2 Using Edge States

In this section, we will make use of edge states, i.e. states where $|m_F| = F$. We will use the relation $|m_F| \leq F$ to restrict the possible Zeeman states of the atom and photon polarization. We will utilize linearly polarized light fields in order to avoid birefringence-induced defects.

First, we present a scheme for generating polarized photons. We begin by pumping to the state $|F = 4, m_F = \pm 4\rangle$. Taking the cavity axis to be $\vec{x}$ and the birefringent modes along $(\vec{y}, \vec{z})$, this is accomplished by applying to the cavity π-polarized light

tuned near $F = 4 \rightarrow F' = 3'$, along with light tuned to $F = 3 \rightarrow F' = 4'$ (which may have any polarization and may come in the side of the cavity). Once the atom has reached one of the dark states, shut off the optical pumping beams and apply an adiabatically increasing coherent-state drive field to the cavity which is also π-polarized and resonant with $F = 4 \rightarrow F' = 4'$. This would drive the atom towards the excited state $|F' = 4', m_F = \pm 4\rangle$. With the cavity tuned to resonance with the $F' = 4' \rightarrow F = 3$ transition, however, the atom will instead be transferred to the ground state $|F = 3, m_F = \pm 3\rangle$ and a photon polarized along $\vec{y}$ will be created in the cavity. The photon cannot be polarized along $\vec{z}$ because conservation of angular momentum would require the atom to end in the state $|F = 3, m_F = \pm 4\rangle$, which does not exist.

Now we describe a scheme for generating a single photon whose polarization is entangled with the Zeeman state of the atom. This scheme does not produce a maximally entangled state, but it is insensitive to birefringence.

We begin again by preparing the atom via optical pumping to be in one of the states $|F = 4, m_F = +4\rangle$ or $|F = 4, m_F = -4\rangle$. Let us assume for the moment that the atom is in the state $|F = 4, m_F = +4\rangle$; the analysis is similar for $|F = 4, m_F = -4\rangle$. Now we will apply to the cavity an adiabatically increasing coherent-state drive field which is polarized along $\vec{y}$ and resonant with $F = 4 \rightarrow F' = 4'$. This would populate the excited state $|F' = 4', m_F = +3'\rangle$. However, with the cavity tuned to resonance with $F' = 4' \rightarrow F = 3$, the system will be adiabatically transferred to the state $(\sqrt{3}|\vec{y}\rangle \otimes |F = 3, m_F = +2\rangle + \sqrt{2}|\vec{z}\rangle \otimes |F = 3, m_F = 3\rangle)/\sqrt{5}$. Here, the first ket denotes the polarization of the single photon and the second represents the atomic state. The ratio of the two terms comes from the Clebsch-Gordan coefficients for the respective atomic transitions. Note that the only difference between this scheme for generating atom-photon entanglement and the above scheme for generating polarized photons is the polarization of the coherent-state drive field. It should therefore be relatively easy experimentally to switch between the two schemes.

Appendix A

Length of the Lab 11 Cavity

This is a summary of what I know about the length of the cavity in Lab 11, based on measurements performed by A. Boca in 2004. I discuss approximations used in finding the length from the resonant frequencies, as well as implications for the CQED and FORT spatial modes. Finally, I compare with previous measurements of these and similar mirrors.

For a cavity made from ideal mirrors, the resonant frequencies would be related to the cavity length by

$$f_N = \frac{cN}{2L} \tag{A.1}$$

where L is the length, c is the speed of light, and N is the mode order number. Since it is usually hard to find N independently, the free spectral range (FSR, the difference of successive resonant frequencies) is commonly used to characterize the cavity:

$$FSR = \frac{c}{2L} \tag{A.2}$$

While this is true for an idealized cavity, real cavities are not so simple. The variation in the measured FSR for different pairs of modes within the reflective band is about 5%. Clearly, we need a better model that goes beyond the limit of ideal mirrors if we want an accurate estimate of the length. In Ref. [34], they use a transfer-matrix formalism to calculate the propagation of a plane-wave through a stack of $\lambda/4$ dielectric layers. This gives an accurate description of each mirror; by calculating the transmission of two mirrors separated by a known gap L as a function

of frequency, they find the resonant modes. From this, they can find the free spectral range as a function of frequency, length, and coating parameters; they can find the length by fitting to the data (free spectral range versus frequency). The agreement between theory and data is quite good (see, for example, Fig. 2 of Ref. [34]), and they claim this method determines L to about 0.5 nm, which is a fractional error $\sim 5 \times 10^{-5}$.

However, this method is rather complicated, so we explore simpler options. Consider the extension of Eq. A.1 for realistic mirrors,

$$f_N = \frac{c}{2L}\left(N - \frac{\phi(f_N)}{\pi} - \frac{\phi_D}{\pi}\right) \tag{A.3}$$

where ϕ is the frequency dependent phase shift caused by one mirror, and ϕ_D is the phase caused by diffraction (called the "Guoy shift;" see Ref. [72] for details, noting that we use a different sign convention). This equation comes from the fact that at any resonant frequency, after a round trip the light will have acquired a phase of 2π times an integer N. Because the cavity under consideration has a much shorter length than the radius of curvature of the mirrors, the resonant modes are nearly plane waves and the Guoy shift is small:

$$\phi_D = -\arccos(1 - \frac{L}{R}) \tag{A.4}$$

where R is the radius of curvature of the mirrors (assuming a symmetric cavity). Since the lab 11 cavity has $L \approx 40\mu\text{m}, R \approx 20\text{cm}$, we have $\phi_D \approx -0.02$. In Ref. [34], they estimate that corrections due to this shift have an effect of about 3nm on the length estimate for the Lab 11 cavity.

Typically, one does not know the N associated with a measured resonant frequency f_N. However, one can make measurements of two resonant frequencies f_N, f_{N+m} separated by a known integer m. In this case, N can be eliminated from the equations, leaving

$$L = \frac{c}{2}\left(\frac{1}{f_{N+m} - f_N}\right)\left(m - \frac{\phi(f_{N+m}) - \phi(f_N)}{\pi}\right) \tag{A.5}$$

Notice that this does not depend on ϕ_D, but we will need a model of $\phi(f)$ in order to determine the length.

Our basic approach is to assume that there is symmetry about some frequency f_c, the center of the coating curve, and perform Taylor expansions about that point. This is reasonable for a mirror made of a $\lambda/4$ stack. There will be some frequency for which the mirrors are nearly perfect, and there will be varying phase shifts as we move away from that center frequency. We expect odd symmetry in phase about the center frequency.

The Taylor expansion of ϕ is given by

$$\phi(f) \approx \sum_k \frac{a_k}{k!}(f - f_c)^k \tag{A.6}$$

$$a_k = \frac{d^k\phi}{df^k}\bigg|_{f_c} \tag{A.7}$$

where $a_k = 0$ for $k > 0$ and even, by symmetry. The phase at the center of the coating curve, a_0, must be a multiple of π. Putting this into Eq. A.3 and keeping terms to third order, we have

$$f_N \approx \frac{c}{2L}\left(N - \frac{\phi_D}{\pi} - \frac{a_0}{\pi} - \frac{a_1}{\pi}(f_N - f_c) - \frac{a_3}{6\pi}(f_N - f_c)^3\right) \tag{A.8}$$

Substituting Eq. A.6 into Eq. A.5 and rearranging gives, to third order,

$$L \approx \frac{c}{2}\left[\frac{m}{f_{N+m} - f_N} - \frac{a_1}{\pi} + \frac{a_3}{6\pi}\left(3f_c(f_{N+m} + f_N - f_c) - f_{N+m}^2 - f_{N+m}f_N - f_N^2\right)\right] \tag{A.9}$$

Notice that this does not depend on N, ϕ_D, or a_0. The term proportional to m is the ordinary relation of the length to free spectral range that we had for ideal mirrors in Eq. A.2. If we ignore the a_3 term, but include the term proportional to a_1 and assume $a_1 = \frac{\pi}{f_c(n_H - n_L)}$ [73], we get

$$L \approx \frac{c}{2FSR} - \frac{\lambda_c}{2(n_H - n_L)} \tag{A.10}$$

which is the simple answer (appropriate near the center of the coating curve) for physical length given in Ref. [34], where $\lambda_c = c/f_c$.

The full form of Eq. A.9 gives us a more accurate way to compute the length from known frequencies, but it requires knowing the value of a_3. According to Seeley [74], we have

$$\phi(f) \approx -\arctan\left(\frac{\sin(\pi f/f_c)}{n_H - n_L}\right), \tag{A.11}$$

near the center of the coating curve if x, the number of high index layers in the dielectric stack, is large enough that $\left(\frac{n_H}{n_L}\right)^x > 15$, which is valid for our mirrors. Under this approximation, we find

$$a_3 \approx \left(\frac{-\pi^3}{f_c^3(n_H - n_L)}\right)\left(1 + \frac{2}{(n_H - n_L)^2}\right) \tag{A.12}$$

We could use Eq A.11 together with Eq A.5 to estimate length directly, but Devoe [73] found that numerical calculations of a_3 only agreed with experimental measurements to 25%. Therefore, we will only use Eq A.12 as a starting point, and fit a_3 to our data.

Typically, our data consist of measurements of several resonant frequencies separated by known numbers of orders. We would like to find values of (L, f_c, a_3) which are consistent with all measurements. In principle, we could take all possible pairs of measured frequencies and use Eq A.9 to adjust f_c and a_3 until we had a consistent value for L (Eq A.9 cannot be used to find a_1 since $\frac{ca_1}{2\pi}$ is a constant offset to L). This is not very convenient, however, so we will take an approach which may seem more circuitous, but is easier to implement. Rearranging Eq A.8 and substituting $a_1 = \frac{\pi}{f_c(n_H - n_L)}$, $a_0 = 0$, and Eq A.4, we find

$$N = \frac{2Lf_N}{c} - \frac{\arccos(1 - \frac{L}{R})}{\pi} + \frac{f_N - f_c}{f_c(n_H - n_L)} + \frac{a_3}{6\pi}(f_N - f_c)^3 \tag{A.13}$$

If we had a list of resonant frequencies $\{f_N\}$ and their associated order numbers $\{N\}$, then we could use Eq A.13 to perform a curve fit with $\{N\}$ as the independent variable, $\{f_N\}$ as the dependent variable, (L, f_c, a_3) as the fit parameters, and $(R, n_H - n_L)$ as

known constants. However, we generally do not know $\{N\}$ in advance, so we must use a boot-strapping process whereby we first estimate $\{N\}$, then take advantage of the fact that $\{N\}$ must be integers to fix $\{N\}$ and fit (L, f_c, a_3).

We start by finding a reasonable estimate of f_c. We can find this in many ways. If we have a transmission versus wavelength plot (a coating curve), then we can estimate f_c as the average of two frequencies with the same transmission (note that frequencies should be averaged, not wavelengths). If we have many successive resonant modes, then we can plot the difference of two successive frequencies versus the average of those two frequencies (similar to Fig. 2 in Ref. [34]). Then, if we fit a parabola to this curve, the center of the parabola will give an estimate of f_c.

Once we have an estimate of f_c, we can estimate L using Eq A.10, Eqs A.5,A.11 or Eqs A.9,A.12. With estimates of these parameters, we can use Eq A.13 to associate a value of N to each f_N. If these values are close to integers, then we round them and use Eq A.13 to fit (L, f_c, a_3).

For example, consider the measurements taken by A. Boca in August 2004, summarized in Table A.1. Note that only the first two wavelengths are successive modes of the cavity. First each wavelength is converted to a frequency (the second column of Table A.1). Now we need to get reasonable starting estimates for (L, f_c, a_3). We start with f_c, which we will estimate to be ~ 352 THz since we know the coating curve should be centered near 852 nm. Next, we will estimate L using Eq A.10 and computing the FSR from the first two frequencies in Table A.1. Taking $(n_H, n_L) = (2.0564, 1.4440)[34]$, this gives $L \sim 42.2$ μm. Now we apply Eq A.13 ignoring the term proportional to a_3 (which should be of order $|\frac{f-f_c}{f_c}|^3 \lesssim 10^{-3}$) to find an initial estimate of N for each f_N (third column of Table A.1). Since all of these are close to integers, we may round them and proceed to fit (L, f_c, a_3) without further effort to improve our initial estimates.

Taking $\{N\}$ to be as shown in the fourth column of Table A.1, we now use Eq A.13 to find $(L, f_c, a_3) \approx (42.207 \pm 0.005$ μm, 358 ± 2 THz, $1.7 \pm 0.3 \times 10^{-41}$ s^3), where uncertainties represent one standard deviation from the fit. The residual error of the fit to the data is less than the uncertainty in the measurement, i.e., the resonant

Table A.1: These are the resonant wavelengths of the lab 11 cavity recorded by A. Boca using the Burleigh wavemeter with a precision of 0.001 nm. The cavity was held on resonance with a probe laser which was locked to a Cs transition (third line of the table). The New Focus locking laser was tuned over one free spectral range to measure the wavelengths in the first and second lines of the table. The FORT laser was used to measure the fourth line.

λ_N [nm]	f_N [THz]	N (estimated)	N	$2L/\lambda$
827.685	362.206	101.987	102	101.988
835.750	358.711	100.987	101	101.004
852.357	351.722	98.988	99	99.036
935.586	320.433	90.036	90	90.226
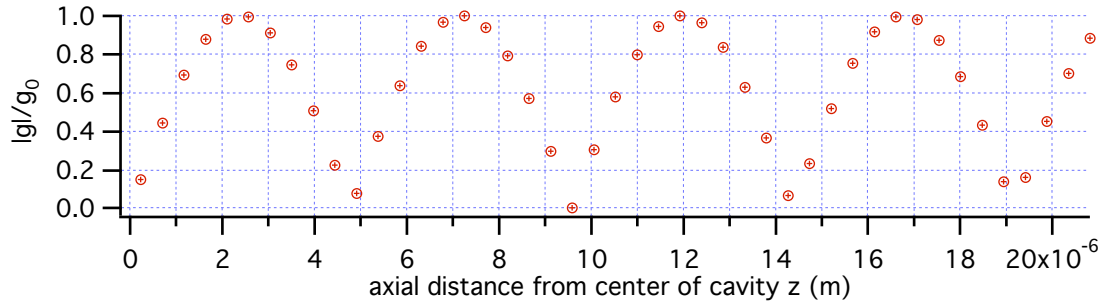
Figure A.1: Absolute value of g at each antinode of the FORT. Note that g is symmetric about the center of the cavity.

wavelengths predicted with these parameters are within 0.001 nm of the measured wavelengths.

Now that we know the length of the cavity to reasonable accuracy, we can calculate the structure of the cavity modes. Since this is a symmetric cavity, we assume that the intensity of any mode must be symmetric about the center of the cavity. Therefore, it will be useful to define the cavity axis z to be zero at the center of the cavity. Thus, the mirror faces are at $z = -L/2$ and $z = L/2$. Between the mirrors is vacuum, so the fields will vary as $\sin(2\pi z/\lambda)$ or $\cos(2\pi z/\lambda)$, where $\lambda = c/f$ is the vacuum wavelength of the field in question (diffraction will only give small additional phase shifts which we will ignore since $L \ll R$). To determine whether the field is even or odd symmetric, we will find how many half-wavelengths there are between the mirrors. Since we expect the field to be close to zero near the mirror face, we will

Table A.2: These are the resonant wavelengths recorded by D. Vernooy [75].

wavelength [nm]	N (estimated)
817.222	107.497
824.772	106.498
832.468	105.499
840.309	104.499
848.303	103.499
856.449	102.499
864.747	101.500
873.209	100.500
881.832	99.502
890.619	98.506

take the field to be odd (even) symmetric if the number of half-wavelengths $2L/\lambda$ is close to an even (odd) number. For example, the probe mode (the third row of Table A.1) will be proportional to $\cos(2\pi z/\lambda_{probe})$, while the FORT mode (fourth row) is proportional to $\sin(2\pi z/\lambda_{FORT})$. The registration of the two modes is displayed in Fig. A.1, where $|\cos(2\pi z/\lambda_{probe})|$ is plotted versus z with a marker at each maxima of $\sin^2(2\pi z/\lambda_{FORT})$.

For comparison, let us consider earlier measurements of the cavity length. When the Lab 11 cavity was assembled by D. Vernooy and J. Ye, its length was measured using resonant modes around 848 nm. The cavity was held at fixed length and a Ti:Sapph laser was scanned to find 10 successive resonant modes. The wavelength of those resonant modes was measured on a wavemeter. The wavelengths are reproduced from Table 6.5 of Ref. [75] in Table A.2. It should be noted that the corresponding frequencies listed in Ref. [75] are not accurate, since D. Vernooy took the speed of light to be exactly 3×10^8 m/s instead of keeping significant digits. D. Vernooy gives no estimate of error due to drift in the cavity length. It is unclear if these are wavelengths in vacuum or wavelengths in air (a correction of $\sim 3 \times 10^{-4}$). I will assume that these are wavelengths in vacuum, since that is what the Burleigh wavemeter reads.

In Fig. A.2, I plot the difference of successive frequencies (FSR) versus their average $\bar{f}$. Note that this does not look like Fig. 6.14 of Ref. [75], though it should. The data in the plot of Ref. [75] (Fig. 6.14) does not correspond to the data in the
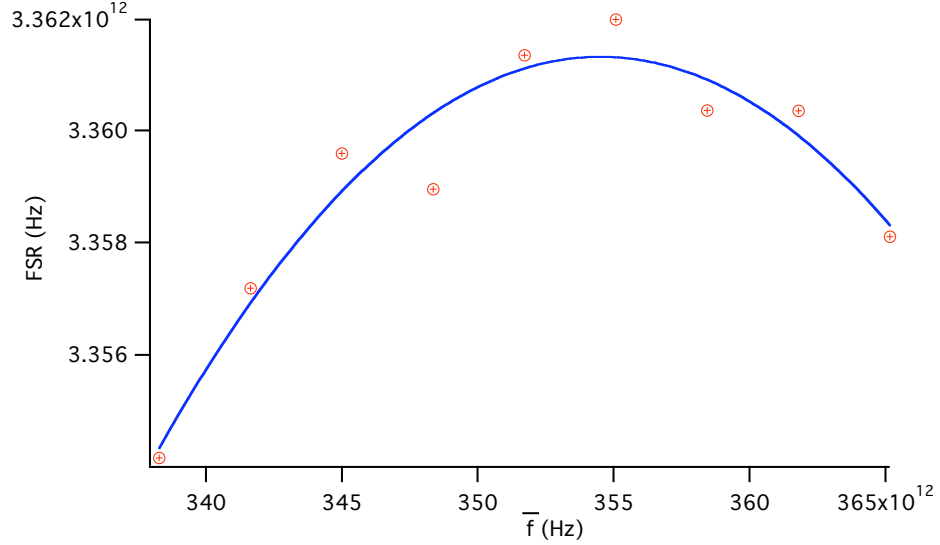
Figure A.2: Difference of successive resonant mode frequencies FSR versus the average of those frequencies $\bar{f}$, based on data from [75]. The curve is a parabola fit to the data.

table. We use the data from the table and ignore the data in the plot. We also fit the data to a parabola, $FSR = FSR_0 + k(\bar{f} - f_c)^2$. Using $a_3 = \pi k/FSR_0^2$ [73] and using FSR_0 in Eq A.10, we estimate $(L, f_c, a_3) \approx (43.904 \ \mu m, 355 \ \text{THz}, -7.37 \times 10^{-42} \ \text{s}^3)$. However, using Eq A.13 to estimate $\{N\}$ yields half-integers (see the second column of Table A.2). We are unable to proceed with our analysis to find more precise values of (L, f_c, a_3).

We will now analyze the measurements of Ref. [34]. Those measurements were performed on a cavity made from mirrors that were coated at the same time as those in the Lab 11 cavity, so we expect that the parameters (f_c, a_3) should be similar. The measured resonant wavelengths are reproduced in the first column of Table A.3. The estimated error in each measurement is 0.01 nm due to drift in the cavity length.

We start by estimating $(f_c, L) \sim (354 \ \text{THz}, 9.4 \ \mu m)$. This center frequency corresponds to a wavelength of 847 nm, which is the approximate center wavelength quoted in Ref. [34]. This value of L is derived from the first two measurements in Table A.3 in conjunction with Eq. A.10. Using these estimates and ignoring a_3, we produce the estimated values of $\{N\}$ displayed in the third column of Table A.3. We

Table A.3: These are the resonant wavelengths of another cavity constructed from mirrors in the same coating run as the Lab 11 cavity mirrors, from Ref. [34].

λ_N [nm]	f_N [THz]	N (estimated)	N	$2L/\lambda$	model λ [nm]
787.170	380.848	24.0065	24	23.8610	787.168
818.651	366.203	23.0204	23	22.9434	818.666
853.255	351.352	22.0204	22	22.0129	853.244
890.800	336.543	21.0233	21	21.0851	890.797

round these numbers as before and use Eq. A.13 to find $(L, f_c, a_3) \approx (9.391 \pm 0.002$ μm, 353.3 ± 0.8 THz, $1.4 \pm 0.1 \times 10^{-41}$ s^3), where uncertainties represent one standard deviation from the fit. The resonant wavelengths predicted by Eq. A.8 using these parameters are displayed in the fourth column. The discrepancy of these wavelengths from the measured values is close to the estimated error of the measurements. The value of f_c from this fit is comparable to that found for the Lab 11 cavity; the values of a_3 are consistent.

Appendix B

Ultra-High Vacuum Chambers

B.1   Overview

These are notes containing general information about UHV systems. Some of this comes from my own experiences in building the Lab 1 chamber, but most of it is from the collective wisdom and experience of the entire group (because the plural of "anecdote" is "data"). Some of the people I talked to are Theresa Lynn, Cristoph Nägerl, Dave Boozer, Hideo Mabuchi, Ben Lev, Sergey Polyakov, Russ Miller, and Liz Wilcut. Of course, much of what they know they were taught by their elders, in a fine oral tradition which I will refer to as The Lore That Has Been Passed Down Lo These Many Years. I have attempted to write down as much of this as possible together with what I learned from talking to technical support staff at various companies, reading catalogs, surfing the web [76, 77], and perusing a few books on vacuum technology [78, 79]. These notes are by no means complete, and quite probably not entirely accurate. I hope that this will be a living document which will evolve and grow with the group's experiences.

Here are the major steps in creating a vacuum system: designing the system, ordering the parts, cleaning and preparing them for use, assembling the system, pumping it down, baking it, and loading the Cesium.

B.2   Design Considerations

It's a good idea to put a lot of thought and planning into any vacuum system. Getting a vacuum system working can be a slow process, and discovering problems along the way can make it a lot slower. With careful planning you can catch a lot of the problems and design around them. You'll probably still find a few things you didn't think of or didn't expect, so try to leave some room for flexibility in the plan. Before you design your system, read through this entire set of notes and think about the whole process. You probably will also want to read the books in the bibliography, and look through the catalogs. When designing your vacuum chamber, here are some of the major considerations:

Good Conductance

There will always be some residual outgassing from all surfaces in your vacuum chamber. To achieve a low pressure, you need good conductance to the pumps. In the molecular flow regime (mean free path much larger than the size of the chamber), the conductance of a pipe (in units of liters/second) is about $(12.4D^3/(L + 1.33D))$ for nitrogen (N_2) at 295 K, where D and L are the diameter and length of the pipe in cm. This formula is supposed to be accurate to about the 10% level. Conductance scales as $(T/M)^{(1/2)}$ where T is the absolute temperature and M is the mass of the molecule. For greater accuracy or more sophisticated shapes see Refs. [78, 79].

Materials

Parts that will be inside the chamber should be made of low outgassing materials, and should be cleanable and bakeable. Stainless steel is the preferred material; 304L and 316LN are the most commonly used alloys for vacuum systems; 304LN and 316L are also OK. Christoph has used 303 steel (a magnetic alloy). Be aware that you cannot screw one piece of clean steel into another without it seizing. You can use gold as a lubricant (gold plate one part); the gold will rub off when you screw it together, so if

you want to re-use a part you will need to re-plate it. OFHC copper is vacuum safe and nonmagnetic (the stainless steel alloys are labeled "nonmagnetic," but anything with iron should be used with care if you are sensitive to magnetic fields). Copper is difficult to clean (see Section B.5), so we now prefer to gold plate our copper for vacuum use. If you get a copper piece gold plated, be sure to specify that you do *not* want them to use nickel in the plating process (by default they will first plate the copper with nickel, then with gold, which will make the piece ferromagnetic). Teflon (PTFE) and Mica/Macor are recommended for nonconductive materials. Glass is acceptable, but be careful not to allow thermal gradients or sudden cooling as this can cause it to crack. Most organic materials (e.g., plastic and rubber) have high outgassing rates and are not useable. Some exceptions are viton and RTV, which we have used in the vibration isolation stack inside our chambers. We have also used optical fibers which have acrylate coatings. Still, it is recommended to keep such materials to a minimum. Most epoxies are also not vacuum compatible. TorrSeal is a specially designed epoxy for use in high vacuum, but should still be used sparingly. We have also used small quantities of Dynaloy Inc 325 electrically conductive epoxy and MasterBond EP30LTEND (for matching the thermal expansion coefficient of glass). Other materials we have used include: EBL 3 shear mode PZTs, kapton insulated wire from MWS (36HML, DN-15376-1, 67429-03, PO#PP212167-77,Class 220 Type M2, J-W-1177/15), Kester Sn62 .015 solder with "44" rosin core, 100% Tin solder without rosin. All materials should have a smooth finish to reduce the effective surface area to as little as possible. Where dissimilar materials meet, remember that the system will be baked, so take into account the different coefficients of thermal expansion. In addition to low-outgassing, cleanability and bakeability, you should also consider what mechanical, electrical, thermal, optical, acoustic, and chemical properties you need for materials in your system.

Virtual leaks

Take care not to have any trapped volumes inside your chamber. Any region that cannot be effectively pumped will act like a "virtual leak," loading your chamber with gas. For example, if you must screw something into a blind hole, make sure that there will be some access from the hole to the pump (e.g., use vented screws, which have a hole through their center along their length).

The term "virtual leak" can also refer to dirty objects that have high outgassing rates. You can avoid this problem by choosing materials carefully and following a good cleaning procedure.

Assembly/Flanges

ConFlat (CF) is the standard for UHV flanges. It is good to the lowest pressures and at temperatures up to 400 C. There are two types of flanges: rotatable and non-rotatable. Be aware that if you attach two non-rotatable flanges to each other then your choice of orientations is limited. You can attach two rotatable flanges to each other, but it can be a pain (especially if you have to attach them in a vertical orientation; see Section B.6). One rotatable attached to one non-rotatable is usually most convenient. For very large sizes, ConFlat is replaced with wire seal (which is much the same, except that instead of a pre-formed copper gasket, you use a piece of copper wire). When you only need pressures down to 10^{-7} Torr, you can use QuickFlange (also called KwikFlange, KleinFlange, QF, KF, or, inexplicably, NW). It is good up to 200 C, depending on what materials are used in the clamp and the O-ring. QuickFlange is convenient because it can be quickly assembled and disassembled (hence the name) and the elastomer O-rings are re-used. However, it is not good for UHV, so it should only be used in situations with higher pressures (e.g., between a turbopump and its backing pump). ISO and ASA flanges are similar to QF. For more information on flanges and O-rings, see the Kurt J. Lesker catalog.

There is another type of seal we have used in our vacuum systems: the large (6") windows on the Lab 1 chamber used to be held on with a double viton O-ring

connection. The chamber had ConFlat ports, but instead of using a copper gasket, there was a viton O-ring in the triangular cross section groove next to the knife edge. This formed a seal between the chamber and the glass. The glass was held in place with a metal ring that had bolt holes that aligned with the ConFlat port. Between the glass and the metal ring was another viton O-ring. Bolts held the metal ring against the chamber and compressed both O-rings. This was a pain to assemble because the O-rings would slip out of position. It was also a pain to leak detect the system because viton is permeable to helium (see troubleshooting section). The vacuum system with these windows pumped down to a pressure of 10^{-8} Torr.

Access

You should consider how your vacuum system will interface to the rest of your experiment. This means, for example, providing optical access for beams and cameras. You should consider how many windows you will need and whether they will require antireflective coatings. AR coated windows are more delicate, so windows should not be coated unless it is necessary. If you need electrical access to your chamber, you should consider how many pins you need and how much noise is allowable. If you need low noise then you may want to use coaxial feedthroughs, but if you need many pins on a small flange then this will not be possible. Anecdote: we once had an electrical feedthrough that had long metal pins that went through a piece of ceramic. Electrical connection was made to the pins on the outside by soldering. The feedthrough developed a leak, which was attributed to mechanical stress on the pins causing a leak in the ceramic. Since then, we have had success using feedthroughs that end in BNC jacks. Liz Wilcut has successfully used fiber optic feedthroughs based on a Swagelock fitting with a Teflon ferrule (following Ref. [80]) in chambers achieving 10^{-9} Torr.

Finally, you should consider how your chamber is mechanically connected to the outside world. For experiments with cavities that are very sensitive to vibration, the vibration isolation stack inside the chamber is supplemented by the support system of the chamber itself. The chamber is held by aluminum clamps that grip the flanges.
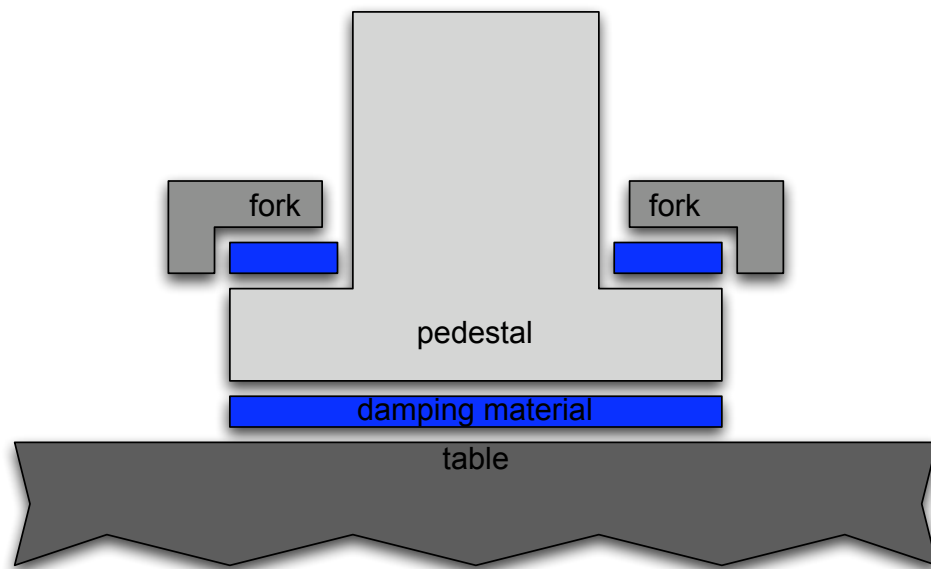
Figure B.1: How to sandwich vibration isolation material between a fork, a pedestal, and the table. The body of the fork is behind the pedestal in this view.

Between the flange and the clamp are layers of damping materials. The clamps are attached to New Focus pedestals which rest on more damping materials, and are held down by a fork which is also padded with damping material (see Figure B.1). The idea is to avoid metal to metal contact since this transmits high frequency acoustic noise.

Pumps and Gauges

Any vacuum system will need an ion pump to achieve and maintain low pressures. You should choose an ion pump such that your pumping rate will be limited by the conductance to the pump, and not by the pump itself. This means choosing a pump with a pumping speed (in liters/sec) higher than the conductance of the chamber (also in liters/sec). You should take into account the dependence of the pumping speed on pressure, the type of gas being pumped, and the saturation of the pump. In this lab, we have always used Varian ion pumps with StarCell elements (which are supposed to pump a wider range of gasses and work better at 10^{-8} and above than the Diode elements) with one exception: a Perkin-Elmer ion pump was once

used. Ion pumps can also be used in combination with titanium sublimation pumps (TSPs) (as in the lab 2 chamber) or non-evaporable getter pumps (NEGs) for greater pumping speed at lower pressures. However, TSPs and NEGs do not work on inert gasses and cannot be used alone. In principle, some turbo pumps could be used to very low pressures, but they lead to a lot of mechanical vibrations.

You will also need an ion gauge to monitor the pressure. Although you can use the ion pump current to give you some indication of the pressure, it is not that accurate so you probably don't want to rely on it. We have always used Bayard-Alpert type ion gauges from Varian. In the past, we have mostly used the standard glass enclosed gauges (the 571 for example). For very low pressures we used "extended range" nude gauges (e.g., the UHV-24p). For future chambers, I would discourage the use of glass encapsulated gauges since it is preferable to eliminate glass to metal seals whenever possible, and we have had no problems with nude gauges.

It should be noted that gauges are not necessarily accurate over the entire range for which they give a reading; the response can be grossly distorted, especially at very low pressures (10^{-9} for ordinary gauges, 10^{-10} for extended range gauges). They tend to read higher than the actual pressure. Also, they depend on the nature of the gas; according to the Lesker catalog, they will typically read 28 times higher for acetone than for an equal pressure of helium. The displayed pressure usually assumes the gas is N_2. For very low pressures, it may also be possible to use inverted magnetron gauges, but we have never used them. It should also be possible to use residual gas analyzers (RGAs), which give not only the pressure, but will also use mass spectrometry to tell you the composition of the gas. We have not used RGAs in this lab before, but Russ Miller used them at Michigan and recommends them.

Valves

Finding good valves has been a real problem. So far the only valve we have found that we trust for UHV is the VAT all metal right angle valve. Before we have used: Varian and MDC linear gate valves (not reliable against air pressure; have elastomer

seals, which are not very good for vacuum and degrade in the presence of Cs), Varian right angle elastomer valves (more reliable, but still has elastomer), MDC right angle all metal valves (unreliable), and a Swagelock valve (this was just a bad idea).

Cesium Reservoir

There is no consensus at this point on the best design of a Cesium reservoir. Some points that should be taken into consideration are the loading technique, the separation of the reservoir from the main chamber, and the ease with which the Cesium can be monitored. Of the two techniques that have been used for loading Cesium ingots (see Section B.9), the breaking-in-a-bellows method is now preferred for its relative simplicity and cleanliness, but it is not without its problems. If you use this technique, be sure to use a bellows with a 3/4" *outer* diameter, such as that sold by Varian. It is easy to accidentally use 3/4" inner diameter, such as that sold by Lesker, which then makes it very hard to break the ampule.

There is more debate over whether the reservoir should be separated from the main chamber by one valve or two. The idea of a two valve system is to make a Cesium "airlock"; that is, some Cesium is transferred from the reservoir to an intermediate space, then from there to the chamber. If there is always one valve closed at any time, then it should reduce the chance of accidentally flooding the chamber with too much Cesium. However, more valves means more complication, more parts to fail, a bigger system to pump, more cost, etc., and in practice it can be hard to use the "airlock" transfer technique effectively.

Another design point which is still under debate is the use of windows in the Cesium section. The advantage of a window is it makes it a lot easier to tell what is happening with the Cesium. You can see if it becomes oxidized, whether it is solid or liquid, and where most of it is. On the other hand, windows are much more likely to fail than steel parts, so there is a desire to keep the number of windows to a minimum. A window on the reservoir may be particularly vulnerable because the reservoir may be heated and cooled often. More than one system has been killed by failure of a

window on a reservoir. Anecdote: the window on the Cesium reservoir of the Lab 2 chamber started to leak in December 2000 for no apparent reason. The Cesium was oxidized. The leak was located by spraying methanol and appeared to come from one region of the glass to metal seal on the window (made by MDC).

A new technique for introducing Cesium to the chamber is the use of Cesium-rich "getter wires." These are designed to sublime Cs (among other elements) into a vacuum chamber when a high current is run through them (using an electrical feedthrough). They have been successfully used in the second chamber of the atomic ensemble experiment and the microtoroid chamber.

Cesium getters present a different set of design constraints and trade-offs. The advantage of using them is that they release very little Cesium and are easier to control. When the current to the wires is off, there is very little free Cs loose in the chamber. The major disadvantage is that they have a limited life span. After they have expelled all of their Cs, the chamber must be opened and they must be replaced. At this time, we do not know how long they last. According to the manufacturer, the total amount of Cs they carry is about 4.3-4.4 mg per centimeter of active length (although they have plots which show the yield asymptote near 2.2 mg/cm at 6.5 Amps and 3.9 mg/cm at 7.5 Amps). The second atomic ensemble chamber, which uses 1/2" getters, has been running for more than a year, with the getters on all day (but turned off at night) about 5 days a week.

Another design constraint when using getters is that they require line of sight from the wire to the target (where the MOT will form). This is because they do not have enough Cs to plate the walls of the chamber, so any Cs that comes off of them will fly in a straight line until it hits a surface, where it will stick permanently due to chemical reactions.

Bellows

In addition to their use in the Cesium reservoir, bellows can also be used to make two parts of a vacuum system meet even if they aren't perfectly aligned. This can be very

useful. However, it's generally best to keep the number of bellows to a minimum, since they are harder to clean and have a greater risk of failure than ordinary steel parts. Bellows should be hydroformed (not edge-welded) for greater robustness. It is good to have rigid mounts at both ends of a bellows so that it does not move as the system is evacuated (an inevitable exception is the Cesium reservoir). Air pressure can compress a bellows beyond its minimum length (20% less than its natural length; maximum length is 15% longer than the natural length).

B.3   Ordering Parts

Most vacuum parts can be ordered from Varian Vacuum Technologies or Kurt J. Lesker Company. You can also get general accessories from Huntington. Specialty items: We get our valves from VAT. We buy windows from Larson Electronic Glass with coatings by Guernsey. Larson has been slow and expensive, however, so one could also investigate buying the windows and sending them out to be coated independently. Sergey has tested windows from Huntington and found them acceptable. We have gotten small spherical hex chambers and larger octagonal chambers from Kimball Physics. The large chambers in lab 1 and lab 11 were custom made by Nor-Cal. We have gotten electrical feedthroughs from ISI. GCG Corp (in Glendale) does gold plating. We have had bad experiences when buying from MDC (in particular, problems with valves and windows) so we don't buy from them anymore. We bought Cesium getters (listed under "alkali metal dispensers with terminals") from SAES Getters. Order plenty of getters, and try to use as many as possible from different lots (since there are rumors that different lots can be very different in quality, and you want to minimize the chance of having all low-quality getters).

There are also a lot of general supplies that you will need. You should have large quantities of oil-free aluminum foil (from All-Foils), lint-free cloth (clean room polyester cloth from McMaster-Carr), powder free gloves (latex or nitrile aka N-Dex are OK and can be found at the Bio stock room), lens paper, solvents, and Fel-Pro C-100 Hi-Temp molybdenum disulfide anti-seize lubricant (from Varian).

Other miscellaneous stuff you may need: glove bags (from I-squared R, Instruments for Industry and Research), epoxies (TorrSeal from Varian or equivalents (e.g., Huntington Bond*Seal*Repair, or any other name for Dexter Hysol-1C) for general use in vacuum, MasterBond EP30LTEND for attaching mirrors to substrates, Dynaloy 325 electrically conductive silver epoxy from Lesker), EBL 3 shear mode PZT's (1.0" sq. 020 thick PO#PV292756 EL24460 from Staveley Sensors Inc, East Hartford CT). You can get wire from MWS wire industries. You can get vented screws, hardware made of different alloys, raw materials, rosin-free solder, etc. from McMaster-Carr. Selco is the distributor for Watlow heating bands. Cole-Parmer has heater tapes. Mindrum Precision will machine glass parts. You can order Cesium ingots from Aldrich. You can get ultrasound accessories from Process Equipment and Supply Inc.

For each ConFlat joint, you will need nuts, bolts, and gaskets. Nuts come in two types: hex and plate. Plate nuts have two threaded holes in them side by side. They are convenient to use since they cannot turn once both screws have been started, so you don't need to hold them with a wrench while tightening the bolt. Bolts come with different heads, lengths, and finishes. For size 8-32 screws we have always used socket heads. For sizes 1/4-28 and 5/16-24 you have the choice of hex or 12-point cap head. If you are attaching a window you will have to use a cap head since the hex head is too large and will cover part of the glass. The cap screws are usually more convenient to use, but the hex heads are good in some spaces where you can't fit a ratchet, but you can slide in a wrench from the side. You probably will want to use washers with hex head screws.

The length of the screw you need depends on how it is being used. If one of the flanges has a tapped hole (you are not using a nut), then you will use a shorter screw than if you were attaching two flanges with clear holes (using a nut). Table B.1 has a list of what screws go with what flanges, from the Lesker catalog. I don't know why they have a different length of screw for plate nuts vs. hex nuts on the 2 3/4" flange. You also have the choice of getting either regular stainless steel screws or silver-plated steel screws. The silver is supposed to act as a dry lubricant preventing seizing. I

Table B.1:   Appropriate type of screw for common sizes of ConFlat flanges.

flange OD [in.]	screw	length [in.] (tapped flange)	length [in.] (untapped flange)
1 1/3	8-32	1/2	3/4
2 3/4	1/4-28	7/8	1 1/4 (plate nut) 1 3/8 (hex nut)
4 1/2	5/16-24	1 1/4	2
6	5/16-24	1 1/4	2 1/4

haven't used them, so I don't know if it works or not. You should order a lot more (1.5x as many) screws and nuts than you need since some of them will have defects in the threads. You will also need to get gaskets for each ConFlat joint. For most joints you can use regular copper gaskets. For situations where you want the piece to have as little stress as possible during assembly, you should use fully annealed copper gaskets (which are softer than the regular kind). If you are worried about chemical reactions involving the copper then you can get gaskets which have been plated with silver or gold (note that Cs, however, reacts even with gold). Buy lots of extra gaskets (see Section B.6).

B.4   General Cleaning Procedures

This covers most structural components of a UHV system, including flanges, blanks, nipples, bellows, elbows, T's, crosses, 5-ways, 6-ways, multi-port chambers, and anything else made of stainless steel. It should be noted that the amount of effort spent on cleaning the components depends on how low a pressure is desired for the system. The microtoroid chamber was assembled from components which were solvent cleaned but never baked, and that chamber achieved pressures of $\sim 10^{-9}$ Torr. In order to get the lowest pressures, however, we have used the following procedures.

Parts should first be inspected for obvious contaminates, e.g., chunks of dirt or Cesium oxide. If there are large quantities of gunk, these should be removed first by hand using lens paper and solvent. Also, this is a good time to check that the knife-edges are in good condition. If they are notched, scratched, bent, or blunted

then there's no point cleaning it – you're going to need a new one. If the part has been exposed to oil (e.g., it has been machined) then it should be ultrasounded in soapy water (tap water + Alconox) for ten minutes and then ultrasounded in clean water (tap water OK) for ten minutes to remove the soap. One exception is bellows: the Red Book vacuum specification CS/05/95 [77] says bellows should *not* be cleaned with alkalines (soap) because it can leave precipitates in the grooves. Once a piece has had the oil removed and is visibly clean (swiping with lens paper and solvent does not make the paper dirty), then it is ready for vacuum cleaning.

Varian tech support recommends cleaning such components with a solvent like acetone or isopropanol, then storing in lint-free cloth.

The Lore suggests the following:

1. Ultrasound the parts for 15 minutes in acetone. Place parts in the solid basket (make sure this is clean first!) and pour in acetone to completely submerge all parts. There should be some water under the basket for good acoustic contact between the ultrasound generator and the acetone-filled basket. Afterwards, acetone should be poured into empty acetone bottles and marked WASTE. From this point on, you should not touch the parts with your bare hands. Wear gloves and only set parts down on clean foil.

2. Rinse the parts with isopropanol. Hold the part by an external surface and spray with isopropanol from a squirt bottle. This is just to eliminate any residue from the acetone. Allow the parts to dry in air. If you are in a hurry you can use a blast of nitrogen.

3. Bake the parts in the small vacuum oven. To do this, place the piece or pieces on a sheet of foil, place in the small vacuum oven along with a thermometer, close the door, and start the pump. Make sure that the valve to the pump is open and the valve to air is closed. Getting the door to make a good enough seal for the oven to pump down can be tricky – if the pressure does not rapidly decrease, stop the pump, open the door, pull off the orange rubber door seal, rotate it 90 or 180 degrees, and try again. Also, you can try pushing on the glass

part of the door while the pump is going. Once it makes a good seal, then you quickly get 15 pounds/sq.inch helping you, so you can let go. Notice that the vacuum gauge is in strange units where "zero" means atmosphere and evacuated is around 30. Once the oven is *completely* evacuated (wait 1 hour), turn on the oven and increase the temperature. For steel, you don't have to worry about the temperature too much, so just turn it all the way up. Bake for about 48 hrs. Turn off the heat, and allow parts to cool. You should be able to see the temperature on the thermometer, but be aware that the temperature is not uniform within the oven and the thermometer may not be at the temperature of the vacuum parts. When the parts have cooled to room temperature, valve off the pump and shut it off. Then carefully open the valve to air. If you have small parts that may blow away (e.g., screws), then you should open this valve slowly.

4. Wrap the parts in foil for safe storage. If you have a heavy piece which must be rested on a knife edge (e.g., a big multiport chamber), then you might rest it on a piece of soft material (with many layers of foil between for safety, since the knife edge can cut through the foil).

Alternative cleaning procedures have been used with similar results. For example, ultrasounding in isopropanol and skipping the rinse step can be appropriate for parts that aren't very dirty. The pre-bake step may not be important if the chamber will be baked anyway. Here's the general rule for solvents: Acetone is an aggressive solvent that works for a range of contaminates, but may leave a residue. The alcohols do not dissolve as many substances, but evaporate without leaving residue. Methanol is the most aggressive and quickest to evaporate and is good for swabbing at visible dirt. Isopropyl is the gentlest and safest to use when you are worried about damaging a material. It also evaporates more slowly, so it's convenient to use in large quantities, such as when ultrasounding. Ethanol is in between. If you are going to ultrasound with a solvent that evaporates quickly, or if you choose to ultrasound for a long period of time, you may want to cover the ultrasound basket with clean foil to reduce the

amount of vapor in the room.

In general, according to Roth [78] you actually want to use solvents first followed by an alkaline (soap) step. This is also the order used by the Red Book [77] standard. However, since we have access to pure solvents, but not to clean (distilled and/or deionized) water, we prefer to use the water based steps earlier.

B.5 Special Cleaning Procedures

More complicated or delicate parts should be cleaned separately, each following a procedure appropriate for that part. It is best to check with the manufacturer of the item before doing anything to it... even things printed here.

Windows

1. Clean by hand with lens paper and methanol. Clean entire glass face, glass-metal seal (there may be a lot of dirt here), and metal that will be in vacuum.

2. Ultrasound in methanol. Place windows (inside surface facing down) in a wire mesh basket inside the solid basket in ultrasound. Be careful not to trap air bubbles under the glass.

3. Rinse with isopropanol. Let dry in air on clean foil.

4. Bake in vacuum oven. Turn up temperature slowly – try to keep rate of temperature change below 20 C/hr (you can do this by going from room to max temperature in about 3 steps). Keep at max temp for 48 hrs. It is OK to turn off heat all at once since it takes more than 8 hrs for the oven to cool to room temp. Window temperature should never exceed 250 C (this temperature should not be possible in the vacuum oven anyway, but it's worth checking). Excessive temperature can damage coatings.

5. Place "lint free" clean room polyester cloth on *outer* face of window to prevent it from being scratched (inner face should be recessed anyway). Be aware that

"lint free" cloth is not, in fact, free of lint. Wrap in clean foil for storage.

Glass Ion Gauges (and Guages)

1. Clean accessible parts (basically, the steel) by hand with lens paper and methanol, very carefully. Pay special attention to the grooves.

2. Bake in small oven. Do not immerse gauges in solvent.

Ion Pumps

If the ion pump has been used before, then it should just be cleaned by hand with lens paper and methanol around the steel flange (but not the functional parts). If it has not been used before, then it has a pinched copper tube bolted to the front and is evacuated inside. Leave it alone until you are ready to assemble your chamber.

According to Jun Ye (as reported by Theresa Lynn), an ion pump that is very dirty can be cleaned by removing the pump body from the case and vapor degreasing it with acetone, "occasionally banging it against the table to knock stuff loose." Theresa has vapor degreased an ion pump once without hitting it, and found that it was not improved (it started out "marginal" and remained so).

Viton Parts

Viton should be cleaned by swiping with lens paper and isopropanol. Acetone makes viton brittle and should not be used (also, viton dissolves in acetone). Viton should be baked in the vacuum oven. The first time viton is baked it emits a large quantity of gas, so viton which has not been previously used/baked should not be put into a chamber.

Vapor degreasing

This is a technique we use occasionally. The part to be cleaned is held by a piece of bare copper wire over a bath of boiling solvent (usually acetone). The vapor condenses
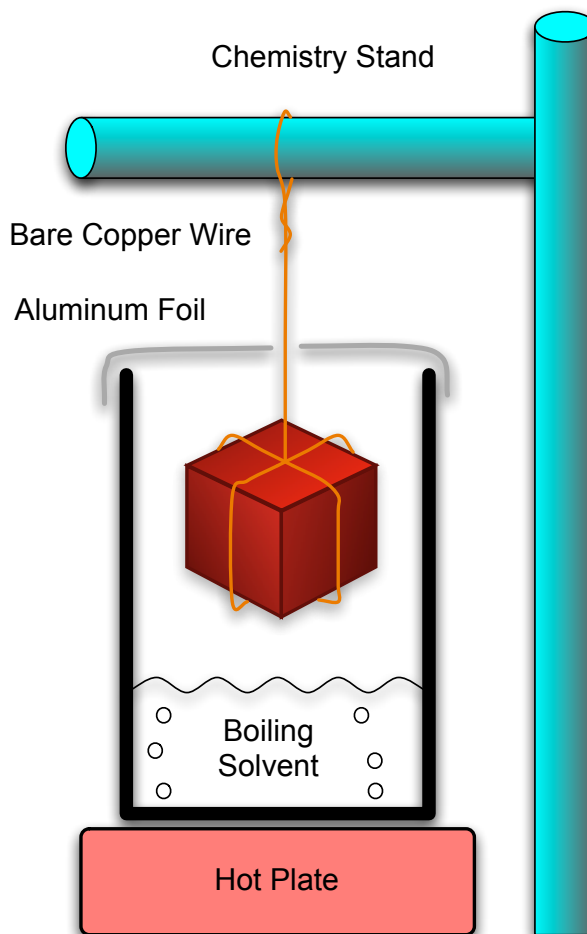
Figure B.2: Diagram of how to vapor degrease an object.

on the part and drips back into the bath. This way the solvent that touches the part is always clean. The amount of solvent that escapes can be minimized by using a tall beaker and covering the top in clean foil (see Figure B.2). Vapor degreasing should always be done in the fume hood. Be extremely careful, since there is a risk of setting the solvent on fire.

PZTs

According to The Lore, PZTs should be wiped with solvent, ultrasounded for a maximum of 5 minutes, rinsed with alcohol, and left to dry in air. It is now preferred to bake them after they have been glued in place. Check the maximum temperature

allowed for PZTs before baking them. The Curie temperature is 190 C for the shear mode PZTs we use (raising a PZT above its Curie temperature will depolarize it completely).

Electrical Feedthroughs

The Lore recommends solvent cleaning by hand, then baking in the small oven. Check the maximum bake temperature for the part. The feedthrough on the Lab 1 chamber has a maximum temperature of 200 C.

Copper

This procedure was obtained from Ali Farvid, the supervisor of the SLAC metal finishing shop. He can be reached at farvid@slac.stanford.edu or (650)926-2580. We have modified it slightly. Note that this procedure involves strong acids and presents serious safety risks. Never try this alone.

1. Vapor degrease in acetone.

2. Soak in Enbond Q527 for 5 minutes at 180 F (0.5 lb/gallon = 60 g/L). Enbond is made by Enthone Inc. New Haven, CT.

3. Rinse in cold tap water for 2 minutes.

   Prepare the fume hood for the next few steps. You will need a large bin filled with clean water for the rinse steps. From this point forward you need to perform rinse steps *immediately* with as little exposure of the piece to air as possible. For a rinse step, you will first dump the piece into the bin, give it a once-over with your gloves to get the acid off the surface, then transfer to a bucket in the sink with water constantly running in it. Keep wiping all the surfaces with your gloves, paying special attention to corners and hard to reach places. Try to keep to the timing as well as you can. You will have to prepare your solutions in advance. You should use teflon coated tongs to remove pieces from acid solutions.

4. Immerse in 50% hydrochloric acid at room temperature for 1 minute.

5. Rinse for 2 minutes.

6. Immerse in the following solution (at room temperature) for 1 minute:

   Phosphoric Acid, 75%   697 mL

   Nitric Acid, 42° Baumé (68%)   232 mL

   Acetic Acid, glacial   66 mL

   Hydrochloric Acid, analytical grade   5 mL

7. Rinse for 2 minutes

8. Immerse in the following solution until the part is covered with white film (do
   not immerse part for more than 5 seconds):

   Sulfuric Acid, 66° Baumé (94%)   431 mL

   Nitric Acid, 43° Baumé   232 mL

   Water   332 mL

   Hydrochloric Acid, 20° Baumé (31%)   3.9 mL

9. Rinse for 2 minutes.

10. Immerse in solution of Oxyban 60 (1% by volume) for 2-5 minutes. Thiokol/Dynachem
    Oxyban 60 can be ordered from Triteck Circuit Products, (714)279-1060.

11. Rinse for 1 minute.

12. Immerse in room temperature deionized water for 1 minute (minimum resistivity
    1Mohm-cm).

13. Immerse in hot deionized water for 1 minute (minimum resistivity 1Mohm-cm).

14. Immerse in analytical reagent grade isopropyl alcohol at 115 F for 30 seconds.

15. Blow dry with nitrogen. Do *not* touch with gloves!

16. Place on clean foil in small vacuum oven. Pump down for 1 hour, bake for 48
    hours. Do *not* expose to air while hot.

Cesium Getters

Sergey says Cesium getters should not be pre-cleaned or baked prior to vacuum chamber assembly.

B.6   Assembly

Before you begin assembly, you should check the following:

- Have all the vacuum parts been cleaned and pre-baked (if possible)?

- Do you have all the necessary copper gaskets, nuts, and bolts?

- Do you have plenty of gloves, foil, lens paper, solvents, and anti-seize compound?

- Do you have all the structural supports you need to hold your chamber?

- Have you installed the heating elements on your ion pumps?

To install the heating element in an ion pump, follow the directions in the manual. If you have to open the pump case, be very careful. There are strong permanent magnets inside that can come dislodged, fly together, and damage themselves (or objects in the nearby vicinity). If you remove the pump body from the case, it's a good idea to put a wooden spacer in its place to hold the magnets apart.

When you have all the components prepared, you are ready to assemble the chamber. Follow these steps for each ConFlat joint:

1. Prepare the screws and nuts. Select out how many you will need and put them on a tray or in a convenient place where they can be easily reached. Be sure to have extra in case some are defective (having 1.5x as many as you need is very safe). If you are using anti-seize, carefully apply it to the end of the screw and smear it into the grooves using your gloved fingers. Make sure that the part of the screw which will eventually be in the nut or the tapped flange is thoroughly coated, but do not leave large amounts of excess since you do not want to smear it all over your chamber. Be very careful not to get it on the

head of the screw, and leave enough of the screw clean that you can pick it up without getting your gloves dirty. *You don't want to get any anti-seize in your chamber.* Set the screws down on a clean piece of foil in such a way that you can pick them up without getting your gloves dirty. One way is to use a rectangular tray and put the screws with the ends in the corner and the heads fanning out towards the center of the tray. You might need to change pieces of foil in the tray between doing flanges because the anti-sieze can get all over the place. Taking these precautions is not always necessary but it can make it a lot easier because you will not have to be as concerned about what your gloves are touching.

2. Inspect the knife edges and clean them with methanol. Put on clean gloves, unwrap the foil off of the flanges that you will join, and carefully inspect the knife egdes. If they are damaged, you need a new part. Remember when working on a part that has multiple flanges not to get the other flanges dirty (keep them wrapped in foil) or damage them (do not let a knife edge rest or press against a hard surface). Swipe the knife edge with lens paper and methanol. Look for any bits of lint on the accessible surfaces. It's OK if you see some as long as you can remove them with lens paper and methanol or a blast of nitrogen. If you are attaching a window, carefully inspect the inside surface. It may help to have a flashlight or a strong light source nearby. Do not hold the window inner face upwards for a long period of time since dust will settle on it. There will be a substantial amount of lint on the outer face from the "lint free" cloth – don't worry about this since it can be cleaned later. Try to get the inside face as clean as possible using methanol and lens paper. Using a blast of nitrogen is acceptable, but be very careful. It may help to move the window onto a fresh piece of foil since the foil it was wrapped in may have lots of lint from the "lint free" cloth.

3. Carefully place the gasket between the knife edges. Only touch a gasket with clean gloves, and try to touch it only around the outer edge (where it will not

be in the vacuum). If it touches a dirty surface (i.e., anything that is not a fresh sheet of clean foil), throw it away and get a new one. It may be difficult to keep the gasket in place while assembling the joint, especially if the gasket has to remain vertical. It may help if the chamber has a slight tilt so that the gasket will remain in its seat without falling out. It helps if you can put it in the non-rotateable flange first. Also it sometimes helps to hold the top edge of the gasket in place by sliding a poky tool (inoculating needle) down the groove in the flange (some, but not all, flanges have grooves that go between the screw holes) and using the tip to hold the gasket from falling forwards. Carefully put the flanges together and make sure the copper gasket is properly seated. You may drop a lot of gaskets while putting together vertical joints – don't worry about it. It may help to have two people so that one person can hold the gasket and the other can bring up one of the flanges, and then one person can hold the flange together while the other puts in the screws.

4. Put the bolts in place and tighten them. Put them all in and get them finger tight before tightening any of them with a wrench. If getting the screw finger tight is difficult or if it feels like the threads are bad, throw away the nut or screw responsible and use your spares. If the gasket falls out while you are putting the screws in, be aware that you may have smeared anti-seize on the flanges. If the gasket falls out, you will have to go back to step 3 with a new gasket, and it will require great care and much checking of your gloves when you try to put the joint back together. When the joint is held together by the screws and nuts, with the gasket properly seated and in place, you are ready to tighten. You want to make sure that the seal is even all the way around, so you will go around the flange many times tightening each screw by a small amount. It is adviseable to use a "star-shaped" pattern for tightening, where the next screw you tighten is as far away as possible from the screws you just tightened. See Figure B.3 for flanges with 6, 8, and 16 screws.
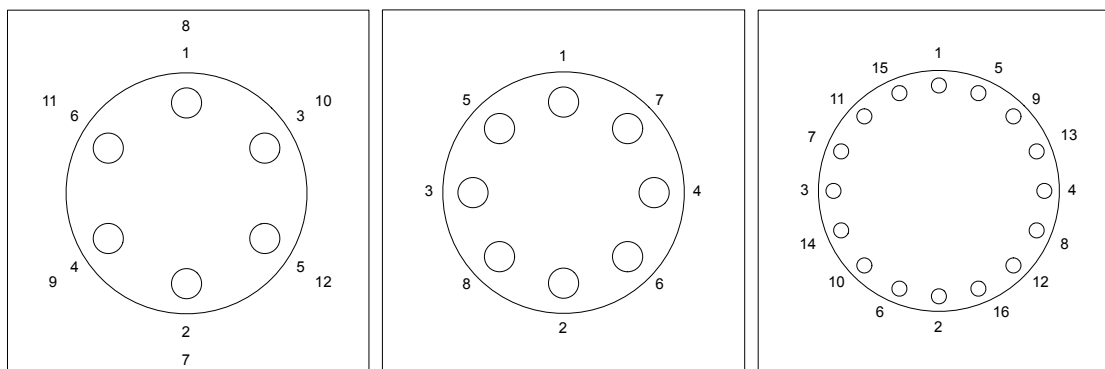
Figure B.3: The order in which to tighten bolts on ConFlat flanges with 6, 8, and 16 screws.

Table B.2: Recommended torque for ConFlat flanges.

1 1/3"	51in.lb.
2 3/4"	96in.lb.
4 1/2" or greater	192 in.lb.

If you are using annealed gaskets, the Lesker catalog recommends no more than 1/16th of a turn on each screw per round. Varian tech support has a recommended torque for each size of ConFlat flange (see Table B.2). Be careful not to damage the heads on any of the screws. It is especially easy to damage the heads of the 8-32 screws (used on 1 1/3" ConFlat joints).

Christoph says that there should always be some room between the steel edges of the flange (that is, you should always be able to see some of the gasket from the outside). It's OK if this room isn't very much (e.g., just enough to slide a sheet of paper or foil between the edges) as long as it isn't zero. The reason is that if the steel parts are touching each other, then a torque on the joint will have more leverage to separate the knife edge off of the copper. Also, it will be impossible to further tighten the joint if a minor leak occurs some time later.

Unsealing an Ion Pump

1. Check the manual for special instructions for your model.

2. Clean off the end of the pinched copper tube with lens paper and methanol.

3. Slowly crush the end of the tube between the jaws of a machinist's vise. Crush along the long dimension of the pinch. You should hear a hissing sound when the copper springs a leak. You want to use a vise and not a cutter or saw because air is going to rush in and you don't want metal shavings or other junk to fly into the pump body.

4. When the hissing stops it is safe to undo the ConFlat fitting holding the copper piece on. It may be very difficult to undo the bolts.

5. Clean off steel flange with methanol and lens paper. Now it's ready to be attached to your system.

Preparing Cesium Getters

The Cesium getters that we buy have a cross section which is roughly square (about 1 mm on a side), have a variable length (usually about 1-2 cm), and end in flat tabs. These getters must be connected to an electrical feedthrough in order to use them. This has been done using crimp connectors which come with the feedthrough. The crimp connectors are metal sleeves (hollow cylinders) which slide over the pins on the feedthrough. The tabs at the end of the getters are bent and inserted into the sleeves, which are then crushed with pliers in order to hold the tabs and make electrical contact. Note that the getters have a preferred direction; one side should have a groove which will emit the Cs. Be sure that this points toward the target region of the chamber where you will form the MOT. We do not have much data on the reliability of the crimping technique but it has worked so far. Be careful not to damage the feedthroughs. The manufacturers say not to bend or cut the pins, since any stress on them can cause leaks.

B.7 Pumping

When your system is fully assembled, you are ready to pump it down. You can use a turbo pumping system to get from room pressure to high vacuum.

A turbomolecular (or turbo) pump is a stack of rapidly spinning blades. It works by transferring momentum from the blades to gas particles, sending them to the output port. Turbo pumps may have greased bearings in them, but are designed to minimize the flow of oil molecules back into the system. Some turbo pumps use magnetically levitated bearings to eliminate lubricants altogether, but these pumps may be easily damaged by bumping them and displacing the rotors (according to Hideo). Turbo pumps may be rated with a compression ratio (max value of (pressure at the exhaust port / pressure at the intake port), usually for N_2). Note, however, that they are designed only to work in a certain pressure range, so this compression ratio is a function of pressure. Also, the compression ratio is better for heavy molecules than for light molecules since it depends on the thermal velocity of the molecule relative to the speed of the blade. Be aware that turbo pumps can be damaged by being suddenly exposed to high pressure, or by large particles (e.g., flakes of dust) entering the pump during operation.

Turbo pumps do not work with the exhaust port at air pressure so they must be backed by another pump. There are two kinds of pumps commonly used for this purpose: rotary vane pumps and diaphragm pumps. Each has its advantages. Rotary vane pumps are generally more powerful and will usually give the system a better pumping speed and a better ultimate pressure. However, they are extremely dirty. Diaphragm pumps are usually not as powerful but are oil-free which makes them more convenient and safer to use.

If you have a turbo backed by a rotary pump then there are a few things to consider. One is that there must be a trap between the pumps to prevent oil molecules from the rotary pump from contaminating the turbo and eventually the vacuum chamber. The trap is basically just a volume filled with densely packed metal fibers which makes the diffusion time very long for the oil. According to Varian, traps are

maintenance-free, but the Lesker catalog recommends baking and pumping on traps frequently to prevent them from getting saturated with oil. The Lesker catalog has a lot of information on how oil can get into your system and how to prevent it in its technical notes on traps and traps and filters. As far as I know, we have never cleaned the traps on our system. Another thing to consider is that you never want to have a pressure imbalance in the system that will suck air/oil from the rotary pump into the trap/turbopump. This means, for example, that the system must be vented upstream of the trap before the rotary pump can be turned off. Since the order of operations for starting and stopping the pumping system, and the timing of the venting that will quickly bring the turbo to rest without damaging the blades, is tricky and very important, it is best to have a system with a master controller that performs these functions automatically.

Around the labs we have two pumping stations on carts, each with a turbo pump, a rotary pump, a trap, an automatic valve for venting, and a controller (Hideo also has a turbo/diaphragm combined unit). The controller should take care of most situations so as to prevent oil backstreaming, but be aware that if the power is suddenly cut then there will be problems: (1) the valve will automatically vent, so everything, including whatever the pump is attached to, will be filled with air; (2) the valve has a built-in delay, so for a few seconds the rotary pump will not be pumping but the system will still be at low pressure, meaning oil will be sucked through the trap and into the turbo pump and whatever it is attached to (e.g., your chamber). This is very bad.

Here are the basic steps to pumping down your chamber:

1. Check the oil in the rotary pump. If it is dark then you should probably replace it. Check the manual for instructions on changing the oil. Basically, you unscrew plugs on the top and on the front and let the oil drain out, tipping it forward to get the last bit out. Then you put the front plug back in and fill from the top until you see the level in the sight glass is between the notches. The oil usually needs to be replaced after about 3 weeks of pumping.

2. Clean the bellows. As a precaution, we usually pump and bake on everything attached to the pump (e.g., a long bellows, an ion gauge, a T or cross, maybe an elbow or a valve, etc.) before exposing the chamber to it. This can be done either by blanking the bellows where it would be attached to the chamber or by attaching to the chamber but having the valve separating them be closed. For more information on baking, see the next section. The turbo unit can be baked to 120 C (check manual first), but we don't usually bake the turbo itself at all (though it might be a good idea). As you bake and pump, you can monitor the pressure on the ion gauge, which you can turn on after the system has been pumping at "normal operation 70kRPM" for an hour. The gauge will probably need frequent de-gassing. We usually start the pumping, then start baking the next day, then watch the pressure until it stops falling, turn off the bake, then wait for everything to come back to room temperature before moving to the next step. If you were going to clean the trap (which we have never done as far as I know, but might be a good idea), you should probably do it before pumping and baking the bellows or turbo. You would clean the trap by disonnecting it from the turbo, blanking the end, and pumping on it with the rotary pump while baking it.

3. Pump on the chamber. If you cleaned the bellows with a blank, then shut off the pump, take off the blank, attach the bellows to the chamber with the valve open, and start the pump. If the bellows is already attached to the chamber but the valve is closed, then you need to slowly and carefully open the valve. You don't want to hit the turbo pump with too much gas too quickly. You can watch the pumping speed on the front of the controller to give you some indication of how much stress the pump is under. You cannot use the ion gauge at this time because the pressure will be too high; turn off the gauge before you start to open the valve.

B.8   Baking

In order to achieve low pressure you must bake your system as it is pumped. Baking increases the outgassing rates, and in general the hotter you bake the faster you get your chamber clean.

In this lab there have been two basic approaches to baking. One is to cover the chamber with heating elements over every part and adjust the power to each element to achieve the desired temperature. The other is to put the entire chamber inside a large oven (or build a large oven around the entire chamber). There are problems with both approaches. If you use lots of heating elements, then you need lots of controls and lots of sensors. Getting a uniform temperature that changes at a specified rate is very difficult and requires a lot of attention and adjustments. High temperatures may not be accessible at all. On the other hand, building a big oven requires enormous amounts of power, lots of irritating fiberglass insulation, a spare room (which will be uninhabitable due to heat, baking smells, fiberglass particles, possibly exposed high voltage... Don't even think of doing this in your lab) and a chamber which has been designed (with its mounts) to be transported without stressing the joints.

Here are some tips and caveats for the many-heater method. If you are baking your chamber on an optical table, be careful not to get the table too hot. According to Newport, optical tables have damping materials inside that degrade at 50 C (check for your table – Ben's is good to 80 C). Use heating bands where you can, and remember to put a thermocouple under each one so you can monitor the temperature. Use tapes on pipes and irregular shapes. If you have tape over glass (e.g., on a glass ion gauge), you might want to put a layer of aluminum foil underneath the tape to help distribute the heat (though this can make it harder to get high temps due to reflection). It's better to avoid having a heating element directly on a piece of glass if you can avoid it. Remember that steel is a poor thermal conductor and glass is worse. Be careful not to heat glass unevenly because you can crack it. Cooling it quickly is also very dangerous. Steel is less sensitive, but remember that if you leave a cold spot, the stuff that comes off as you bake will condense or stick to the cold

region; a bake is only as hot as the coldest point. Cover the face of every window with foil to distribute the heat across the surface, but do *not* allow the foil to touch the glass anywhere (if the foil touches the face of the window at one point, it will rapidly conduct heat to/away from that point and will lead to thermal stress). For windows we have used a heating band around the outside of the steel with foil wrapped over the face, stretched between the bolts so as to not touch the glass. Cover everything over with layers of aluminum foil (with some air between the layers) to give as good an insulating layer as you can. Fiberglass insulation should be used with caution. It can be very effective, but it can leave a real mess of nasty irritating dust and fibers. Heating elements can be powered by variacs (variable autotransformers) or dimmer switches (solid state power controls). Mostly we have used variacs, but they are expensive and are really more than you need. You can get dimmer switches for lamps from Home Depot that work up to 500 watts, but the slider controls are not linear and they can be a pain to adjust. You can also order just the components from electronic catalogs and wire up a knob and a power cord, but it takes longer to make the boxes and do the soldering. When ramping the temperature, go slowly and watch all your sensors. Try to keep everything at about the same temperature. You should have at least one sensor for every heating element, with extras for long tapes or for locations without direct contact from a heater.

As I am writing this, Tracy Northup and Russ Miller are looking into large commercial ovens that could be used for baking vacuum chambers. This seems highly preferable over our previous methods. Our attempt at using a homemade oven (for baking the first Lab 2 chamber) was very unpleasant.

General points: Check the maximum temperature of all your components. You may want to assemble your chamber in stages so that you can bake different parts to different temps. For example, the lab 2 chamber was first baked with steel blanks where the windows go. Then they replaced the blanks with windows (while keeping the chamber overpressured with dry nitrogen) and baked again to a lesser temperature. Windows should not be ramped faster than 20 C/hr (check with your manufacturer); valves no more than 60 C/hr. Dave Boozer once had a valve get stuck in

Table B.3:   Maximum bake temperatures.

Steel	450 C
Uncoated windows	400 C
Coated windows	200-250 C
All-metal valves	450 C open, 350 C closed
Nude ion gauges	450 C
Ion pumps	350 C
Viton	150-200 C, depends on type
ISI feedthrough with 4 BNCs	200 C
Kapton insulated wire	220 C
Cesium getters	500 C

the open position after a bake, so he now recommends leaving valves almost, but not completely open while baking.

If possible, you want to bake to at least 200 C since around 180-190 C is supposedly a "magic temperature" at which water in thin films on surfaces evaporates (as told by Christoph, and as sort of confirmed by Varian tech support, though they were pretty vague). Table B.3 lists some maximum temperatures for various components. You should check with the manufacturers to find the maximum temperature of all of your components before you bake.

This would also be the time to do a special bake of the Cs getters. The second atomic ensemble chamber was the first test of using getters as a Cs source. This chamber was not baked because it was not necessary in order to get to the desired pressure range (10^{-8}-10^{-9} Torr). However, the getters needed a special bake before they could be used. That is because they operate at very high temperatures (the manufacturers say 550-850 C) and they give off a lot of other substances before they get hot enough to release their Cs. Sergey's technique for baking off these unwanted substances was

1. With the turbopump pumping on the chamber, run 1 amp through the getter. This raised the pressure of his system to 10^{-4} Torr. Wait until the pressure falls back to what it was without current (around 10^{-7}-10^{-8} Torr for his chamber when hooked up to the turbopump). This took about 24 hours for him.

2. Increase the current to 2 amps. Again the pressure will greatly increase at first and then return to a low pressure, this time over several hours.

3. Again increase the current to 3 amps. It took his chamber about an hour for the pressure to come back down.

4. Turn off the current to the getter. It is now ready for operation. Repeat this process for each getter in the chamber. For the second atomic ensemble chamber, there were 3 getters so this process was done twice. The third getter was left alone in case there was a problem with this method.

At the end of this procedure he switched over to the ion pump and was ready to use his chamber.

If doing a full chamber bake, continue to bake (while turbopumping) until the pressure is not falling (usually about a week). After it cools down, you can close off the valves, and turn on the gauges and pumps. With the turbo pump still pumping on the chamber, turn on the chamber ion gauge. Make sure that it is working and giving a reasonable reading (typically somewhat higher than the reading of the gauge on the turbopump, depending on your chamber geometry). Then turn on the ion pump. According to The Lore (from Jun Ye via Theresa), we "burp" ion pumps when we first turn them on. This means that we turn them on and off a few times. The reason for this is that when you first turn on an ion pump after a bake it has a high pump current and it seems to increase the pressure of nearby gauges. So we turn it on and off at first to get the stuff out of it (and hopefully have it removed from the system by the turbopump). Then when the pump current is lower, at a level corresponding to the ion gauge readings, we leave it on. You should now be able to see the pressure on the ion gauge falling due to the action of the ion pump. When you have confirmed that the ion pump is working, close off the valve to the turbopump. Congratulations, you have yourself a vacuum system!

Peugeot

B.9 Loading Cesium

Now that you have a beautiful clean vacuum system, the first thing you get to do is contaminate it with some nasty Cesium. There are three techniques we have used to add Cesium to a vacuum system: pouring the Cesium into the chamber inside a glove bag (not recommended), breaking an ampule of Cesium in a bellows, and running current through a Cesium getter.

Pouring Inside a Glove Bag

Starting state: chamber is evacuated, pumps and gauges are off, nitrogen line (which has been flushed) is connected to closed valve. This takes at least two people (one with their hands inside the bag and one outside) and preferably three (one to monitor/adjust the flow of nitrogen or pressure of the bag).

1. Attach glove bag to chamber. You will have to cut open the narrow end to attach it. We have used electrical tape to make a seal from the glove bag to the chamber and it seems to work fine.

2. Put needed items in the glove bag. These include wrenches to open and close the chamber, plenty of gloves (you need to wear disposable gloves inside the glove bag to prevent the built-in gloves from getting dirty or punctured), fresh gaskets, the Cs ampule, etc. Make sure the nitrogen hose is securely in place inside the bag. You can close off the wide end of the bag with a twist tie or the Ziploc style plastic things that come with the bag. It's good to have something that is easily adjustable so that you can maintain the pressure in the bag without having it deflate or explode.

3. Fill and flush the bag with nitrogen. Let it fill and then compress it, expelling the gas through the wide end of the bag. Repeat about 4 times so that the oxygen/water content of the bag is very little.

4. Open the chamber. Slowly open the valve to the nitrogen line (which should be overpressured). You want the chamber pressure to be greater than room

pressure, but not so large that you risk damaging delicate components (e.g., glass ion gauges or cells). A few kPa above room pressure is OK. For added safety, you can use a "blowout" valve on the nitrogen line to prevent the pressure from getting too high. When the chamber is filled with nitrogen, unbolt the accessible flange of the vacuum chamber. If you are using a right angle valve with an elastomer seal on the moving part of the valve, be careful not to blow the elastomer out of its seat as you open the valve. Keep the nitrogen line at a modest pressure until just after the valve has started to open, then crank up the pressure. Once the chamber is open (a flange is unbolted) you don't have to worry about overpressuring any components, so you can turn up the nitrogen to get a good flow rate (so the bag isn't deflating nor inflating so fast it's in danger of popping).

5. Break the ampule. Make sure all Cesium is at the bottom of the ampule – you can warm it with your fingers to get it to flow. Hold the ampule against a hard vertical surface (e.g., the chamber). Hit the top of the ampule (above the notch) with a small wrench. It should snap off.

6. Pour the Cs into the chamber. Use the warmth of your fingers to keep the Cesium liquid. Try to get as much of it out as you can. Carefully tape (electrical tape is OK) the ampule in an upright position to a disposable item (e.g., a small cardboard box) inside the bag, taking care not to let Cesium touch anything.

7. Close the chamber. See Section B.6 for details. After the chamber is sealed, close the valve to the nitrogen.

8. Dispose of the remaining Cesium. Quickly but carefully detach the bag from the chamber, keeping it filled with nitrogen. Take the bag and contents outside, dump it in a bucket (metal trash can), and pour water over it. Try not to get close since as the water hits the Cesium it might splatter Cesium hydroxide which is a strong base. Also, the reaction will release hydrogen gas, which may ignite. Poke it with a long stick and make sure all the Cesium has reacted before

you approach it. Dilute it with lots of water before disposing of it.

9. Pump on the chamber. Keep the Cesium reservoir cold so you don't overly contaminate your pumps. Start with the turbo then switch to the ion pumps when the pressure is low enough.

Breaking Ampule Inside a Bellows

Starting state: chamber is clean and evacuated, pumps and gauges are off, nitrogen line is connected to valve (which is closed).

1. Gather the materials you will need. This includes gloves, ConFlat gaskets, etc. (see Section B.6). The ampule should be prepared by scraping off the label, removing the glue using acetone, then following the procedure for cleaning glass for vacuum.

2. Open the chamber. Slowly open the valve to the overpressured, flushed nitrogen line. Be careful not to raise the pressure of the chamber too high (see step 4 of previous section). When the chamber is filled with nitrogen, carefully unbolt the access flange on the Cesium reservoir. This could be done in a glove bag but usually isn't for the sake of convenience.

3. Insert the ampule into the bellows.

4. Close the chamber and pump. Bolt the flange back together (see Section B.6). Close the valve, switch from the nitrogen line to a turbopump, open the valve and start the pump.

5. Bake and pump the chamber. After the chamber has pumped down, bake it again to clean off anything on the outside of the ampule. When the pressure stops falling, allow the chamber to cool, while still pumping with the turbo pump.

6. Bend the bellows to break the ampule. You should feel the crunching of glass. Remember that there is buffer gas which must be pumped away, so turn off the

ion gauges and don't be surprised to see a load on the turbopump. Keep the Cesium arm cool to reduce contamination of the pump.

7. Look for the Cesium. Turn on the ion gauge to monitor the pressure. Turn on the ion pump and close off the valve to the turbopump. You should now look for Cesium vapor. You can adjust the vapor pressure by changing the temperature of the reservoir, while watching the ion gauge reading. You can see vapor using a resonant beam, or for greater sensitivity, forming a MOT. Be aware that it may take a while (possibly weeks at room temperature) for Cesium to migrate from the reservoir to the main part of your chamber, depending on the geometry.

This is because Cs atoms will react with pretty much anything, and will remain chemically bonded to any surface. The main exception to this is that Cs will come off of a Cs coated surface. Since Cs atoms travel in straight lines through the vacuum, in order to get Cesium to go around a corner you must wait for enough Cs to evaporate from the reservoir to essentially plate the interior of your chamber with Cs. Once a section has been plated, it acts as a source to coat more parts of the chamber. We used to "chase" the Cs from one section of the chamber to another with a heat gun, but this was far too uncontrollable. We once accidentally moved the entire mass of Cs from the reservoir to a little nook between two flanges. We didn't find it until we were disassembling the chamber. Now we leave the reservoir at room temperature or slightly above and wait patiently for the Cs to travel.

Using Cesium Getters

If Cesium getters are installed, then you should be able to get Cesium vapor in your chamber by running the right amount of current through them to heat them to the correct temperature. The manufacturers state that the activation current (start of evaporation) is around 4.7 ± 0.2 Amps and the operating current is 6.5-7.5 Amps. However, they envision dispensing all of the Cs in about 20 minutes, whereas we

want these sources to last for years usually. You should therefore operate at a lower current. Sergey finds that 3.6-3.8 amps works for his chamber. You should not use more current than necessary, and you should turn off the current when you don't need it since there is a limited amount of Cs in the dispenser. Sergey finds that his MOT falls off in brightness within 5-10 minutes after shutting off the current to the getter, so this gives an estimate of how long it takes for the getter to cool off and stop emitting Cs.

B.10 Troubleshooting

- *Something is wrong with the rotary pump.*

  We once had a rotary pump that was leaking oil out of the casing. I took the thing apart and replaced all the gaskets and all the other plastic and rubber bits. It's a real mess but it's not that hard. You can get a set of replacement parts by ordering a "maintenance kit" from Varian. There are instructions in the manual but they aren't that helpful. After putting it back together it worked fine. I hope this helps.

- *The pressure of my chamber is way too high. I think my vacuum system is leaking. Help!*

  If you think you have a leak in your chamber, the first thing to try is squirting methanol on various parts of the chamber and watching the pressure. If you have a large leak, the pressure should change when the methanol enters the leak. A more sophisticated method is to hook up the leak detector. The leak detector is a turbo pump with a mass spectrometer set to look for helium. Hook up the leak detector and let it pump down. When the pressure is low enough (you may need to bake the hose), open it to your chamber. Spray a small amount of helium around different parts of your chamber, waiting after each to see if the mass spectrometer lights up (read its instruction manual for details). Remember that it can take a while for the helium to migrate so you should

spray a little helium in one place, wait a minute for the reading, then move on.

If you find that a ConFlat joint is leaky then you can try to tighten it, or decide to re-seal it (take it apart and put it back together). If you find that it is a bad glass-to-metal seal, or a bellows, then you will have to replace the part. These are the most common sources of leaks.

Liz Wilcut has also mentioned that Swagelock/Teflon fiber optic feedthroughs [80] develop a leak after a bake, but this can be fixed by tightening the Swagelock nut.

- *What happened to my Cesium?*

  Sometimes it seems like you can't see any Cesium vapor in your chamber – you don't get any fluorescence from resonant beams and you can't form a MOT. Here are some things to check: If you have optical access to the reservoir, then look at the Cesium. Does it look shiny or more like a flat grey? If it is grey then it has probably oxidized, likely because of a leak that allowed air to come into the chamber. You have to find and repair the leak and replace the Cesium. If you do not have optical access to the Cesium, then you might try warming it and watching the pressure and the MOT/fluorescence. It could just be that the Cesium is too cold to have an appreciable vapor pressure. Another thing to consider is the time it takes Cesium to get from the reservoir to the main chamber. This can be a long time, depending on the geometry of your chamber. It seems that the vapor pressure of Cesium is more temperature sensitive than that of Cesium oxide/hydroxide so if the Cesium is corrupted the pressure will not change as rapidly under heating. There are anecdotes of a Cesium puddle with an oxidized crust, where tapping the chamber could disturb the crust and let fresh Cesium vapor out (increasing the pressure and showing up in the MOT).

- *I don't think my ion pump is working.*

  Ref. [81] has a lot of good information on troubleshooting ion pumps. One

problem they mention is that after a long period of heavy use, the sputtering action of the pump can cause a metallic film to build up between the electrodes. This means that the current will flow through the film instead of through the vacuum, so there will be no pumping action. This problem can be diagnosed by measuring the resistance between the pump electrodes with an ohm-meter (with the pump controller disconnected). For low voltages, the pump should appear as an open circuit. Finite resistance means the pump needs to be replaced.

Another possible problem is field emission leakage. This is caused by fine metallic whiskers forming on the electrodes, which form regions of very high local electric fields where electrons can enter the vacuum. This does not actually impair the effectiveness of the pump, but it causes an anomalously high (and often noisy) pump current. It can be diagnosed by measuring current as a function of voltage in the kV range. Ion pump current should be roughly linear in applied voltage; field emission leakage will make it exponential. If you need to use the pump current to measure pressure, you can eliminate the metallic whiskers by banging on the pump to break them or applying 15-20 kV to melt them.

- *I need to do a bit of minor repair on my system, but it already has Cesium in it. Do I have to start over?*

We have done glove bag operations on a chamber with Cesium in it before. It can be done successfully without reacting all the Cesium if you are quick and careful. See the Section B.9 on loading Cesium in a glove bag for more information.

B.11   Disassembly

Here are some tips for taking things apart: Loosen all the bolts on a flange slightly before loosening any of them all the way. This reduces stress on the part. If you are going to store the pieces, leave the copper gasket on one of the flanges. It will help protect the knife edge. Always wrap parts in clean foil for storage. You can

write notes with a sharpie on the outside of the foil indicating what the piece is and any important information (e.g., "broken" "leaky" "OK" "removed MM/DD/YY" "Meow" etc.). If a gasket is stuck on a flange and you need to remove it, try sliding something under it along the outer groove of the flange. If the flange doesn't have a groove along the outside, carefully grip the gasket in a machinist's vise and pull on the vacuum part. If this still doesn't work, you can crush the gasket in the vise, which should free it from the flange without damaging the knife edge. Never touch the inside of a vacuum piece and always wear clean gloves.

Bibliography

[1] H. Mabuchi and A. C. Doherty. Cavity quantum electrodynamics: coherence in context. *Science*, 298:1372, 2002.

[2] E.T. Jaynes and F.W. Cummings. Comparison of quantum and semiclassical radiation theories with application to the beam maser. *Proc. IEEE*, 51:89, 1963.

[3] C. J. Hood, M. S. Chapman, T. W. Lynn, and H. J. Kimble. Real-time cavity QED with single atoms. *Phys. Rev. Lett.*, 80:4157, 1998.

[4] J. McKeever, J.R. Buck, A.D. Boozer, A. Kuzmich, H.-C. Naegerl, D.M. Stamper-Kurn, and H.J. Kimble. State-insensitive cooling and trapping of single atoms in an optical cavity. *Phys. Rev. Lett.*, 90:133602, 2003.

[5] S. M. Spillane, T. J. Kippenberg, K. J. Vahala, K. W. Goh, E. Wilcut, and H. J. Kimble. Ultra-high-q toroidal microresonators for cavity quantum electrodynamics. *quant-ph/0410218*, 2004.

[6] B. Lev, K. Srinivasan, P. Barclay, O. Painter, and H. Mabuchi. Feasibility of detecting single atoms using photonic bandgap cavities. *quant-ph/0402093*, 2004.

[7] C. J. Hood, T. W. Lynn, A. C. Doherty, A. S. Parkins, and H. J. Kimble. The atom-cavity microscope: single atoms bound in orbit by single photons. *Science*, 287:1447, 2000.

[8] C. J. Hood. *Real-time Measurement and Trapping of Single Atoms by Single Photons.* PhD thesis, California Institute of Technology, 2000.

[9] T. W. Lynn, K. M. Birnbaum, and H. J. Kimble. Strategies for real-time position control of a single atom in cavity QED. *J. Opt. B, Semiclass. and Quant. Opt.*, 2005. Submitted.

[10] T. W. Lynn. *Measurement and Conrol of Individual Quanta in Cavity QED*. PhD thesis, California Institute of Technology, 2003.

[11] A. Boca, R. Miller, K. M. Birnbaum, A. D. Boozer, J. McKeever, and H. J. Kimble. Observation of the vacuum Rabi spectrum for one trapped atom. *Phys. Rev. Lett.*, 93:233603, 2004.

[12] H. J. Kimble. Strong interactions of single atoms and photons in cavity QED. *Physica Scripta*, T76:127, 1998.

[13] J. J. Sanchez-Mondragon, N. B. Narozhny, and J. H. Eberly. Theory of spontaneous-emission line shape in an ideal cavity. *Phys. Rev. Lett.*, 51:550, 1983.

[14] G. S. Agarwal. Vacuum-field Rabi splittings in microwave absorption by Rydberg atoms in a cavity. *Phys. Rev. Lett.*, 53:1732, 1984.

[15] T. Pellizzari, S. A. Gardiner, J. I. Cirac, and P. Zoller. Decoherence, continuous observation, and quantum computing: A cavity QED model. *Phys. Rev. Lett.*, 75:3788, 1995.

[16] L.-M. Duan and H. J. Kimble. Scalable photonic quantum computation through cavity-assisted interactions. *Phys. Rev. Lett.*, 92:127902, 2004.

[17] J. I. Cirac, P. Zoller, H. J. Kimble, and H. Mabuchi. Quantum state transfer and entanglement distribution among distant nodes in a quantum network. *Phys. Rev. Lett.*, 78:3221, 1997.

[18] H.-J. Briegel, S. J. van Enk, J. I. Cirac, and P. Zoller. Quantum networks I: Entangling particles at separate locations. In D. Bouwmeester, A. Ekert, and

A. Zeilinger, editors, *The Physics of Quantum Information*, page 192. Springer-Verlag, Berlin, 2000.

[19] P. Berman, editor. *Cavity Quantum Electrodynamics*. Academic Press, San Diego, 1994.

[20] R. J. Thompson, G. Rempe, and H. J. Kimble. Observation of normal-mode splitting for an atom in an optical cavity. *Phys. Rev. Lett.*, 68:1132, 1992.

[21] J. J. Childs, K. An, M. S. Otteson, R. R. Dasari, and M. S. Feld. Normal-mode line shapes for atoms in standing-wave optical resonators. *Phys. Rev. Lett.*, 77:2901, 1996.

[22] R. J. Thompson, Q. A. Turchette, O. Carnal, and H. J. Kimble. Nonlinear spectroscopy in the strong-coupling regime of cavity QED. *Phys. Rev. A*, 57:3084, 1998.

[23] M. Brune, F. Schmidt-Kaler, A. Maali, J. Dreyer, E. Hagley, J. M. Raimond, and S. Haroche. Quantum Rabi oscillation: a direct test of field quantization in a cavity. *Phys. Rev. Lett.*, 76:1800, 1996.

[24] J. Ye, D. W. Vernooy, and H. J. Kimble. Trapping of single atoms in cavity QED. *Phys. Rev. Lett.*, 83:4987, 1999.

[25] P. Maunz, T. Puppe, I. Schuster, N. Syassen, P. W. H. Pinkse, and G. Rempe. Normal-mode spectroscopy of a single bound atom-cavity system. *quant-ph/0406136*, 2004.

[26] M. Riebe, H. Haeffner, C. F. Roos, W. Haensel, J. Benhelm, G. P. T. Lancaster, T. W. Koerber, C. Becher, F. Schmidt-Kaler, D. F. V. James, and R. Blatt. Deterministic quantum teleportation with atoms. *Nature*, 429:734, 2004.

[27] M. D. Barrett, J. Chiaverini, T. Schaetz, J. Britton, W. M. Itano, J. D. Jost, E. Knill, C. Langer, D. Leibfried, R. Ozeri, and D. J. Wineland. Deterministic quantum teleportation of atomic qubits. *Nature*, 429:737, 2004.

[28] A. Wallraff, D. I. Schuster, A. Blais, L. Frunzio, R.-S. Huang, J. Majer, S. Kumar, S. M. Girvin, and R. J. Schoelkopf. Strong coupling of a single photon to a superconducting qubit using circuit quantum electrodynamics. *Nature*, 431:162, 2004.

[29] I. Chiorescu, P. Bertet, K. Semba, Y. Nakamura, C. J. P. M. Harmans, and J. E. Mooij. Coherent dynamics of a flux qubit coupled to a harmonic oscillator. *Nature*, 431:159, 2004.

[30] J. McKeever. *Trapped atoms in cavity QED for quantum optics and quantum information.* PhD thesis, California Institute of Technology, 2004.

[31] K.L. Corwin, S.J.M. Kuppens, D. Cho, and C.E. Wieman. Spin-polarized atoms in a circularly polarized optical dipole trap. *Phys. Rev. Lett.*, 83:1311, 1999.

[32] D. Boiron, A. Michaud, P. Lemonde, Y. Castin, and C. Salomon. Laser cooling of cesium atoms in gray optical molasses down to 1.1 μK. *Phys. Rev. A*, 53:R3734, 1996.

[33] H. Carmichael. *An open systems approach to quantum optics.* Springer-Verlag, Berlin, 1993.

[34] C. J. Hood, H. J. Kimble, and J. Ye. Characterization of high-finesse mirrors: Loss, phase shifts, and mode structure in an optical cavity. *Phys. Rev. A*, 64:033804, 2001. Available at arxiv.org as quant-ph/0101103.

[35] K. M. Birnbaum, A. Boca, R. Miller, A. D. Boozer, T. E. Northup, and H. J. Kimble. Photon blockade in an optical cavity with one trapped atom. *Nature*, 2005.

[36] T. A. Fulton and G. J. Dolan. Observation of single-electron charging effects in small tunnel junctions. *Phys. Rev. Lett.*, 59:109, 1987.

[37] M. A. Kastner. The single-electron transistor. *Rev. Mod. Phys.*, 64:849, 1992.

[38] A. Imamoḡlu, H. Schmidt, G. Woods, and M. Deutsch. Strongly interacting photons in a nonlinear cavity. *Phys. Rev. Lett.*, 79:1467, 1997.

[39] P. Grangier, D. F. Walls, and K. M. Gheri. Comment on "Strongly interacting photons in a nonlinear cavity". *Phys. Rev. Lett.*, 81:2833, 1998.

[40] M. J. Werner and A. Imamoḡlu. Photon-photon interactions in cavity electro-magnetically induced transparency. *Phys. Rev. A*, 61:011801, 1999.

[41] S. Rebić, S. M. Tan, A. S. Parkins, and D. F. Walls. Large kerr nonlinearity with a single atom. *J. Opt. B*, 1:490, 1999.

[42] S. Rebić, A. S. Parkins, and S. M. Tan. Polariton analysis of a four-level atom strongly coupled to a cavity mode. *Phys. Rev. A*, 65:043806, 2002.

[43] J. Kim, O. Bensen, H. Kan, and Y. Yamamoto. A single-photon turnstile device. *Nature*, 397:500, 1999.

[44] I. I. Smolyaninov, A. V. Zayats, A. Gungor, and C. C. Davis. Single-photon tunneling via localized surface plasmons. *Phys. Rev. Lett.*, 88:187402, 2002.

[45] S. Rebič, A. S. Parkins, and S. M. Tan. Photon statistics of a single-atom intracavity system involving electromagnetically induced transparency. *Phys. Rev. A.*, 65:063804, 2002.

[46] R. J. Brecha, P. R. Rice, and M. Xiao. N two-level atoms in a driven optical cavity: Quantum dynamics of forward photon scattering for weak incident fields. *Phys. Rev. A*, 59:2392, 1999.

[47] L. Tian and H. J. Carmichael. Quantum trajectory simulations of two-state behavior in an optical cavity containing one atom. *Phys. Rev. A*, 46:R6801, 1992.

[48] H. J. Kimble, M. Dagenais, and L. Mandel. Photon antibunching in resonance fluorescence. *Phys. Rev. Lett.*, 39:691, 1977.

[49] L. Mandel and E. Wolf. *Optical Coherence and Quantum Optics.* Cambridge University Press, New York, 1995.

[50] H. J. Carmichael, R. J. Brecha, and P. R. Rice. Quantum interference and collapse of the wavefunction in cavity QED. *Opt. Commun.*, 82:73, 1991.

[51] H. J. Carmichael. Photon antibunching and squeezing for a single atom in a resonant cavity. *Phys. Rev. Lett.*, 55:2790, 1985.

[52] J. McKeever, A. Boca, A. D. Boozer, R. Miller, J. R. Buck, A. Kuzmich, and H. J. Kimble. Deterministic generation of single photons from one atom trapped in a cavity. *Science*, 303:1992, 2004.

[53] F. Diedrich and H. Walther. Nonclassical radiation of a single stored ion. *Phys. Rev. Lett.*, 58:203, 1987.

[54] K. K. Likharev. Single-electron devices and their applications. *Proc. IEEE*, 87:606, 1999.

[55] K. M. Birnbaum, A. Boca, R. Miller, A. D. Boozer, T. E. Northup, and H. J. Kimble. Supplemental information – photon blockade in an optical cavity with one trapped atom. *Nature*, 2005.

[56] J. P. Reithmaier, G. Sek, A. Löffler, C. Hofmann, S. Kuhn, S. Reitzenstein, L. V. Keldysh, V. D. Kulakovskii, T. L. Reinecke, and A. Forchel. Strong coupling in a single quantum dotsemiconductor microcavity. *Nature*, 432:197, 2004.

[57] T. Yoshie, A. Scherer, J. Hendrickson, G. Khitrova, H. M. Gibbs, G. Rupper, C. Ell, O. B. Shchekin, and D. G. Deppe. Vacuum rabi splitting with a single quantum dot in a photonic crystal nanocavity. *Nature*, 432:200, 2004.

[58] D. A. Steck. Cesium D line data. Technical report, Los Alamos National Laboratory, 1998.

[59] S. M. Tan. A computational toolbox for quantum and atomic optics. *J. Opt. B: Quantum Semiclass. Opt.*, 1:424, 1999.

[60] S. M. Tan. *A quantum optics toolbox for Matlab 5.* University of Auckland.

[61] A. D. Boozer. *Raman Transitions in Cavity QED.* PhD thesis, California Institute of Technology, 2005.

[62] H. M. Wiseman. *Quantum Trajectories and Feedback.* PhD thesis, University of Queensland, 1994.

[63] N. Lutkenhaus. Security against individual attacks for realistic quantum key distribution. *Phys. Rev. A*, 61:52304, 2000.

[64] I. L. Chuang and Y. Yamamoto. Simple quantum computer. *Phys. Rev. A*, 52:3489, 1995.

[65] Q. A. Turchette, C. J. Hood, W. Lange, H. Mabuchi, and H. J. Kimble. Measurement of conditional phase shifts for quantum logic. *Phys. Rev. Lett.*, 75:4710, 1995.

[66] E. Knill, R. Laflamme, and G. Milburn. A scheme for efficient quantum computation with linear optics. *Nature*, 409:46, 2001.

[67] L.-M. Duan, A. Kuzmich, and H. J. Kimble. Cavity QED and quantum-information processing with "hot" trapped atoms. *Phys. Rev. A*, 67:032305, 2003.

[68] A. Kuzmich. Simulations of single photon production. Unpublished, 2002.

[69] E. Arimondo. Coherent population trapping in laser spectroscopy. *Progress in Optics*, 35:257, 1996.

[70] J.McKeever, A.Boca, A.D.Boozer, J.R.Buck, and H.J.Kimble. Experimental realization of a one-atom laser in the regime of strong coupling. *Nature*, 425:268, 2003.

[71] J. McKeever, J. R. Buck, A. D. Boozer, and H. J. Kimble. Determination of the number of atoms trapped in an optical cavity. *Phys. Rev, Lett.*, 93:143601, 2004.

[72] A. E. Siegman. *Lasers*, page 761. University Science Books, Sausalito, 1986.

[73] R. G. DeVoe, C. Fabre, K. Jungmann, J. Hoffnagle, and R. G. Brewer. Precision optical-frequency-difference measurements. *Phys. Rev. A*, 37:1802, 1988.

[74] J. S. Seeley. Resolving power of multilayer filters. *JOSA*, 54:342, 1964.

[75] D. Vernooy. *Cold atoms in cavity QED for quantum information processing.* PhD thesis, California Institute of Technology, 2000.

[76] J. A. Venables. UHV resources: Vacuum and materials. Available on the web at http://venables.asu.edu/grad/appmat1.html.

[77] CCLRC Synchrotron Radiation Department Vacuum Support Group. The red book ultrahigh vacuum guide. Technical report, Daresbury Laboratory, 1996. Available on the web at http://srs.dl.ac.uk/vacsci/website%20now%20running%20from%20srdweb4 /Documents/DL_Specifications/redbook/rbconts.html.

[78] A. Roth. *Vacuum Technology.* Elsevier, Amsterdam, 1990.

[79] A. Chambers, R. K. Fitch, and B. S. Halliday. *Basic Vacuum Technology.* Institute of Physics, Bristol, 1998.

[80] E. R. Abraham and E. A. Cornell. Teflon feedthrough for coupling optical fibers into ultrahigh vacuum systems. *App. Opt.*, 37:1762, 1998.

[81] S. Rutherford. Ion pump operation and trouble shooting guide. Available on the web at http://www.duniway.com/images/pdf/pg/Ion-Pump-op-troubleshoot.pdf.